In Memory
of my Mother,
Eythimia S. Kallianteris

ACKNOWLEDGEMENTS

I would like to express my gratitude to those whose support has aided the preparation of this thesis:

Professor Otto Schwelb, for his guidance and many helpful suggestions during the course of the work and the preparation of the manuscript;

The president of Com Dev Ltd., Mr. V. O'Donovan, for his encouragement and support of this project;

Mr. C. M. Kudsia of Com Dev Ltd., for his help in the computer programs;

Mr. K. J. Flood and N. Vouloumanos of Com Dev Ltd., for arranging the fabrication of the experimental filters;

and finally, the National Research Council of Canada for their Industrial Research Assistance Program.

TABLE OF CONTENTS

LIST OF TABLES

LIST OF FIGURES

LIST OF IMPORTANT ABBREVIATIONS AND SYMBOLS

A	Cross sectional area of cavity
A_i	Relative transmission loss or isolation
A_o	Centre frequency insertion loss
A_r	Return loss or reflection loss
A_{rip}	Passband ripple of Chebyshev filters
A_t	Transmission loss or insertion loss
a	Width of interfacing waveguide
a_1	Width of square cavity
B	Susceptance of coupling aperture
BP	Bandpass filter
BW	Bandwidth of BP filter
b	Height of interfacing waveguide
C	Coupling screw
C_N	Number of cross couplings
C_v	Velocity of light
D	Diameter of cavity
dB	Decibels
f	Frequency variable
f_h	High frequency print out point
f_l	Low frequency print out point
f_o	Centre frequency of BP filter

g_m	LP prototype elements of Chebyshev filters
H_t	Constant multiplier in transmission formula
H_r	Constant multiplier in reflection formula
J	Number of transmission zeros
K_c	Coupling coefficient
LP	Low pass filter
ℓ	Length of cavity
ℓ_a	Length of aperture
ℓ_p	Penetrating length of coupling screw
M	Magnetic polarizability of aperture
M_{ij}	Mutual coupling
N	Third index of operating mode
N_p	Number of print out points
n	Number of poles
P_{avail}	Maximum available power
P_ℓ	Dissipated power
P_r	Reflected power
P_t	Transmitted power
Q_e	External quality factor
Q_u	Unloaded quality factor
S	Complex frequency variable
S_{pk}	Poles of LP Chebyshev filters
S_{tJ}	Transmission zeros of filter function

T_o	Centre frequency group delay of BP filter
TE	Transverse electromagnetic mode
T_R	Relative group delay
$Tn(\omega)$	First kind Chebyshev polynomial
T_r	Reflection group delay
T_t	Transmission group delay
t	Transmission coefficient
VSWR	Voltage standing wave ratio
W	Width of coupling aperture
W_λ	Fractional bandwidth
Y_o	Characteristic admittance of guide
δ	Skin depth
δ_d	Dissipation factor
ε	Ripple factor of LP Chebyshev filter
η	Unloaded Q efficiency
λ	Free space wavelength
λ_c	Cut off wavelength
λ_g	Interfacing guide wavelength
λ_{gc}	Cavity guide wavelength
λ_{go}	Arithmetic mean guide wavelength
ρ	Reflection coefficient
σ_{pk}	Real part of S_{pk}
σ_{zJ}	Real part of S_{zJ}
ϕ_t	Total transmission phase

ϕ_{pk}	Phase lag of each pole
ϕ_{zJ}	Phase lag of each transmission zero
ω	Angular frequency variable
ω_{Bp}	Normalized BP frequency variable
ω_c'	Cut off frequency of LP filter
ω_{Lp}	Normalized LP frequency variable

CHAPTER I

INTRODUCTION

The direct coupled cavity microwave bandpass filter is a development of the last two decades.

The first important independent effort in the design of direct coupled cavity filters, which produced a significant technical contribution, is a design procedure introduced in 1957 by Cohn[4]. Using this procedure, microwave bandpass filters with bandwidths less than 20% are designed from the conventional all pole low pass prototype filter elements. Such filters are realized using synchronously tuned rectangular waveguide cavities supporting the TE_{101} mode and coupled through shunt inductive irises or posts.

Another significant contribution in the area of direct coupled cavity filters was the linear phase filter introduced in 1970 by Rhodes[9]. Rhodes conceived the synthesis of linear phase filters and applied this synthesis technique to general waveguide bandpass filters. The generalized direct coupled cavity linear phase filter consists of two identical shunt inductive iris waveguide structures where

adjacent cavities in the two halves are coupled through apertures in the common narrow wall.

The most recent important contribution which resulted from the need to develop optimum amplitude miniaturized microwave bandpass filters for satellite communications is the dual mode filter.

The first TE_{101} and TE_{111} dual mode filters were introduced at the COMSAT Laboratories[6] in 1970, where significant advances in both theoretical and experimental aspects were reported over the following five years[11,14]. Further theoretical work on the same filter was carried out in the TRW Systems Group[12] in 1975. The referenced publications established the basic design steps for the 4 GHz output multiplexer filters of the INTELSAT IV-A and V transponders.

Further work on the dual mode filter, with the objective of increasing its unloaded Q at 12 GHz was carried out at the Com Dev laboratories in 1975. This work resulted in the introduction of the TE_{10_N} and TE_{11_N} ($N > 1$) dual mode filters[16,22]. A further improvement of the TE_{10_N} filter at Com Dev aided the design of the 12 GHz output multiplexers[17] used in the ANIK-B and INTELSAT V transponders. Development of the TE_{10_N} and TE_{11_N} linear phase[10,23] and elliptic filters[15] was carried out at the same laboratory in 1976 and 1977.

Today a set of literature is available on dual mode filters, and several companies manufacture the above filters for earth and space applications.

In this thesis the dual mode Chebyshev filter is analyzed in detail using, whenever possible, existing material available in the literature. The thesis is arranged into four major parts.

Part one presents the amplitude, phase and group delay characteristics of lossless and lossy LP and BP Chebyshev filters. Both transmission and reflection characteristics are considered and are calculated from the locus of the poles and reflection zeros of LP Chebyshev filters. The LP prototype elements of Chebyshev filters are also defined. Relations for computing these elements and the above characteristics are provided and arranged in a form suitable for computer programming.

The second part describes the longitudinal dual mode filter structure, its principles of operation, and the filter types which can be realized using this structure. The equivalent circuit of the dual mode filter, the filter function and responses corresponding to each filter type are also included. Further, in this part, the TE_{10N} and TE_{11N} ($N > 1$) dual mode filter is introduced and described.

In the third part the coupling elements of the dual mode Chebyshev filter are defined. Equations for

computing these elements and techniques for converting them into mechanical dimensions are given. The theoretical and measured unloaded Q's of the dual mode filter are also considered. The design procedure is general and covers square and cylindrical cavity filters operating in $TE_{10}N$ and $TE_{11}N$ modes (N = 1,2,3, ...).

The fourth part deals with the presentation and discussion of the computed and measured results of an 8 pole 4 GHz TE_{111} and of two 6 pole 12 GHz TE_{111} and TE_{103} Chebyshev filters. The differences between the filter characteristics, the dimensions determined from the computer programs, and those actually achieved in practice are discussed. The theoretical and measured unloaded Q's of the experimental filters are also given together with methods for improvement and the advantages and disadvantages of dual mode filters are pointed out.

Finally, in the Appendices, the flow charts of the design program and the response prediction program are presented.

CHAPTER II

AMPLITUDE AND PHASE CHARACTERISTICS OF CHEBYSHEV FILTERS

2.1 DEFINITION OF TRANSMISSION AND REFLECTION LOSS

In Fig. 2.1 a filter is shown terminated by equal source and load resistances. This filter is called "doubly terminated", and permits maximum power transfer from the source to the load.

The power flow from the source through the filter into the load can be expressed in terms of the maximum available power P_{avail}. A fraction P_t of this power will be transferred through the filter into the load. Another fraction P_r will be reflected back to the source, and the rest P_ℓ will be dissipated in the lossy filter. Thus

$$P_{avail} = P_t + P_r + P_\ell . \tag{1}$$

For a doubly terminated filter the logarithmic ratio of the available power P_{avail} to the transferred power P_t is called the "transmission loss" or "insertion loss" of the filter and is given by

$$A_t(dB) = 10 \lg \frac{P_{avail}}{P_t} . \tag{2}$$

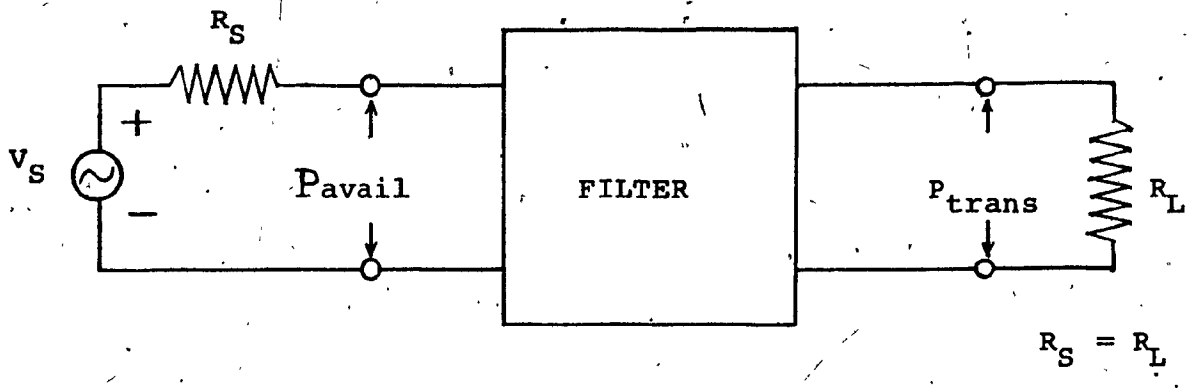

Fig. 2.1 Doubly Terminated Filter

The centre frequency transmission loss is designated by A_o and is a convenient measure of the power P_ℓ dissipated in the filter and it is also related to the unloaded Q of the filter. The stopband transmission loss of a filter minus its loss at centre frequency is called "relative transmission loss" or "isolation". It is given by (3) and determines the order of the filter.

$$A_i(dB) = A_t - A_o \tag{3}$$

Similarly the analogous logarithmic ratio of the available power P_{avail} to the reflected power P_r is called "reflection loss" or "return loss" of the filter and it is given by

$$A_r(dB) = 10 \lg \frac{P_{avail}}{P_r}. \tag{4}$$

The passband return loss of a filter is a measure of the matching condition at its input and output ports, and of the passband ripple in the case of equiripple filters. In general, the passband return loss of a filter gives a good indication of its passband performance. The transmission and reflection losses defined above are frequency dependent quantities.

The transmitted and reflected powers P_t and P_r are also directly related to the transmission and reflection coefficients t and ρ as given by

$$P_t = |t|^2 P_{avail} \tag{5}$$

and

$$P_r = |\rho|^2 P_{avail}. \tag{6}$$

Therefore the transmission loss and reflection loss of a filter can be determined from its transmission and reflection coefficients:

$$A_t(dB) = -20 \lg|t| \tag{7}$$

$$\text{and } A_r(dB) = -20 \lg|\rho| . \tag{8}$$

For a lossless filter $|t|^2+|\rho|^2 = 1$ and the relationship between A_t and A_r is

$$10^{-\frac{A_t}{10}}+10^{-\frac{A_r}{10}} = 1. \tag{9}$$

2.2 AMPLITUDE CHARACTERISTICS OF MICROWAVE FILTERS

A microwave filter is specified by its passband and stopband amplitude characteristics. The specified passband characteristics are: The minimum passband width, the minimum passband return loss and the maximum insertion loss. Since ρ, VSWR and A_r are related by

$$A_r(dB) = -20 \lg|\rho| = -20 \lg \frac{VSWR-1}{VSWR+1}. \tag{10}$$

Any one of these three parameters can be used to specify the minimum passband return loss.

The specified stopband characteristics are the maximum stopband width and the minimum stopband isolation. The above design parameters are shown in Fig. 2.2.

Following standard procedures the first step in in filter design is to find a suitable transmission loss function which meets the specified passband and stopband characteristics. This function is selected in such a way that the transmission loss A_t(dB) falls within the unshaded area in Fig. 2.2.

The classical transmission functions which can be used to approximate a certain amplitude response are the: Butterworth, Chebyshev, inverted Chebyshev and elliptic functions. In this thesis we shall restrict ourselves to Chebyshev approximation.

2.3 TRANSMISSION CHARACTERISTICS OF LOSSLESS LP CHEBYSHEV FILTERS

The typical low pass Chebyshev transmission response is depicted in Fig. 2.3. This response is characterized by an equiripple passband and a monotonic stopband attenuation. The mathematical function which represents the magnitude of this response is given by

$$|t(j\omega)|^2 = \frac{1}{1+\varepsilon^2 T_n^2(\omega)} \quad (11)$$

where $t(j\omega)$ is the transmission coefficient and $T_n(\omega)$ is the nth order Chebyshev polynomial of the first kind defined by

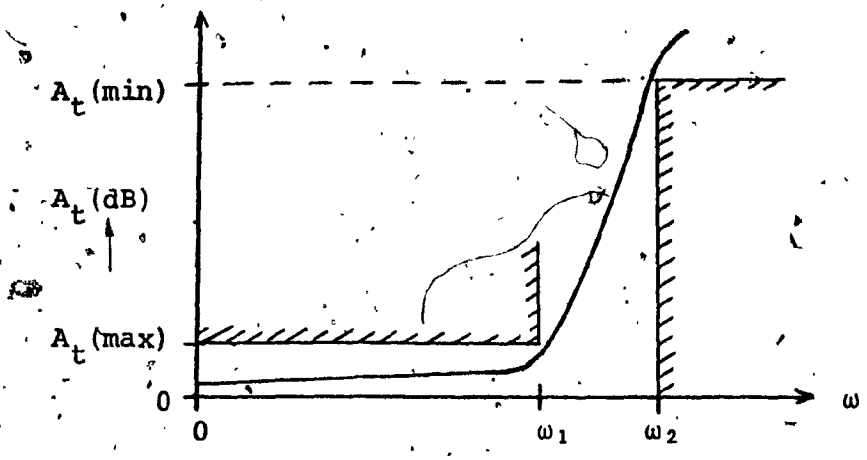

Fig. 2.2 Design Parameters of a LP Filter

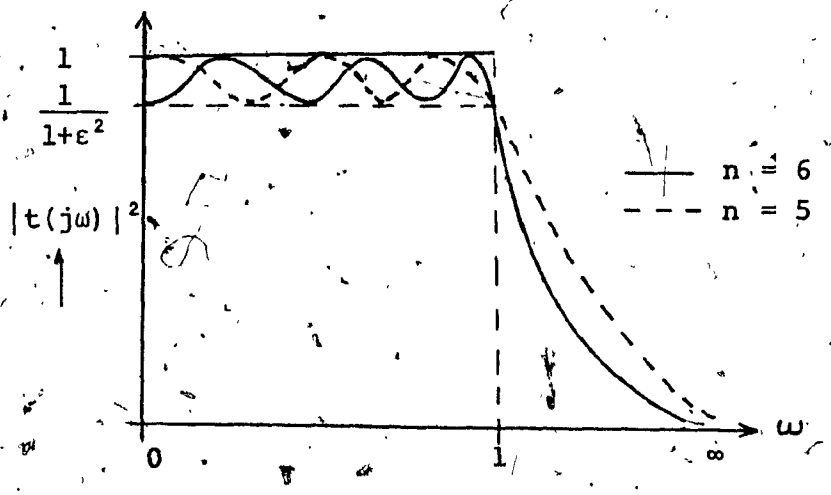

Fig. 2.3 Normalized LP Chebyshev Response

$$T_n(\omega) = \begin{cases} \cos(n\cos^{-1}\omega) & |\omega| \leq 1 \\ (-1)^{nm}\cosh(n\cosh^{-1}|\omega|) & |\omega| > 1 \\ m=0 \text{ for } \omega>1, m=1 \text{ for } \omega<1 \end{cases} \quad (12)$$

The parameter ε is the passband ripple factor of $|t(j\omega)|^2$ which is related to the passband return loss A_r(dB) by

$$\varepsilon^2 = \frac{1}{10^{\frac{A_r}{10}}-1} \quad (13)$$

The subscript n is the order of the Chebyshev polynomial and therefore the order of the filter.

2.4 REFLECTION CHARACTERISTICS OF LOSSLESS LP CHEBYSHEV FILTERS

For a lossless filter the sum of the squared magnitudes of the transmission and reflection coefficients is equal to unity, i.e. $|t(j\omega)|^2+|\rho(j\omega)|^2 = 1$. This relationship can be used to determine the reflection response of lossless low pass Chebyshev filters. Thus

$$|\rho(j\omega)|^2 = 1-|t(j\omega)|^2 = 1 - \frac{1}{1+\varepsilon^2 T_n^{\,2}(\omega)} = \frac{\varepsilon^2 T_n^{\,2}(\omega)}{1+\varepsilon^2 T_n^{\,2}(\omega)} \quad (14)$$

From (14) it can be seen that the reflection function of Chebyshev filters has the same denominator as the transmission function but the numerator is different.

2.5 POLES AND ZEROS OF TRANSMISSION AND REFLECTION FUNCTIONS

The roots of the denominator of the transmission and reflection functions (11) and (14) in the complex frequency plane S give the poles of the low pass Chebyshev filter. Therefore, for $\omega = \frac{S}{j}$ one obtains

$$1+\varepsilon^2 T_n^2\left(\frac{S}{j}\right) = 0 \qquad (15)$$

Solving (15) and considering only its left half plane poles corresponding to a realizable filter[2], we have

$$S_{pk} = -\sigma_{pk}+j\omega_{pk} = -\sinh a \sin\frac{2k-1}{n}\frac{\pi}{2} + j\cosh a \cos\frac{2k-1}{n}\frac{\pi}{2}$$

$$\text{where } a = \frac{1}{n}\sinh^{-1}\frac{1}{\varepsilon} \text{ and } k = 1,2,3, \ldots n \qquad (16)$$

Knowing the left half plane poles S_{pk} of the low pass Chebyshev function we can write (11) in its general form

$$|t(j\omega)|^2 = \frac{1}{C\left(|S-S_{p1}||S-S_{p2}||S-S_{p3}|\ldots|S-S_{pk}|\right)^2} = \frac{H_t}{\prod_{k=1}^{n}|S-S_{pk}|^2} \qquad (17)$$

where $H_t = \frac{1}{C}$ is a constant multiplier to be determined later.

Similarly, by obtaining the zeros of the reflection function we can also write (14) in its general form

$$|\rho(j\omega)|^2 = \frac{H_r \prod_{J=1}^{n} |S-S_{zJ}|^2}{\prod_{k=1}^{n} |S-S_{pk}|^2} \quad (18)$$

where S_{zj} are the zeros of the Chebyshev polynomial given by

$$S_{zJ} = j\omega_{zJ} = \cos \frac{2J-1}{n} \frac{\pi}{2} \quad (19)$$

where $J = 1,2,3,4 \ldots n$, $\omega_{zJ} < 1$ and $H_r = \frac{\varepsilon^2}{C}$ is another constant multiplier.

The transmission loss and return loss of lossless low pass Chebyshev filters is determined by taking the logarithm of (17) and (18). Thus

$$A_t(dB) = 20 \sum_{k=1}^{n} \lg |S-S_{pk}| - H_t(dB) \quad (20)$$

$$\text{and } A_r(dB) = 20 \left[\sum_{k=1}^{n} \lg |S-S_{pk}| - \sum_{J=1}^{n} \lg |S-S_{zJ}| \right] - H_r(dB)$$

2.6 DETERMINATION OF THE CONSTANT MULTIPLIERS H_t AND H_r

The constant multipliers H_t and H_r of the transmission and reflection functions $|t(j\omega)|^2$ and $|\rho(j\omega)|^2$ are determined from the value of these functions at a specified frequency. This frequency is chosen to be unity where the normalized LP Chebyshev response reaches the value $\frac{1}{1+\varepsilon^2}$ which is independent of n (see Fig. 2.3).

Hence, at $\omega = 1$ and $S = j\omega = j$

$$\left|t(j\omega)\right|^2_{\omega=1} = \frac{H_t}{\prod_{k=1}^{n}\left|j-S_{pk}\right|^2} = \frac{1}{1+\varepsilon^2} = 1-10^{-\frac{A_r}{10}}$$

from which we get

$$H_t(dB) = 10\ \lg(1-10^{-\frac{A_r}{10}}) + 20\sum_{k=1}^{n}\lg\left|j-S_{pk}\right| \qquad (22)$$

Similarly at the same frequency

$$\left|p(j\omega)\right|^2_{\omega=1} = H_r\ \frac{\prod_{J=1}^{n}\left|j-S_{zJ}\right|^2}{\prod_{k=1}^{n}\left|j-S_{pk}\right|^2} = \frac{\varepsilon^2}{1+\varepsilon^2} = 10^{-\frac{A_r}{10}}$$

and

$$H_r(dB) = -A_r + 20\left[\sum_{k=1}^{n}\lg\left|j-S_{pk}\right| - \sum_{J=1}^{n}\lg\left|j-S_{zJ}\right|\right] \qquad (23)$$

where $\left|j-S_{pk}\right| = \left|j-(\sigma_{pk}+j\omega_{pk})\right| = \sqrt{\sigma_{pk}^2+(1-\omega_{pk})^2}$

and $\left|j-S_{zJ}\right| = \left|j-j\omega_{zJ}\right| = 1-\omega_{zJ}$

Thus, it has been shown that the transmission and return loss characteristics of lossless low pass Chebyshev filters can be determined from the poles and reflection zeros of the low pass Chebyshev function.

2.7 TRANSMISSION LOSS AND RETURN LOSS SLOPE CHARACTERISTICS

The passband amplitude slope of a microwave filter in dB/MHz is a useful measure of the distortion of signals through the filter. This slope is determined by taking the

first derivative of the transmission loss or return loss with respect to frequency.

Differentiating (20) one obtains

$$\frac{dA_t}{d\omega} = 8.686 \left| \sum_{k=1}^{n} \frac{\frac{d}{d\omega}|S-S_{pk}|}{|S-S_{pk}|} \right|$$

but

$$\frac{d}{d\omega}|S-S_{pk}| = \frac{d}{d\omega}\left[\sigma_{pk}^2+(\omega-\omega_{pk})^2\right]^{1/2} = \frac{\omega-\omega_{pk}}{|S-S_{pk}|}$$

therefore $$\frac{dA_t}{d\omega} = 8.686 \sum_{k=1}^{n} \frac{\omega-\omega_{pk}}{|S-S_{pk}|^2} \qquad (24)$$

Similarly from (21) we get

$$\frac{dA_r}{d\omega} = 8.686 \left[\sum_{J=1}^{n} \frac{\omega-\omega_{zJ}}{|S-S_{zJ}|^2} - \sum_{k=1}^{n} \frac{\omega-\omega_{pk}}{|S-S_{pk}|^2}\right] \qquad (25)$$

Thus, given the location of poles and reflection zeros of low pass Chebyshev filters, one can determine the slope of its passband transmission loss and return loss functions.

2.8 PHASE CHARACTERISTICS OF LP CHEBYSHEV FILTERS

The phase-lag associated with each $|S-S_{pk}|$ or $|S-S_{zJ}|$ term of the transmission and reflection functions (17)

and (18) is determined by replacing S by $j\omega$. Thus, for the kth pole and $\jmath$th zero of the left half plane we have

$$S-S_{pk} = j\omega-(-\sigma_{pk}+j\omega_{pk}) = \sigma_{pk}+j(\omega-\omega_{pk})$$

and

$$S-S_{z\jmath} = \sigma_{z\jmath}+j(\omega-\omega_{z\jmath}).$$

The phase lag associated with the above terms is

$$\phi_{pk}(\omega) = \tan^{-1}\frac{\omega-\omega_{pk}}{\sigma_{pk}} \quad \text{(for the poles)} \qquad (26)$$

and

$$\phi_{z\jmath}(\omega) = \tan^{-1}\frac{\omega-\omega_{z\jmath}}{\sigma_{z\jmath}} \quad \text{(for the zeros)} \qquad (27)$$

The total phase lag of the transmission and reflection functions is the sum of the individual terms of (17) and (18):

$$\phi_t(\omega) = -\sum_{k=1}^{n} \tan^{-1}\frac{\omega-\omega_{pk}}{\sigma_{pk}} \quad \text{(for transmission)} \qquad (28)$$

and

$$\phi_r(\omega) = \sum_{\jmath=1}^{n} \tan^{-1}\frac{\omega-\omega_{z\jmath}}{\phi_{z\jmath}} - \sum_{k=1}^{n} \tan^{-1}\frac{\omega-\omega_{pk}}{\sigma_{pk}}$$

(for reflection) (29)

The group delay T of a filter is defined as the rate of change of phase with frequency and represents the time required by a signal to pass through the filter. Based on this definition one can determine the group delay associated with each term of (17) and (18).

Thus, from (26) we have

$$T_{pk}(\omega) = \left|\frac{d\phi_{pk}(\omega)}{d\omega}\right| = \frac{1}{1+\left\{\frac{\omega-\omega_{pk}}{\sigma_{pk}}\right\}^2}\,\frac{1}{\sigma_{pk}} = \frac{\sigma_{pk}}{\sigma_{pk}^2+(\omega-\omega_{pk})^2} \tag{30}$$

and similarly from (27)

$$T_{zJ}(\omega) = \left|\frac{d\phi_{zJ}(\omega)}{d\omega}\right| = \frac{\sigma_{zj}}{\sigma_{zJ}^2+(\omega-\omega_{zJ})}\,. \tag{31}$$

The total group delay of the transmission and reflection functions is therefore given by

$$T_t(\omega) = \left|\sum_{k=1}^{n} \frac{\sigma_{pk}}{\sigma_{pk}^2+(\omega-\omega_{pk})^2}\right| \tag{32}$$

and

$$T_r(\omega) = \left|\sum_{K=1}^{n} \frac{\sigma_{pk}}{\sigma_{pk}^2+(\omega-\omega_{pk})^2}\right| - \left|\sum_{J=1}^{n} \frac{\sigma_{zj}}{\sigma_{zJ}^2+(\omega-\omega_{zJ})^2}\right|. \tag{33}$$

Differentiating (32) and (33) with respect to frequency one can determine the slope of the transmission and reflection group delay of the filter. From (29), (30), (31) and (32) we have

$$T_t'(\omega) = \frac{dT_t(\omega)}{d\omega} = \left|\sum_{K=1}^{n} \frac{-2\sigma_{pk}(\omega-\omega_{pk})}{(\sigma_{pk}^2+(\omega-\omega_{pk})^2)^2}\right| = \sum_{k=1}^{n} 2T_{pk}^2\,\frac{\omega-\omega_{pk}}{\sigma_{pk}}\,. \tag{34}$$

and

$$T_r'(\omega) = \frac{dT_r(\omega)}{d\omega} \doteq \sum_{k=1}^{n} 2T_{pk}^2 \frac{\omega-\omega_{pk}}{\sigma_{pk}} - \sum_{J=1}^{n} 2T_{zj}^2 \frac{\omega-\omega_{zj}}{\sigma_{zJ}} . \quad (35)$$

We have shown that the phase and group delay of the low-pass Chebyshev filter can be also determined from the location of its poles and reflection zeros. The phase characteristics $\phi(\omega)$, $\frac{d\phi}{d\omega}$ and $\frac{d^2\phi}{d\omega^2}$ together with the amplitude characteristics $A(\omega)$ and $\frac{dA}{d\omega}$ are the essential quantities necessary to determine the signal distortion in a filter.

2.9 PROTOTYPE ELEMENTS FOR LP CHEBYSHEV FILTERS

The first step in the design of microwave filters is to determine the lumped low pass prototype elements for the desired filter approximation. These are represented by the values of shunt capacitors and series inductors of the lossless low pass ladder network which, in the Chebyshev case, give the normalized response of Fig. 2.4. Among the available methods[3] which can be used to generate these elements, Cohn's method[4] is the most suitable for microwave filter design and computer programming.

The element values g_o, g_1, g_2 ... g_n, g_n+1 of the doubly terminated low pass filter are defined in Fig. 2.4.

The odd elements g_1, g_3, g_5 ... are shunt capacitance values in farads; while the even elements g_2, g_4, g_6 ... are series inductances in henries. The prototype filter is doubly terminated with source and load resistances g_o and g_{n+1}. The element values for the doubly terminated Chebyshev prototype of order n are given by

$$g_o = 1 \qquad \text{for every n}$$

$$g_{n+1} = \begin{cases} 1 & \text{for n odd} \\ \coth^2\left(\frac{\beta}{4}\right) & \text{for n even} \end{cases} \tag{36}$$

$$g_1 = \frac{2a_1}{\gamma}\ , \quad g_m = \frac{4a_{m-1}\ a_m}{b_{m-1}\ g_{m-1}} \qquad m = 2,\ 3,\ \ldots\ n \tag{37}$$

$$\text{where } a_m = \sin\left[\frac{(2m-1)\pi}{2n}\right] \tag{38}$$

$$b_m = \gamma^2 + \sin^2\left(\frac{m\pi}{n}\right),\ m = 1,\ 2,\ \ldots\ n$$

$$\text{and } \beta = \ln\left[\coth\frac{A_{rip}}{17.37}\right],\ \gamma = \sinh\left(\frac{\beta}{2n}\right). \tag{39}$$

The quantity A_{rip} represents the passband ripple of the filter which is related to the passband return loss by the relationship

$$A_{rip}(dB) = 10\ \lg\left(1-10^{-\frac{A_r}{10}}\right). \tag{40}$$

From the above equations it can be seen that specifying the order of the filter (n) and its passband return loss (A_r)

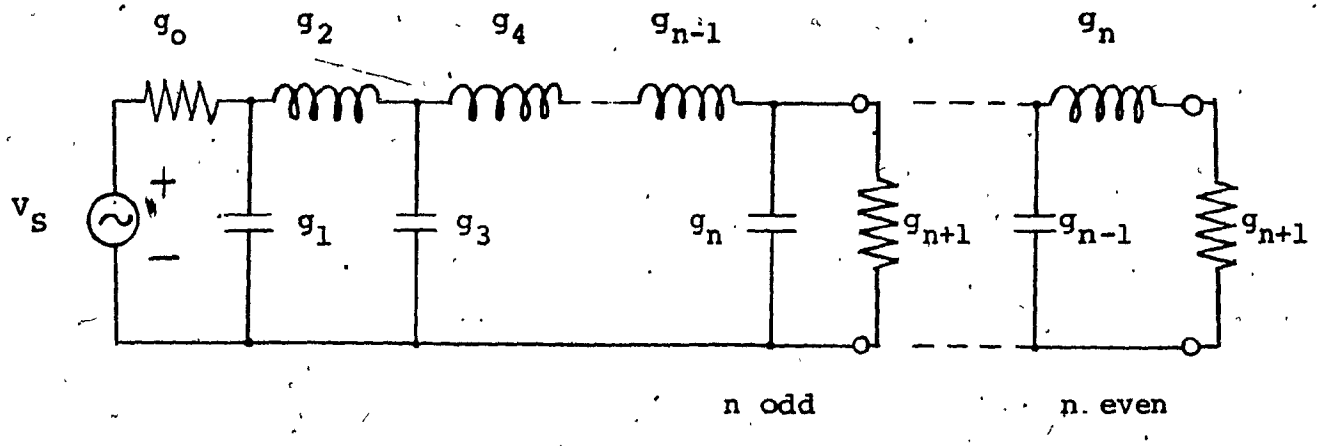

Fig. 2.4 Definition of Prototype Filter Elements

one can generate its prototype elements. These elements will be used later to determine the coupling elements of the filter, and calculate its unloaded Q.

2.10 THE LOSSY PROTOTYPE FILTER

The effect of dissipation on the amplitude and phase response of the prototype filter is treated by the "predistortion" or "precorrection" methods. Among the different ways by which these methods can be applied[5,7], the one which is considered here is Guillemin's method[8].

This method is based on the fact that the farther the poles and zeros are from the $j\omega$ axis, the larger the loss is. Thus, displacing to the right the pole-zero locus of the lossless filter by a predetermined positive real quantity δ_d, one can take into account the effect of dissipation. Such displacement is affected by replacing the variable S by $S+\delta_d$. Hence any particular point $S = S_k$ of the S plane is changed to a point $S+\delta_d = S_k$ or $S = S_k-\delta_d$, and the entire pole-zero pattern is shifted to the left by the value of δ_d as shown in Fig. 2.5.

The effect of replacing S by $S+\delta_d$ in the prototype filter can be assessed by noting that the variable S is always multiplicatively associated with the L and C elements.

Hence the corresponding transformations are:

$$\begin{aligned} S &\longrightarrow S+\delta_d \\ LS &\longrightarrow LS+\delta_d L \\ CS &\longrightarrow CS+\delta_d C \end{aligned} \tag{41}$$

Physically (41) implies that each inductance has associated with it a series resistance $R = \delta_d L$, and each capacitance is paralleled by a conductance $G = \delta_d C$. The lossy prototype filter is depicted in Fig. 2.6.

The positive real quantity δ_d is called the dissipation factor and is related to the unloaded Q of a microwave filter by

$$\begin{aligned} \delta_d &= \frac{1}{Q} \qquad \text{(for a LP filter)} \\ \delta_d &= \frac{fo}{BW} \cdot \frac{1}{Q} \quad \text{(for a BP filter)} \end{aligned} \tag{42}$$

where fo is the centre frequency and BW is the bandwidth of the bandpass filter.

From the realizable unloaded Q of a microwave filter one can compute the dissipation factor δ_d and determine the pole-zero locus of the lossy prototype filter. This locus can then be used to determine its amplitude and phase characteristics.

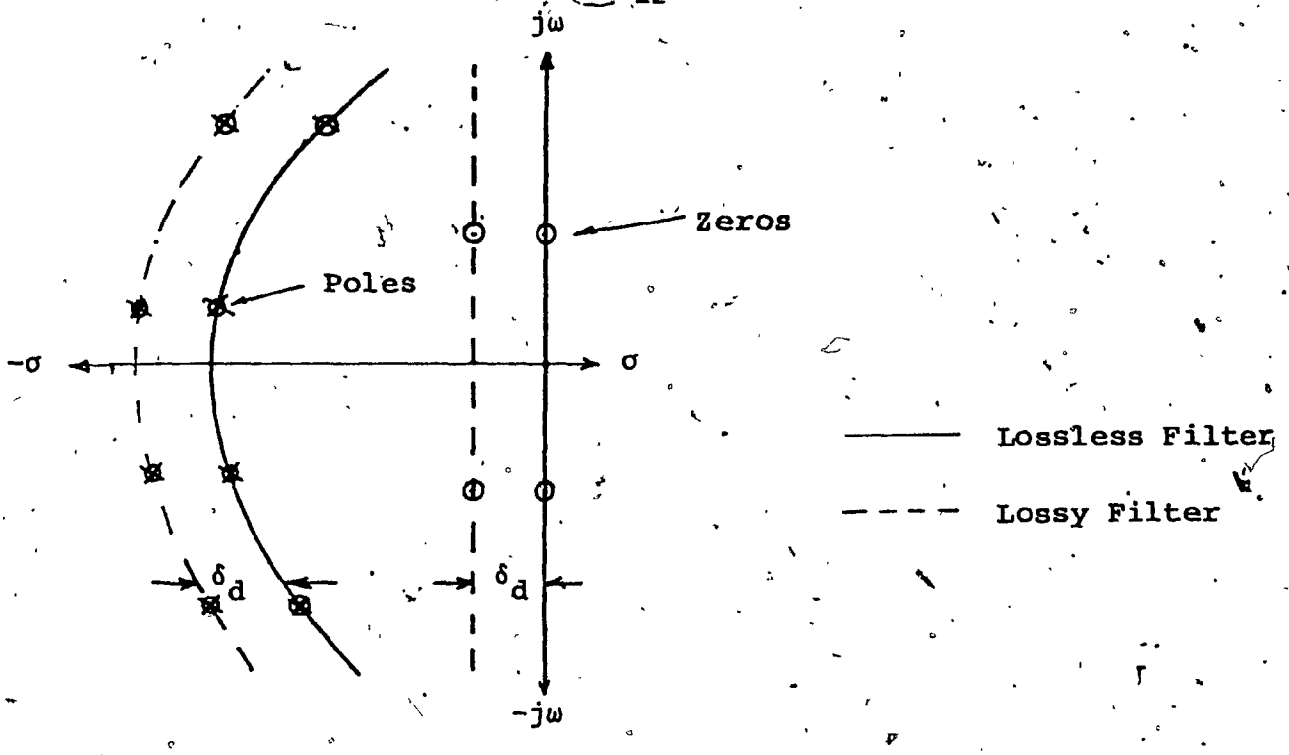

Fig. 2.5 Pole-Zero Pattern of Lossless and Lossy Prototype Filter

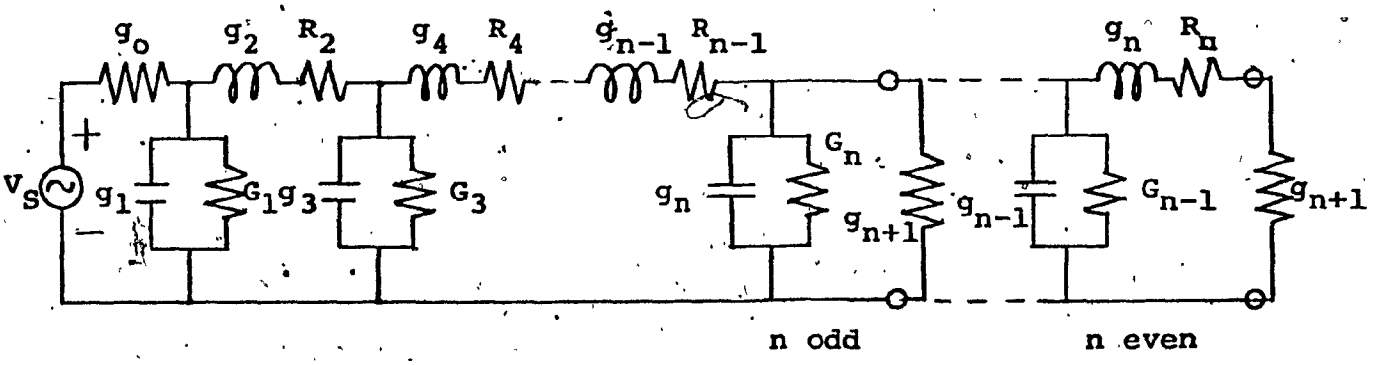

Fig. 2.6 The Lossy Prototype Filter

2.11 LP TO BP TRANSFORMATION

In the previous sections the amplitude and phase characteristics of lossless and lossy low pass Chebyshev filters were considered. These characteristics are evaluated in terms of the normalized low pass frequency variable

$$\omega_{LP} = \frac{\omega}{\omega_c'} \tag{43}$$

where ω_c' is the cut-off frequency of the prototype filter to which the frequency scale is normalized.

The amplitude and phase characteristics of a BP filter are obtained by replacing ω_{LP} in the corresponding LP relations by the normalized bandpass frequency variable ω_{BP}. In the case of direct coupled cavity filters this variable is obtained using the LP to BP transformation introduced by Cohn[4].

$$\omega_{BP} = \frac{\omega'}{\omega_c'}\Bigg|_{BP} = \frac{2(\lambda_{go}-\lambda_g)}{\lambda_{g1}-\lambda_{g2}} \tag{44}$$

where λ_{g1} and λ_{g2} are the guide wavelengths corresponding to the band edges of the bandpass filter and λg_o is the arithmetic mean guide wavelength.

$$\lambda_{go} = \frac{1}{2}(\lambda_{g1}+\lambda_{g2}) \tag{45}$$

The running variable λ_g is the guide wavelength corresponding to the frequency ω. Based on this transformation the normalized bandpass Chebyshev response becomes as shown in Fig. 2.7.

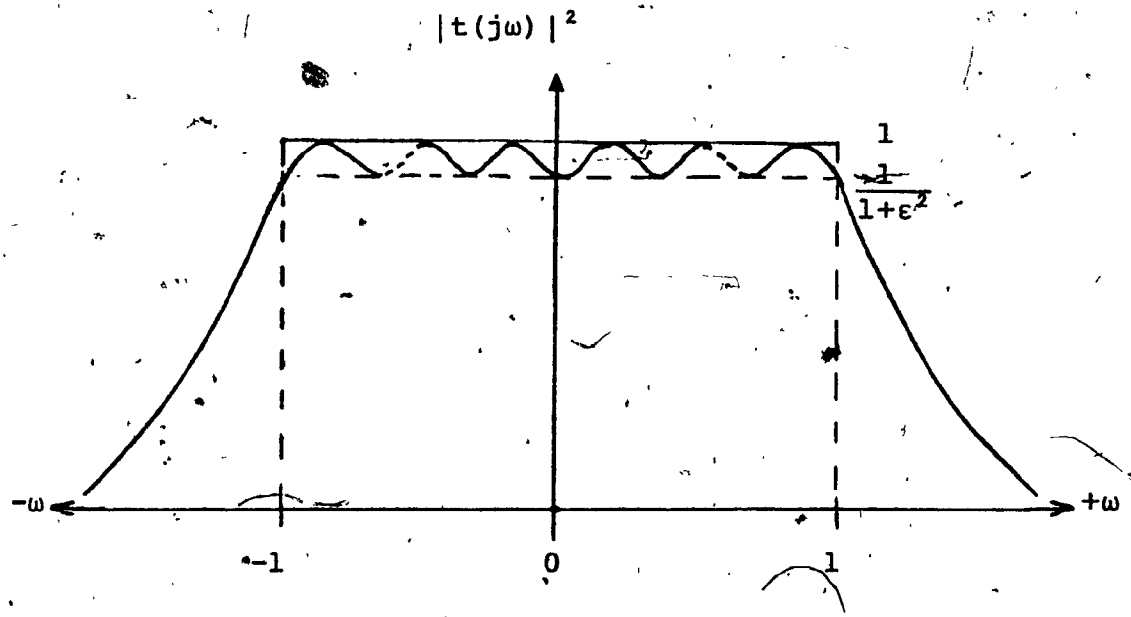

Fig. 2.7 Normalized BP Chebyshev Response

Fig. 2.7 shows that the normalized bandpass Chebyshev response is obtained by appending its mirror image to the low pass response. Thus the amplitude and phase response of a bandpass Chebyshev filter is determined by substituting ω_{LP} by ω_{BP} in the low pass amplitude and phase equations.

2.12 THE SLOPE OF THE AMPLITUDE AND PHASE RESPONSES IN TRANSFORMED VARIABLES

The slope of the amplitude and phase response in the transformed domain is

$$\frac{d\omega_{BP}}{d\omega} = -\frac{2}{\lambda_{g1}-\lambda_{g2}}\frac{d\lambda_g}{d\omega} \tag{46}$$

where $$\frac{d\lambda_g}{d\omega} = \frac{\lambda_g^3}{\lambda_o^3}\frac{d\lambda_o}{d\omega} \tag{47}$$

and $$\frac{d\lambda_o}{d\omega} = -\frac{2\pi C}{\omega^2} = -\frac{\lambda_o}{\omega} \tag{48}$$

Substituting (47) and (48) into (46) results in

$$\frac{d\omega_{BP}}{d\omega} = \frac{2}{\lambda_{g1}-\lambda_{g2}}\cdot\frac{1}{\omega}\cdot\frac{\lambda_g^3}{\lambda_o^2} \tag{49}$$

The first derivatives of the amplitude and phase response in bandpass form are

$$\left.\frac{dA}{d\omega}\right|_{BP} = \frac{d\omega_{BP}}{d\omega}\cdot\frac{dA}{d\omega_{BP}} \quad \text{and} \quad T_{BP} = \left.\frac{d\phi}{d\omega}\right|_{BP} =$$

$$\frac{d\omega_{BP}}{d\omega}\frac{d\phi}{d\omega_{BP}} \tag{50}$$

where $\frac{dA}{d\omega_{BP}}$ and $\frac{d\phi}{d\omega_{BP}}$ are obtained from their LP equivalents by replacing ω by ω_{BP}.

For the second derivative of phase with respect to frequency one finds

$$T'_{BP} = \frac{d^2\phi}{d\omega^2}\bigg|_{BP} = \frac{d^2\omega_{BP}}{d\omega^2} \cdot \frac{d^2\phi}{d\omega^2_{BP}} \tag{51}$$

where $$\frac{d^2\omega_{BP}}{d\omega^2} = -\frac{2}{\lambda_{g1}-\lambda_{g2}} \frac{1}{\omega^2} \frac{\lambda_g^3}{\lambda_o^2} = -\frac{1}{\omega} \frac{d\omega_{BP}}{d\omega} \tag{52}$$

and $\frac{d^2\phi}{d\omega^2_{BP}}$ is determined again from its LP equivalent by replacing ω by ω_{BP}.

The band centre transmission loss and group delay A_o and T_o of a bandpass filter are computed by substituting $\omega_{BP} = 0$, for ω in the LP transmission loss and group delay equations. The relative transmission loss or isolation is computed from (3) while the relative group delay from

$$T_R = T_t - T_o. \tag{53}$$

Both quantities above are generally frequency dependent.

CHAPTER III

THE DUAL MODE FILTER

3.1 DESCRIPTION

The dual mode filter is depicted in Fig. 3.1. It employs a number of waveguide cavities each of which resonates in two orthogonal modes. These cavities may be either square or cylindrical and can resonate either in a square TE_{101} mode or in a cylindrical TE_{111} mode. These modes are chosen because they are the least sensitive, orthogonal, and easily coupled to adjacent waveguides carrying the dominant mode.

Coupling between the orthogonal modes within the cavities is provided by a structural discontinuity such as a probe or a screw. This screw is located at an E field antinode (maximum) and oriented in a 45° angle between the orthogonal E field vectors as shown in Fig. 3.1. Such coupling is called "intracavity" coupling, it is capacitive and couples the E field vectors (1,2), (3,4), (5,6) .... (n-1 , n).

Direct coupling between cavities is provided by polarization apertures located at the common walls between

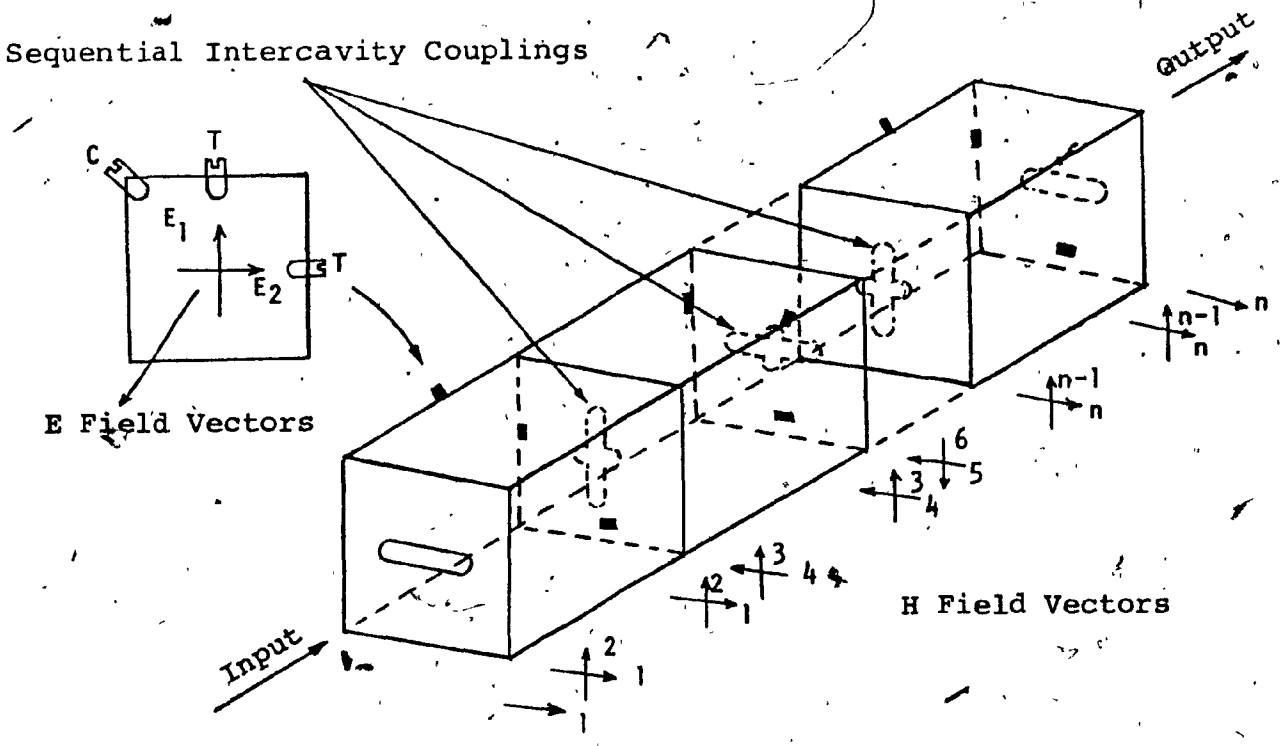

(a) TE_{101} Dual Mode Filter

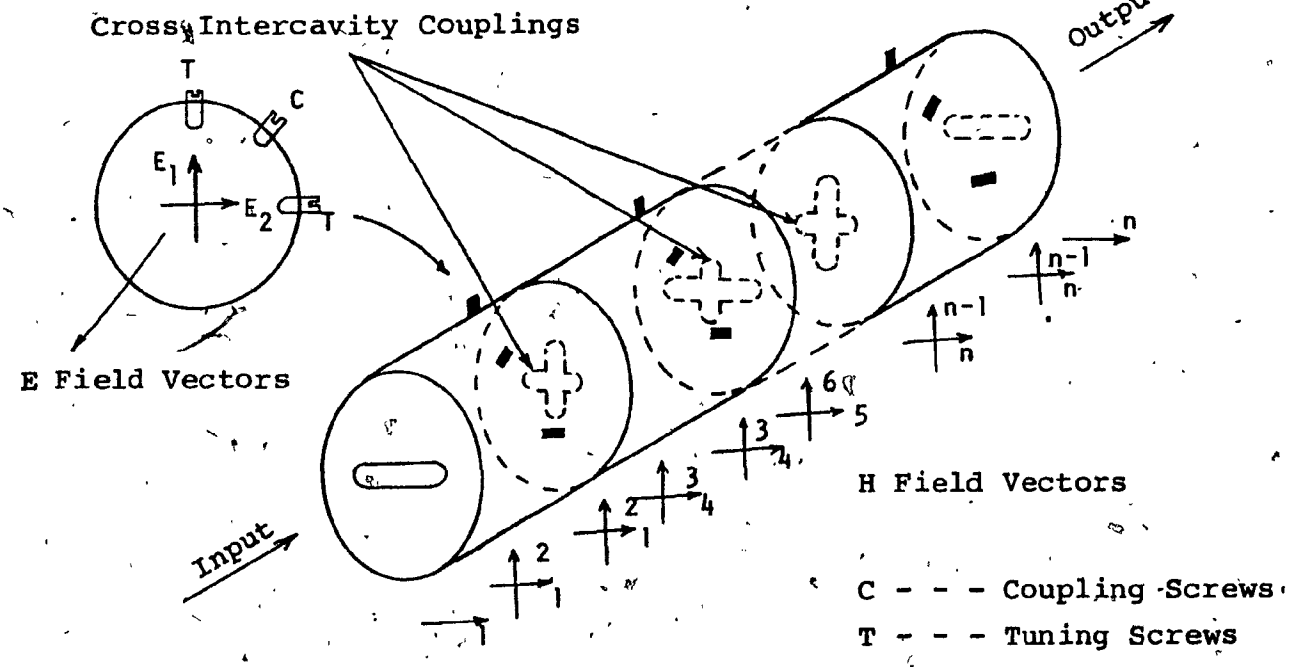

(b) TE_{111} Dual Mode Filter

Fig. 3.1 The Longitudinal Dual Mode Filter Structure

cavities as shown in Fig. 3.1. This coupling is called "intercavity" coupling and is inductive since it couples the H field vectors of the adjacent cavities. There are two types of intercavity couplings: The "sequential" ones which couple the H vectors (2,3), (4,5), (6,7) .... (n-2), (n-1) and the "cross" couplings which couple the H vectors (1,4), (3,6), (5,8) .... (n-3, n).

In addition to the 45° coupling screw which provides the intracavity coupling, each cavity is provided with tuning screws as shown in Fig. 3.1. These project into the cavity parallel to each E field vector and control the frequency of each resonant mode by varying its electrical length.

Using the previously described capacitive and inductive coupling configurations in an alternate manner, one can couple all the resonant modes of the cavities in a sequential order and realize a direct coupled cavity BP filter. This filter has n resonances in n/2 physical cavities and is called "longitudinal" dual mode filter because its input and output ports are in line. The relative orientation of its ports depends on the number of physical cavities employed. These ports are in phase if the filter has an even number of cavities, and are rotated 90° with respect to each other if the number of cavities is odd.

3.2 TYPES OF DUAL MODE FILTERS

The longitudinal dual mode filter shown in Fig. 3.1 is capable of realizing Butterworth, Chebyshev, elliptic, and linear phase filters.

The Butterworth and Chebyshev dual mode filter is realized using only the sequential couplings (1,2), (2,3), (3,4), ... (n-1, n) available in both arrangements in Fig. 3.1. This is obtained by removing the cross intercavity couplings. However, in practice, the finite width of the sequential coupling apertures provides a weak cross coupling which distorts the response of the filter. Such distortion can be reduced by using narrow apertures. In the above filter, critically coupled modes result in a Butterworth response, while over-coupled modes result in the equiripple Chebyshev response.

Linear phase[9,10] and elliptic[11,12] filters are realized by using both sequential and cross couplings. In the linear phase filter the cross couplings couple H field vectors which are in phase. To realize these so called "positive" cross couplings all 45° coupling screws must be in line as shown in Fig. 3.1b. Positive cross couplings in this filter flatten its passband amplitude and group delay characteristics, but degrade its stopband attenuation. These are characteristic of linear phase filters.

In the elliptic filter the cross couplings couple H field vectors which are 180° out of phase. Such couplings

are called "negative" and are realized by coupling screws oriented to have 90^{o} phase difference between each other as shown in Fig. 3.1α. Negative cross couplings create pairs of stopband transmission zeros resulting in the steep passband and stopband characteristics of the elliptic function filter.

3.3 THE EQUIVALENT CIRCUIT

In the vicinity of its resonant frequency a tuned cavity can be represented by a single lumped LC circuit[13]. Thus, the equivalent circuit of a doubly terminated dual mode filter of order n, consists of n coupled, LC circuits as shown in Fig. 3.2.

In this circuit the filter is assumed lossless and of narrow fractional bandwidth $\left(\frac{BW}{fo} \simeq 1\%\right)$. Under this assumption the coupling coefficients m_{ij} are considered independent of frequency. The sequential coupling coefficients m_{12}, m_{23}, m_{34} .... m_{n-1}, n are positive real numbers, while the cross coupling coefficients m_{14}, m_{36}, ... m_{n-3}, n are real numbers which have zero values for Butterworth and Chebyshev filters, positive values for the linear phase filter and negative values for the elliptic filter.

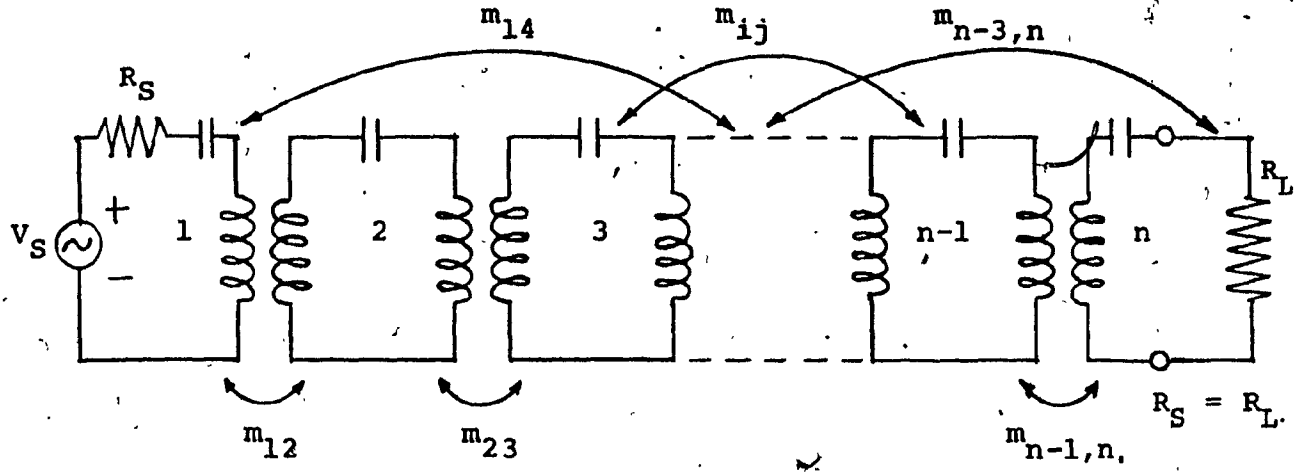

Fig. 3.2 Equivalent Circuit of Longitudinal Dual Mode Filter

3.4 THE FILTER FUNCTION

The power transmission ratio $|t(s)|^2$ of the circuit of Fig. 3.2 is given in low pass form by

$$|t(s)|^2 = H_t \frac{(S^2+S_{T1}^2)(S^2+S_{T2}^2)\ldots.(S^2+S_{TJ}^2)}{(S^2+S_{P1}^2)(S^2+S_{P2}^2)(S^2+S_{P3}^2)\ldots(S^2+S_{Pn}^2)} \quad (54)$$

where S_{p1}, S_{p2} .... S_{pn} correspond to the resonant circuits n of the filter and represent its poles. They always occur on the left half of the S plane, and their values depending on the type of the filter.

The roots S_{T1}, S_{T2}, ...S_{TJ}, of the numerator of (54) represent the transmission zeros. These zeros correspond to the cross couplings of the filter and their location also depends on the type of the filter[14,15]. Negative cross couplings result in pairs of transmission zeros which occur on the $j\omega$ axis of the S plane. Such zeros are called "real frequency transmission zeros" and are characteristic of elliptic function filters.

If the cross couplings are positive the generated pairs of transmission zeros occur either in complex conjugate pairs or on the real axis of S plane. These zeros are characteristic of the linear phase filter. In the case of Butterworth and Chebyshev filters, all the transmission zeros are at infinity and the numerator of (54) is H_t.

There are J transmission zeros in (54). This number depends on the number of cross couplings available in the dual mode filter. Table 3.1 gives the number of cross couplings (C_N) and the value of J for a filter of order of n. Note that only even order filters are considered since cross couplings cannot be realized in single mode direct coupled cavity filters.

Figure 3.3 summarizes the various types of filters which can be realized using the dual mode structure of Fig. 3.1. The normalized amplitude and group delay responses of these filters are shown together with the type of cross couplings and transmission zeros.

3.5 TE_{10N} AND TE_{11N} DUAL MODE FILTERS

The dual mode filters depicted in Fig. 3.1 employ square or cylindrical waveguide cavities supporting orthogonal TE_{101} or TE_{111} modes respectively. The cavities used in these filters have an electrical length of π radians at the centre frequency of the filter. Silver plating such cavities one can obtain an unloaded Q in the range of 5,000-6,000 at 12 GHz.

However, for specific applications such as satellite transponders, where it is necessary to combine narrow bands

TABLE 3.1

NUMBER OF POLES, CROSS COUPLINGS, AND TRANSMISSION ZEROS OF DUAL MODE FILTERS USING 2, 3, ... 7 CAVITIES

NUMBER OF CAVITIES	2	3	4	5	6	7
NUMBER OF POLES (n)	4	6	8	10	12	14
NUMBER OF AVAILABLE CROSS COUPLINGS (C_N)	1	2	3	4	5	6
NUMBER OF TRANSMISSION ZEROS (J)	2	2	4	4	6	6

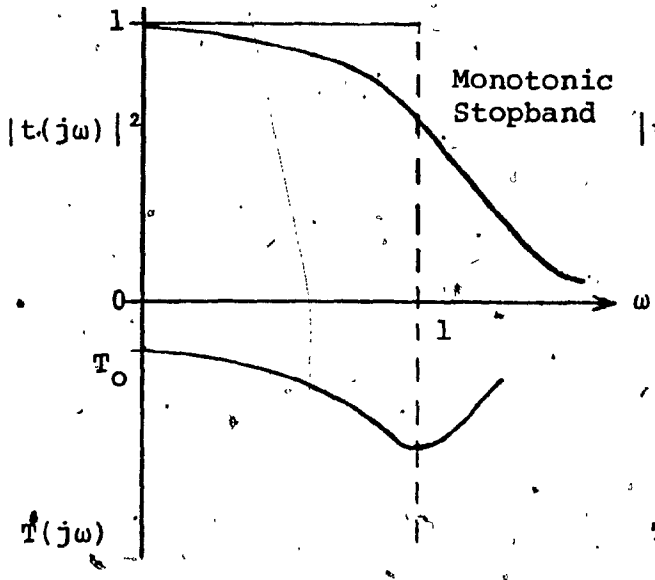

(a) Butterworth Filter (no cross couplings, all trans. zeros at infinity)

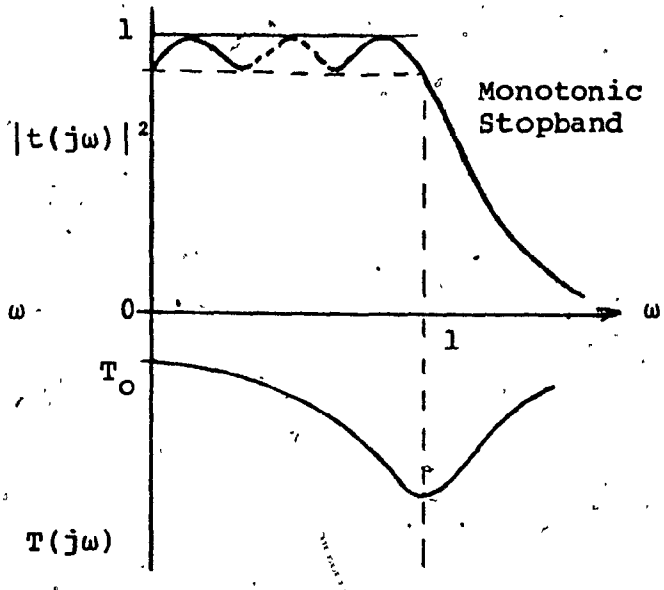

(b) Chebyshev Filter (no cross coupling, all trans. zeros at infinity)

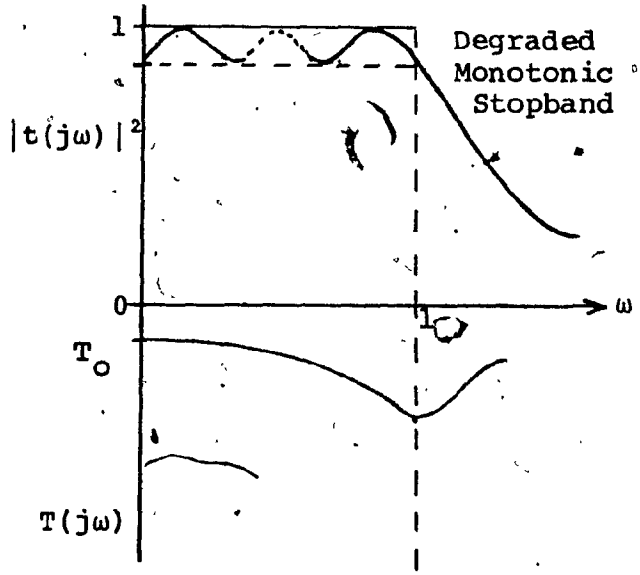

(c) Linear Phase Filter (positive cross couplings, trans. zeros on $-\sigma$ axis or complex conjugate pairs)

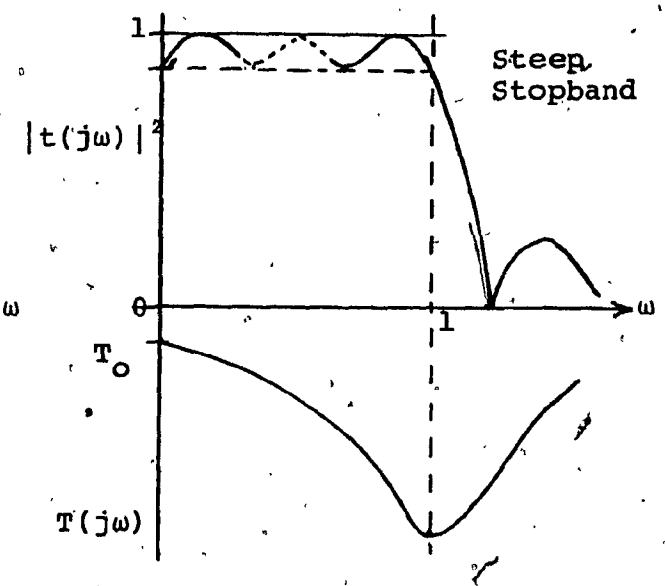

(d) Elliptic Filter (negative cross couplings, all trans. zeros on $j\omega$ axis)

Fig. 3.3 Types of Filters Realized Using the Dual Mode Structure

(less than 1%), these Q's are inadequate. Taking into consideration that the unloaded Q of a cavity increases by increasing the indices of its operating mode, one can employ cavities resonating in TE_{10N} or TE_{11N} modes[16,17] with N>1. These modes permit dual mode operation with Q's in the range of 9,000-15,000 at 12 GHz. The subscript N gives the number of half sinusoids of the E field variations along the direction of propagation. In practice N ranges from 2 to 5.

The basic differences between the N = 1 and N ≠ 1 cavities are the electrical length (Nπ radians), and the location of the coupling and tuning screws. These screws are placed at the E field antinodes located at a distance $\frac{\ell\ I}{2N}$ from each cavity end, where I = 1, 3, 5 ... N and ℓ is the cavity length. Filters with odd index N have their coupling and tuning screws at the centre of their cavities and are more attractive because they exhibit mechanical symmetry.

The design procedure for fundamental and higher order mode Chebyshev filters is the subject of the next chapter.

CHAPTER IV

DESIGN OF THE DUAL MODE CHEBYSHEV FILTER

4.1 COUPLING ELEMENTS

The coupling elements employed by the dual mode Chebyshev filter are (see Fig. 3.1):

(a) The normalized susceptance of the input and output apertures,

(b) The normalized susceptance of the sequential intercavity apertures, and

(c) The coupling coefficients of the intracavity couplings.

The following sections deal with the design of these elements.

4.2 END APERTURE SUSCEPTANCES

The inductive coupling between the interfacing waveguides and the end cavities of the filter is treated in two steps. In the first step the susceptance of an aperture located at the junction wall between two waveguides of different cross sections is considered. While in the second

one, the magnetic polarizability of the aperture is related to the geometry of the cavity and its external Q. The resulting formulas are used to calculate the end aperture susceptances.

Marcuvitz[18] has shown that the normalized susceptance B/Y_o of a coupling aperture connecting two rectangular waveguides of different cross sections, as shown in Fig. 4.1, is given by

$$\frac{B}{Y_o} = - \frac{\lambda_g ab}{4\pi M} \qquad (55)$$

where a, b, and λg are the dimensions and the guide wavelength of the interfacing waveguide A, and M is the magnetic polarizability of the aperture. From (55) we see that the normalized susceptance depends on the frequency, the geometry, and the magnetic polarizability of the aperture. Further, it is assumed that $\ell a/w >> 1$ and that the aperture is centred on the interface consisting of an infinitesimally thin transverse conductor. Equation (55) holds also if the larger guide B is square or cylindrical[18].

The magnetic polarizability M of the coupling aperture is related to the external Q of the end cavity[19] and its dimensions (see Fig. 4.2). For an inductive aperture connecting to a cavity operating in TE_{10N} mode

$$M^2 = \frac{\ell^3 ab\lambda_g A}{4\pi N^2 Q_e \lambda^2} \qquad (56)$$

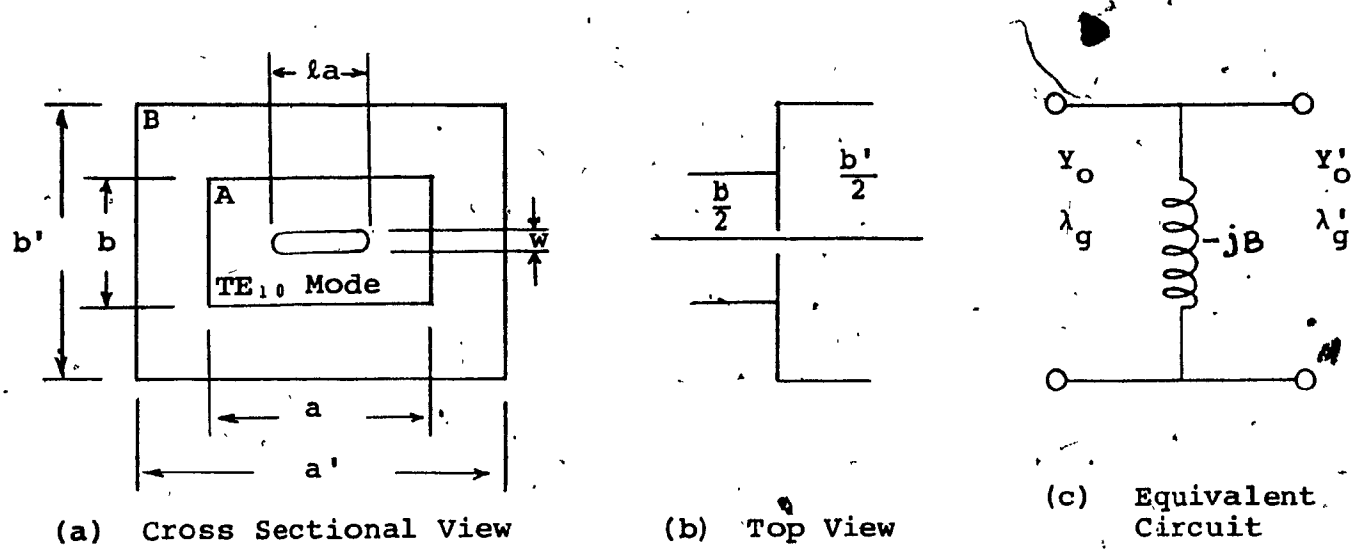

(a) Cross Sectional View (b) Top View (c) Equivalent Circuit

Fig. 4.1 Aperture Coupling Between Two Rectangular Guides of Different Cross Sections

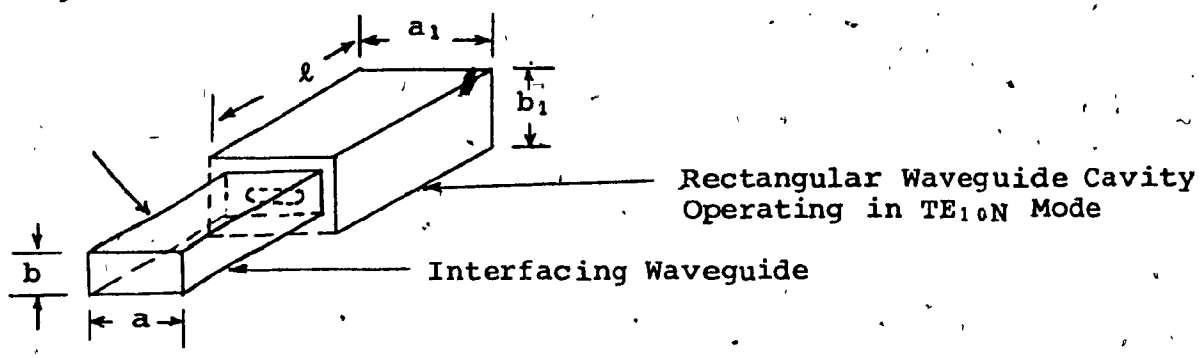

Fig. 4.2 Aperture Coupling Between the Interfacing Guide and the End Cavity

where λ is the free space wavelength, A is the cross sectional area of the cavity, and Qe the external Q which is related[19] to the prototype elements of the filter by

$$\text{Qe (for the input cavity)} = \frac{g_o g_1}{\omega\lambda}$$

$$\text{Qe (for the output cavity)} = \frac{g_o g_{n+1}}{\omega\lambda} \qquad (57)$$

where $\omega\lambda$ is the fractional bandwidth of the filter:

$$\omega\lambda = \frac{\text{Bandwidth of Filter}}{\text{Centre Frequency}} = \frac{BW}{fo} \qquad (58)$$

For meaning of the other parameters, refer to Fig. 4.2. In doubly terminated filters the input and output Qe's are equal since the products $g_o g_1$ and $g_n g_{n+1}$ are identical.

From (56) we see that the magnetic polarizability M is a function of the cross sectional areas of the interfacing guide (ab) and the cavity (A). Thus for a square cavity supporting the TE_{10N} mode, where $A = a_1^2$, we have

$$M^2 \text{ (for square cavity)} = \frac{\ell^3 ab\lambda_g a_1^2}{4\pi N^2 Q_e \lambda^2} . \qquad (59)$$

while for a cylindrical cavity operating in TE_{11N} mode $A = \frac{\pi D^2}{4}$ (D is the cavity diameter) and

$$M^2 \text{ (for cylindrical cavity)} = \frac{\ell^3 abD^2\lambda_g}{16N^2 Q_e \lambda^2} . \qquad (60)$$

Substituting (59) and (60) into (55) we get the relations for the end aperture susceptances of the dual mode filter:

Thus

$$\frac{B}{Y_o}(TE_{10N}\text{ mode}) = -\sqrt{\frac{N^2 Q_e \lambda^2 \lambda_g ab}{4\pi \ell^3 a_1^2}} \tag{61}$$

and

$$\frac{B}{Y_o}(TE_{11N}\text{ mode}) = -\sqrt{\frac{N^2 Q_e \lambda^2 \lambda_g ab}{\pi^2 \ell^3 D^2}} \tag{62}$$

4.3 INTERCAVITY COUPLING APERTURE SUSCEPTANCES

The normalized susceptances of the intercavity coupling apertures are determined using a similar procedure as the one used for the end apertures. The normalized susceptance of a centred aperture connecting two adjacent square or circular guides carrying the dominant mode[18] is given by (see Fig. 4.3)

$$\frac{B}{Y_o}(\text{for square guides}) = -\frac{\lambda_{gc} a_1^2}{4\pi M} \tag{63}$$

and

$$\frac{B}{Y_o}(\text{for circular guides}) = -\frac{3\lambda_{gc} D^2}{16\pi M} \tag{64}$$

where it is again assumed that $\ell a/w >> 1$, and that the transverse wall is infinitesimally thin, and where λ_{gc} represents the cavity guide wavelength given by

$$\lambda_{gc} = \frac{\lambda}{\sqrt{1-\left(\frac{\lambda}{\lambda_c}\right)^2}} \tag{65}$$

with λ_c being the cut-off wavelength of the guide

$$\lambda_c \text{ (for square guide)} = 2a_1 \qquad (66)$$

$$\lambda_c \text{ (for circular guide)} = 1.706D.$$

The polarizability M of a small aperture which couples two rectangular waveguide cavities of identical cross sections and resonating in a TE_{10N} mode[19] as shown in Fig. 4.4 is given by

$$M = \frac{\ell^3 A K_c}{N^2 \lambda^2} \qquad (67)$$

where K_c represents the coupling coefficient between two adjacent resonant cavities m-1 and m. This coefficient is related[19] to the prototype elements of the filter by

$$K_c = \frac{\omega\lambda}{\sqrt{g_m g_{m+1}}}, \quad m = 2, 3, \ldots n \qquad (68)$$

If the coupled cavities of Fig. 4.4 are square, the polarizability of the coupling aperture is obtained by replacing A by a_1^2 in (67).

Thus

$$M \text{ (for square cavities)} = \frac{\ell^3 a_1^2 K_c}{N^2 \lambda^2} \qquad (69)$$

Similarly, for circular waveguide cavities A is replaced by $\frac{\pi D^2}{4}$ and M becomes

$$M(\text{for circular cavities}) = \frac{\ell^3 \pi D^2 K_c}{4N^2 \lambda^2} \qquad (70)$$

The final equations for the intercavity aperture susceptances

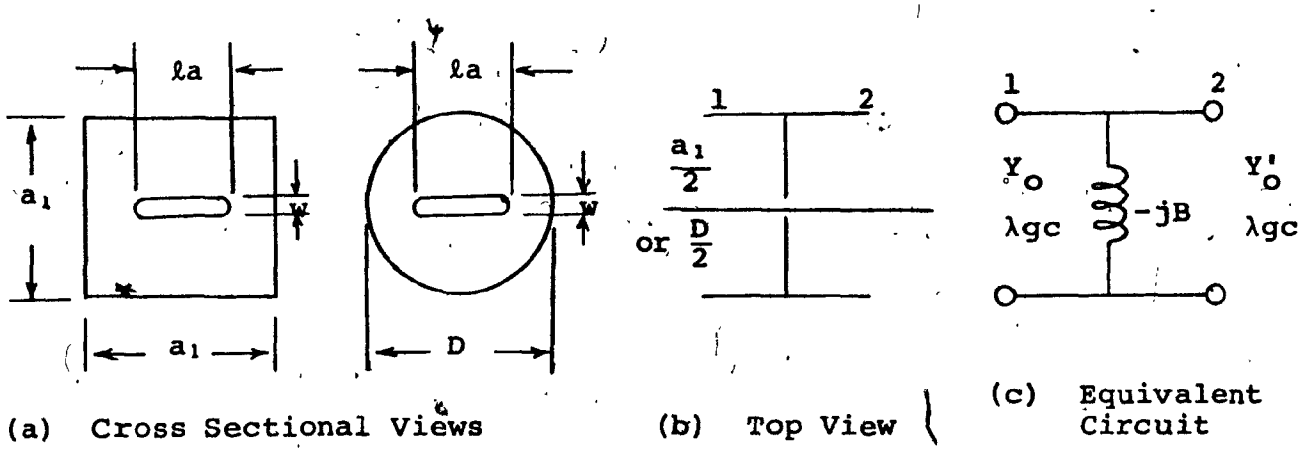

(a) Cross Sectional Views (b) Top View (c) Equivalent Circuit

Fig. 4.3 Aperture Coupling Between Two Square or Two Circular Guides of the Same Cross Section

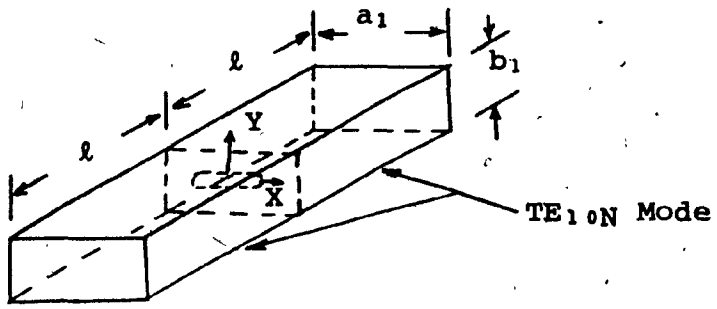

Fig. 4.4 Aperture Coupling of Two Rectangular Cavities

are obtained by combining (63) with (69) or (64) with (70) for square or circular cavities respectively.

Thus

$$\frac{B}{Y_o} \text{ (for } TE_{10N} \text{ mode)} = -\frac{N^2\lambda^2\lambda_{gc}}{4\pi\ell^3 K_c} \tag{71}$$

$$\text{and } \frac{B}{Y_o} \text{ (for } TE_{11N} \text{ mode)} = -\frac{3N^2\lambda^2\lambda_{gc}}{4\pi^2\ell^3 K_c} \tag{72}$$

From (71) and (72), it can be seen that the susceptances of the intercavity apertures are independent of a_1 and D, since the cavities have the same cross sections.

4.4 INTRACAVITY COUPLINGS IN DUAL MODE FILTERS

The intracavity coupling provided by the structural discontinuity of the 45^o coupling screw is determined by evaluating the coupling coefficient K_c from (68). Knowing this coefficient one can determine the screw penetration ℓ_p from a set of measurements of K_c versus ℓ_p.

These measurements are based on the fact that the Chebyshev response is overcoupled, and are obtained from tests[19] conducted on a single cavity two pole filter with known unloaded and external Q values. With reference to Fig. 4.5, the resonant modes of the dual mode cavity are adjusted using the frequency tuning screws for a symmetrical

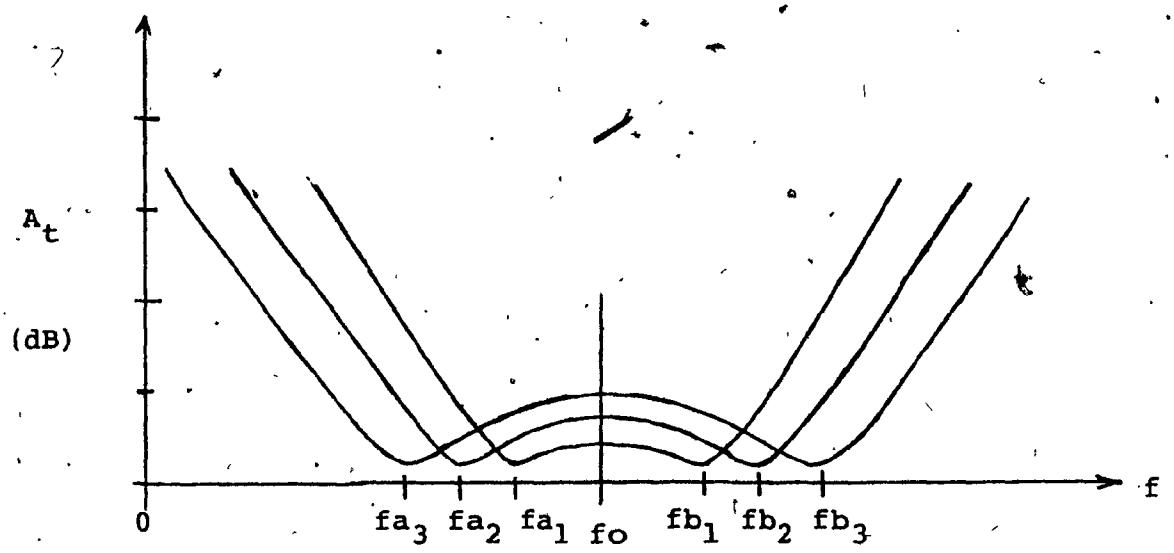

Fig. 4.5 Measurement of Intracavity Coupling in the Dual Mode Cavity

overcoupled response. Then, for different coupling screw penetrations, the set of responses shown on Fig. 4.5 are obtained.

The coupling coefficient corresponding to each of these responses is given by

$$K_c = \left(\omega_m^2 + \left(\frac{1}{Qe} + \frac{1}{Qu}\right)^2\right)^{1/2} \qquad (73)$$

where $\omega_m = \frac{fb-fa}{fo}$

Thus, knowing the desired value of K_c required to realize a Chebyshev filter, one can determine the penetration of the coupling screw by performing the above measurement. Typical graphs of K_c versus ℓ_p at 4 and 12 GHz are given in the next chapter. In practice any inaccuracies in determining ℓ_p are corrected by varying the coupling screw penetration during the tuning of the filter.

4.5 CAVITY LENGTH

The physical length of a single mode cavity which is resonating in TE_{10N} mode and coupled to adjacent cavities or guides through apertures of normalized susceptances[19] B_1/Y_o and B_2/Y_o as shown in Fig. 4.6(a) is given by

$$\ell = \left\{N\pi - \frac{1}{2}\left[\tan^{-1}\frac{2Y_o}{B_1} + \tan^{-1}\frac{2Y_o}{B_2}\right]\right\}\frac{\lambda_g c}{2\pi} \qquad (74)$$

From (74) it can be seen that the coupling apertures load the cavity and make its effective length shorter than $N\frac{\lambda_{gc}}{2}$, which is the length of a cavity coupled to a source through an infinitesimally small aperture.

In the case of the dual mode cavity (74) gives two ℓ's, corresponding to the susceptances B_1/Y_o and B_2/Y_o of the polarized apertures as shown in Fig. 4.6(b). Neglecting the weak loading of the cavity caused by the intracavity coupling, and assuming that $\frac{B_1}{Y_o} < \frac{B_2}{Y_o}$ the cavity length ℓ corresponding to the normalized susceptance $\frac{B_1}{Y_o}$ is given by

$$\ell = \left(N\pi - \frac{1}{2}\tan^{-1}\frac{2Y_o}{B_1}\right)\frac{\lambda_{gc}}{2\pi}. \qquad (75)$$

In practice this length is made 0.5% shorter to allow the cavity to resonate at a higher frequency than that required, and to facilitate the tuning of the filter using its tuning screws. This is necessary since tuning screws make the effective length of the cavity longer and shift the frequency of the filter down. Fig. 4.6(c) shows the relative penetration of the tuning screws T_1 and T_2 in the dual mode cavity. The cavity length corresponding to the normalized susceptance $\frac{B_2}{Y_o}$ is greater than that corresponding to $\frac{B_1}{Y_o}$.

The increase in cavity length can be achieved by an increase of the T_2 screw penetration.

The relative values of the coupling susceptances for the doubly terminated dual mode filter are shown in Fig. 4.7. These filters are symmetrical structures in the sense that $B_{o1} = B_{no}$, $B_{23} = B_{n-2,\ n-1}$, $B_{45} = B_{n-4,\ n-3}$, etc.

The physical length of each cavity is determined by using in (75) the susceptance corresponding to the aperture which is closer either to the input or to the output port of the filter.

The final values of B/Y_o and ℓ are then computed by obtaining estimate values of B/Y_o and, by using these values iteratively in (75), (61), (62), (71) and (72) to determine the final values of ℓ and B/Y_o. The approximate susceptance values are obtained by substituting $\ell \simeq N \frac{\lambda_{gc}}{2}$ in (61), (62), (71) and (72).

The approximate end aperture susceptances are:

$$\frac{B}{Y_o} \text{ (for } TE_{10N} \text{ mode)} = -\sqrt{\frac{2Q_e\lambda^2\lambda_g ab}{\pi N\lambda_{gc}^3 a^2}} \qquad (76)$$

and

$$\frac{B}{Y_o} \text{ (for } TE_{11N} \text{ mode)} = -\sqrt{\frac{8Q_e\lambda^2\lambda_g ab}{\pi^2 N\lambda_{gc}^3 D^2}} \qquad (77)$$

Similarly, for the intercavity apertures:

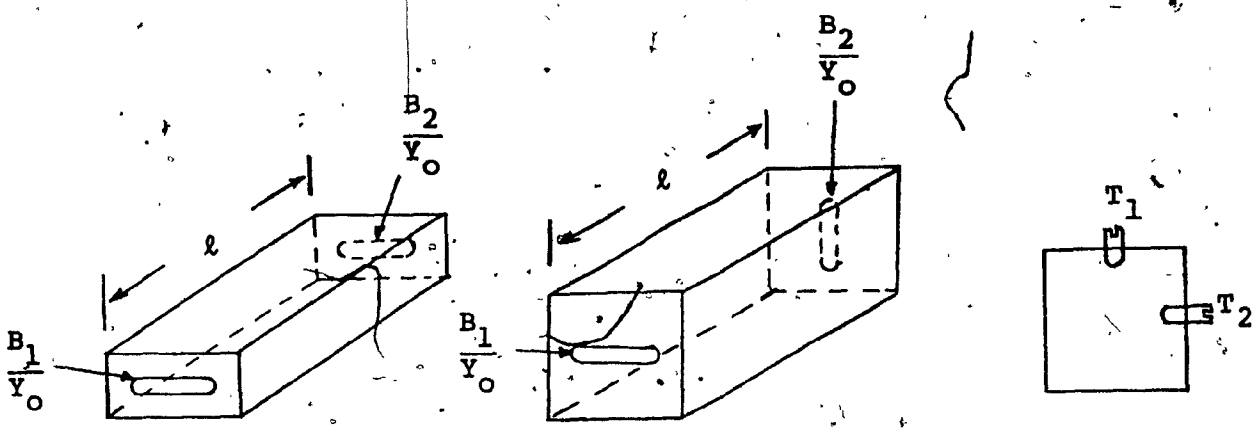

(a) Single Mode Cavity (b) Dual Mode Cavity (c) Tuning Screw Penetration

Fig. 4.6 Aperture Loading of Single and Dual Mode Cavities

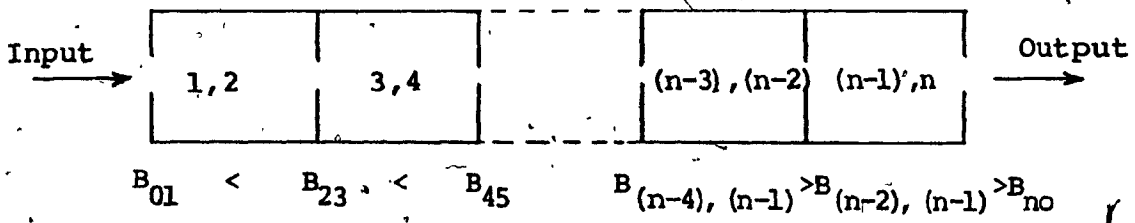

Fig. 4.7 Relative Values of Coupling Susceptances for the Doubly Terminated Dual Mode Filter

$$\frac{B}{Y_o} \text{ (for } TE_{10N} \text{ mode)} = -\frac{2\lambda^2}{\pi N \lambda_g c^2 K_c} \qquad (78)$$

and

$$\frac{B}{Y_o} \text{ (for } TE_{11N} \text{ mode)} = -\frac{6\lambda^2}{\pi^2 N \lambda_g c^2 K_c} \qquad (79)$$

From the above relations it can be seen that in higher order mode filters the end and intercavity susceptances are related to the corresponding susceptances of dominant mode filters by $\frac{1}{\sqrt{N}}$ and $\frac{1}{N}$ respectively. Since lower susceptance values correspond to larger apertures the above factors make the TE_{10N} and TE_{11N} filters less sensitive to aperture dimensions.

4.6 THE THEORETICAL UNLOADED Q

The theoretical unloaded Q of the dual mode filter is the average Q of the physical cavities employed by the filter.

The unloaded Q of a square cavity[20] supporting the TE_{10N} mode is given by

$$Qu = \frac{\lambda}{\delta} \frac{a_1 \ell}{2} \frac{(P^2+r^2)^{3/2}}{3P^2\ell + r^2(\ell+2\alpha_1)} \qquad (80)$$

where δ is the skin depth, $P = \frac{1}{\alpha_1}$ and $r = \frac{N}{\ell}$.

Similarly the unloaded Q of a cylindrical cavity[20] operating in TE_{11N} mode is given by

$$Qu = \frac{\lambda}{\delta} \frac{\left[\lambda - \left[\frac{1}{1.841}\right]^2\right]\left[1.841^2 + P^2R^2\right]^{3/2}}{2\pi\left[1.841^2 + P^2R^3 + (1-R)\left[\frac{PR}{1.841}\right]^2\right]} \quad (81)$$

where $P = \frac{N\pi}{2}$ and $R = \frac{D}{\ell}$.

Equations (80) and (81) are represented graphically in Fig. 4.8 where the $\frac{Q\delta}{\lambda}$ values are plotted for several values of N as a function of $\frac{a_1}{\ell}$ for the square cavity and $\frac{D}{\ell}$ for the cylindrical cavity. From this figure we see that dominant mode filters have optimum Q's for $\frac{a_1}{\ell}$ or $\frac{D}{\ell} \simeq 1$, while for higher order mode filters the unloaded cavity Q gradually increases with $\frac{a_1}{\ell}$ or $\frac{D}{\ell}$.

4.7 SELECTION OF GEOMETRICAL PARAMETERS FOR THE DUAL MODE CAVITY

The dimensions a_1 or D of the dual mode cavity must be chosen in such a way that the spurious passbands caused by the unwanted modes supported by the cavities occur as far as possible from the band of interest, while still maintaining a near optimum unloaded Q.

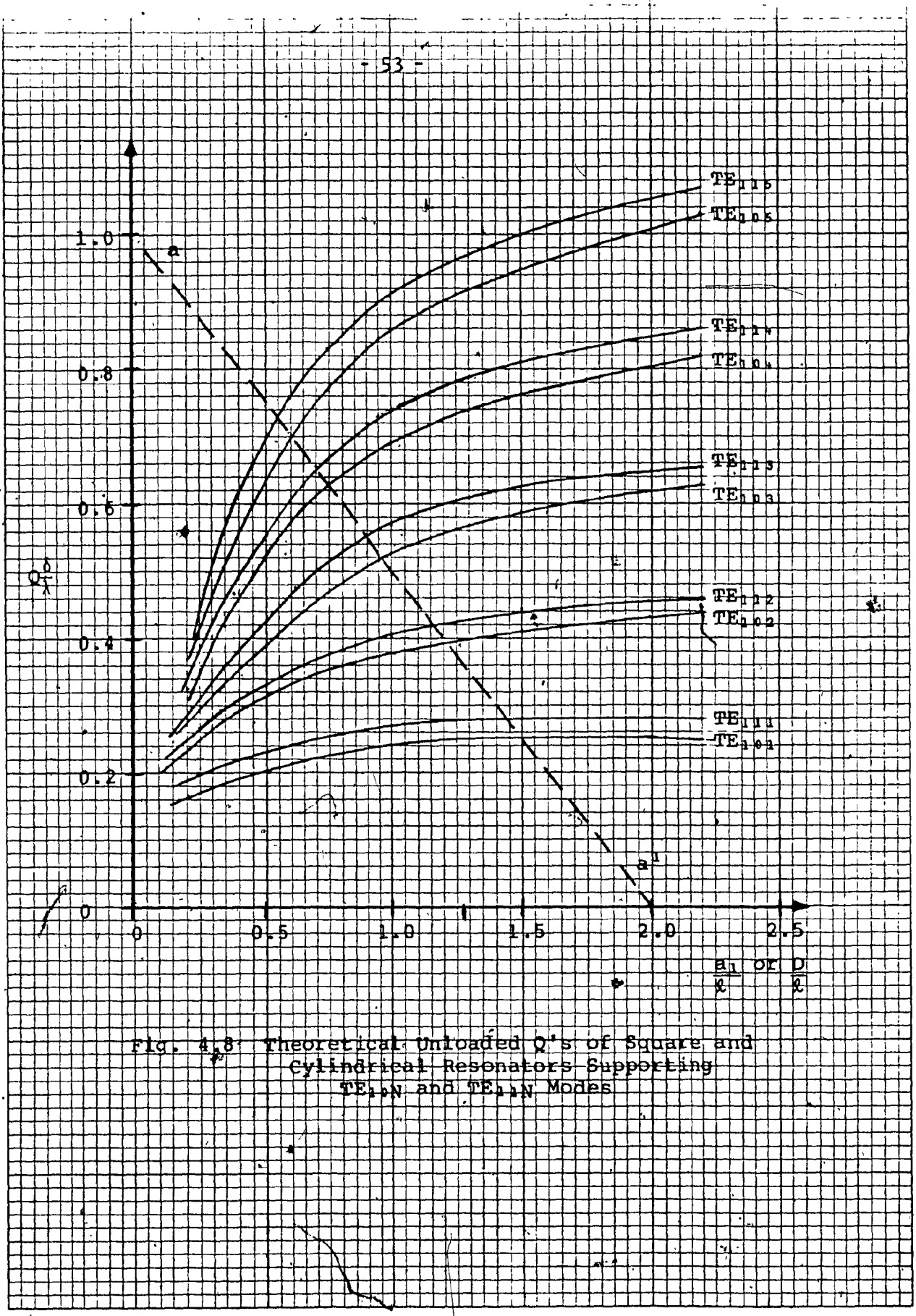

Fig. 4.8 Theoretical Unloaded Q's of Square and Cylindrical Resonators Supporting $TE_{1,0,N}$ and $TE_{2,1,N}$ Modes

In order to obtain a band free from spurious transmissions, one must select the proper $\frac{a_1}{\ell}$ or $\frac{D}{\ell}$ ratio for the cavity and for the operating mode. To aid this selection mode charts as shown in Figs. 4.9 and 4.10 are used for square or cylindrical resonators respectively. With these charts the spurious free operating ranges or "mode windows" and the frequencies of the spurious passbands are determined. Examples of the mode windows for the modes TE_{101}/TE_{111}, TE_{102}/TE_{112} and TE_{103}/TE_{113} are shown by the shaded areas in Figs. 4.9 and 4.10.

From the mode charts and the unloaded Q curves of Fig. 4.8, we see that dominant mode filters can be designed to operate on optimum $\frac{a_1}{\ell}$ or $\frac{D}{\ell}$ ratios. But for higher order mode filters, the above ratios can vary according to the spurious specifications required by the filter. Practical values of the $\frac{a_1}{\ell}$ or $\frac{D}{\ell}$ ratios for the modes with indices N = 1, 2, 3, 4 and 5 are on the left of the dotted line a-a' of Fig. 4.8, because in practice it is difficult to find mode windows with higher ratios. Once A or D is selected, the length of the cavity is obtained using the previously described procedure.

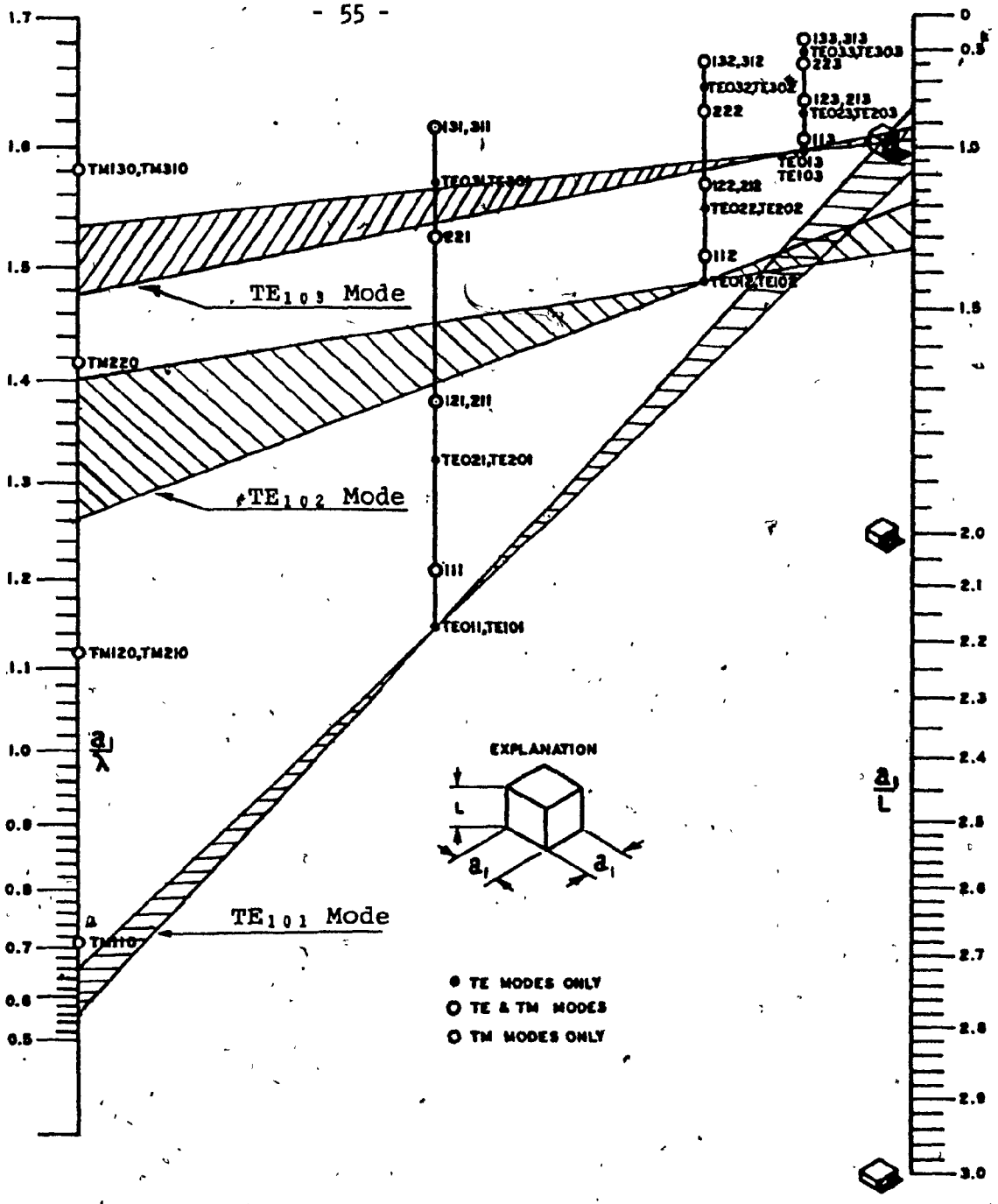

Reprinted from Mode Lattice for Square Prism Resonators, R. N. Bracewell, Proceedings of the IRE, Aug., 1947.

Fig. 4.9 Mode Chart of Square Cavity Resonators

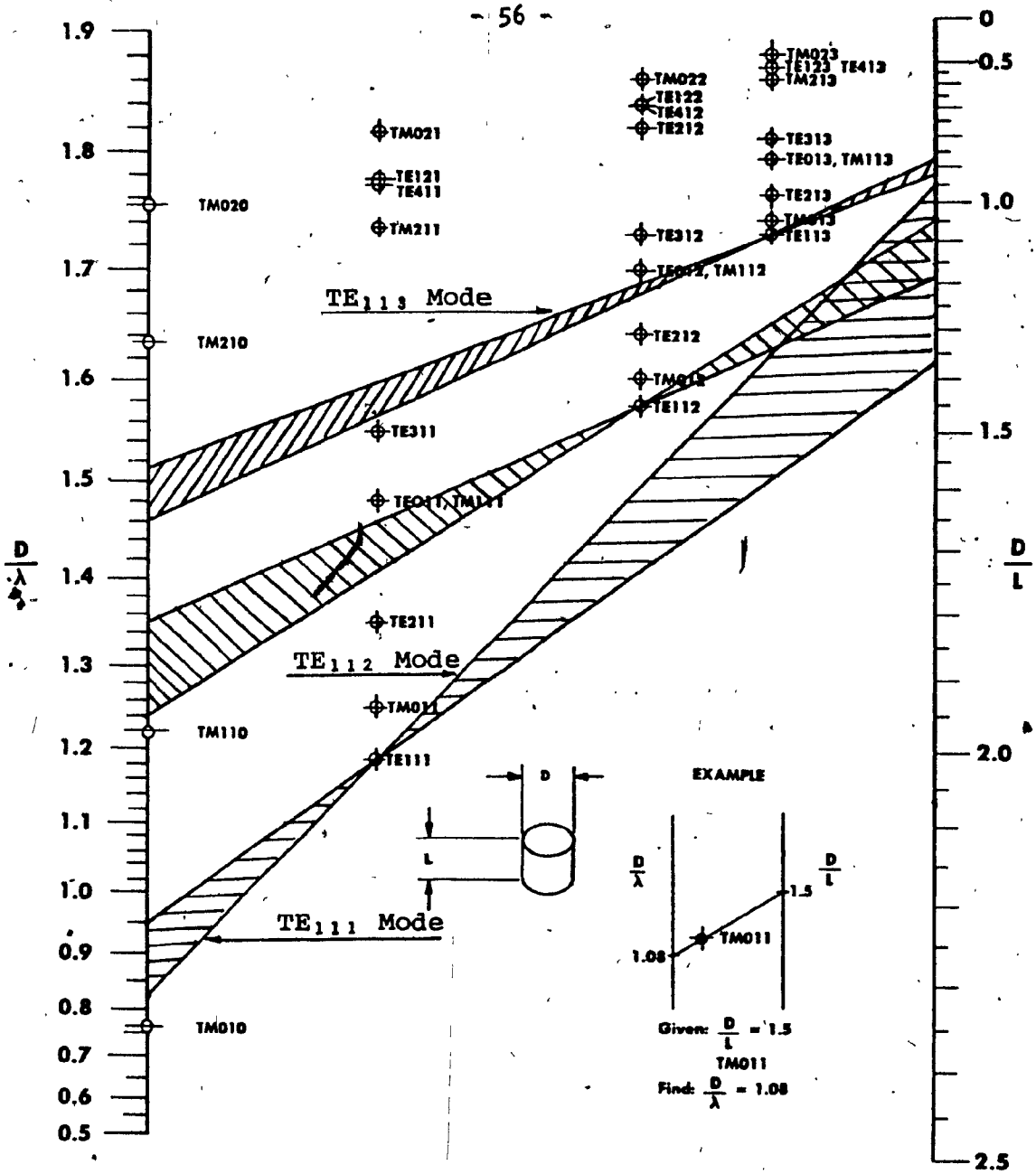

Reprinted from Charts for Resonant Frequencies of Cavities, R. N. Bracewell, Proc. of the IRE, Aug. 1947.

Fig. 4.10 Mode Chart of Cylindrical Cavity Resonators

4.8 MEASURED UNLOADED Q'S OF DUAL MODE FILTERS

The realized unloaded Q of the dual mode filter is computed[5], by measuring its centre frequency insertion loss and apply

$$Qu = \frac{4.343\ fo \sum_{m=1}^{n} g_m}{BW\ A_o} \quad (82)$$

where $\sum_{m=1}^{n} g_m$ represents the summation of the LP prototype elements of the filter. Table 4.1 gives the sums of these elements for Chebyshev filters of order 3 to 9 and for different return loss levels A_r. The $\sum_{m=1}^{n} g_m$ elements of filters with any return loss in the range of 16 to 40 dB are obtained by interpolating between the values of Table 4.1.

The ratio of the measured and theoretical unloaded Q's of the filter gives the unloaded Q efficiency η. In microwave dual mode filters η is a measure of the surface roughness, the quality of plating, the screw penetration, the electrical contact between adjacent cavities, and in general the manufacturing quality of the filter.

4.9 APERTURE DIMENSIONS IN DUAL MODE FILTERS

A conventional method for determining the dimensions of the apertures for the dual mode filter is to employ Cohn's technique[21]. According to this technique the computed

TABLE 4.1

SUMS OF g_m ELEMENTS FOR CHEBYSHEV FILTERS WITH n = 3, 4, 5 ... 9 AND A_r = 16, 20, 26, 34, 40 dB

n	A_r=16 dB	A_r=20 dB	A_r=26 dB	A_r=34 dB	A_r=40 dB
3	2.2636	2.8109	2.2600	1.6862	1.3492
4	5.0590	4.5687	3.9207	3.1782	2.7031
5	7.0789	6.4942	5.7443	4.8752	4.2985
6	8.9761	8.3964	7.6201	6.6800	6.0339
7	11.0511	10.3974	9.5586	8.5538	7.8559
8	12.9738	12.3397	11.4985	10.4630	9.7299
9	15.9672	14.3655	13.4763	12.4017	11.6398

polarizabilities of given apertures are first corrected for the length and finite thickness of the slots and then plotted versus slot dimensions. Next, from (59), (60), (69) and (70), the required polarizabilities necessary to realize a certain filter are computed and the above plots are used to determine the aperture dimensions.

In the case of high frequency narrow band microwave filters, the above technique is inaccurate because:

(a) The small diffraction theory of Bethe does not predict accurately the polarizabilities of long thin slots, and

(b) The correction formula uses an empirical constant which varies with frequency within the band of interest.

Alternatively, a simple and accurate approach for determining the aperture dimensions is through susceptance measurements of given slots. Such an approach has advantages because it takes into account automatically the thickness and length corrections. The aperture susceptance is obtained by measuring either the VSWR or the transmission loss of the slot and apply

$$\left|\frac{B}{Y_o}\right| = \frac{VSWR - 1}{\sqrt{VSWR}} = 2\sqrt{10^{\frac{At}{10}} - 1} \qquad (83)$$

This measurement is effected by placing coupling disks with slots of constant width and variable length between two square or circular guides which carry dominant mode. For filters with fractional bandwidths less than 1% where large values of susceptances are required, the transmission loss measurements provide more accuracy, since it is difficult to measure accurately large VSWR values. The coupling disks are assumed lossless.

In the design of higher order mode filters, the measured susceptances are scaled by $\frac{1}{\sqrt{N}}$ for the end apertures and by $\frac{1}{N}$ for the intercavity apertures. Plots of measured susceptances versus slot dimensions are shown in the next chapter.

CHAPTER V

EXPERIMENTAL FILTER DESIGN AND MEASUREMENT RESULTS

5.1 COMPUTER PROGRAMS

The amplitude and phase equations of the first chapter and the design equations of the third chapter are compiled in two computer programs.

The first program deals with the design of the filter. The inputs are: n, A_r, BW, fo, a_1 or D, a, b and N. The computer output prints the design parameters of the filter, its intercavity coupling coefficients K_c, the normalized susceptances of its apertures $\left|\frac{B}{Y_o}\right|$, and the length of the cavities. Since the program designs dual mode filters, only even order is considered.

The second program computes the amplitude, phase, and group delay response of Chebyshev filters. The inputs to this program are: n, A_r, BW, fo, Qu and the lowest, highest and total frequency print out points fℓ, fh and Np. The computer output prints either the transmission or the reflection amplitude and phase characteristics for every specified frequency point Np. These characteristics are: $A(\omega)$, $A_i(\omega)$, $\frac{dA}{d\omega}$, $\phi(\omega)$, $T(\omega)$ and $\frac{dT}{d\omega}$.

The above computer programs are described in terms of their flow charts in Appendix B. The maximum number of poles that can be handled by these programs is 12.

5.2 EXPERIMENTAL FILTER DESIGNS

Three dual mode Chebyshev filters were designed, fabricated and evaluated. These filters are:

(a) 4 GHz, 8 pole TE_{111} mode filter

(b) 12 GHz, 6 pole TE_{111} mode filter, and

(c) 12 GHz, 6 pole TE_{103} mode filter.

The design parameters, coupling elements, and dimensions of the above filters are listed in the computer outputs of the design program shown in tables 5.1 to 5.3. The aperture dimensions are obtained from the $\left|\frac{B}{Y_o}\right|$ versus aperture length (ℓa) graphs of Figs. 5.1 to 5.3 as described in Section 4.9.

Similarly, the penetration lengths (ℓp) of the intracavity coupling screws are determined from the K_c versus ℓp plots of Figs. 5.4 to 5.6. These plots are determined from single cavity tests as described in Section 4.4.

Photographs of the three experimental filters are shown in Figs. 5.7, 5.12 and 5.16. From these photographs it can be seen that the 4 GHz filter has negative cross couplings, while the 12 GHz filters have positive cross

TABLE 5.1

DESIGN PARAMETERS AND DIMENSIONS OF

4 GHz TE_{111} EXPERIMENTAL FILTER

========== INPUT DATA ==========

TYPE OF FILTER:	CHEBYSHEV		
ARITHMETIC CENTER OF PASSBAND:	(FO)	3960.00	MHZ.
BANDWIDTH:	(BW)	38.00	MHZ.
PASSBAND RETURN LOSS:	(RL)	-26.00	DBS.
NUMBER OF SECTIONS	(N)	8	
WIDTH OF INTERFACING W/G	(A)	2.290	INCH.
HEIGHT OF INTERFACING W/G	(B)	1.145	INCH.
THIRD INDEX OF MODE	(NN)	1	
CYLINDRICAL CAVITY (DIAMETER)	(D)	2.120	INCH.

========== INTERMEDIATE DESIGN DATA ==========

DESIGN CENTER OF PASSBAND:	(FR)	3959.62	MHZ.
CAVITY CUTOFF FREQUENCY:	(FC)	3263.41	MHZ.
CAVITY GUIDE WAVELENGTH AT FR	(CWL)	5.263	INCH.
INTERFACING GUIDE WAVELENGTH	(RGWL)	3.925	INCH.

========== THE FILTER ELEMENTS ARE ==========

INTERCAVITY COUPLINGS		INTRACAVITY COUPLINGS		CAVITY LENGTH (inch)
Aperture Susceptances $\lvert B/Y_o \rvert$	Length of Apertures ℓa (inch)	Coupling Coefficients K_c	Length of Coupling Screws (inch)	
3.582	1.057			
		0.00891	0.210	2.418
33.345	0.842			
		0.00552	0.132	2.593
37.046	0.820			
		0.00552	0.132	2.593
33.345	0.842			
		0.00891	0.210	2.418
3.582	1.057			

TABLE 5.2

DESIGN PARAMETERS AND DIMENSIONS OF

12 GHz TE_{111} EXPERIMENTAL FILTER

========== INPUT DATA ==========

TYPE OF FILTER:	CHEBYSHEV		
ARITHMETIC CENTER OF PASSBAND:	(FO)	12000.00	MHZ.
BANDWIDTH:	(BW)	80.00	MHZ.
PASSBAND RETURN LOSS:	(RL)	-26.00	DBS.
NUMBER OF SECTIONS	(N)	6	
WIDTH OF INTERFACING W/G	(A)	.750	INCH.
HEIGHT OF INTERFACING W/G	(B)	.375	INCH.
THIRD INDEX OF MODE	(NN)	1	
CYLINDRICAL CAVITY (DIAMETER)	(D)	.780	INCH.

========== INTERMEDIATE DESIGN DATA ==========

DESIGN CENTER OF PASSBAND:	(FR)	11999.63	MHZ.
CAVITY CUTOFF FREQUENCY:	(FC)	8869.79	MHZ.
CAVITY GUIDE WAVELENGTH AT FR	(CWL)	1.460	INCH.
INTERFACING GUIDE WAVELENGTH	(RGWL)	1.303	INCH.

========== THE FILTER ELEMENTS ARE ==========

INTERCAVITY COUPLINGS		INTRACAVITY COUPLINGS		CAVITY LENGTH (inch)
Aperture Susceptances $\lvert B/Y_o \rvert$	Length of Apertures ℓa (inch)	Coupling Coefficients K_c	Length of Coupling Screws (inch)	
4.733	0.374			
		0.00641	0.141	0.684
63.975	0.273			
		0.00412	0.084	0.723
63.975	0.273			
		0.00641	0.141	0.684
4.733	0.374			

TABLE 5.3

DESIGN PARAMETERS AND DIMENSIONS OF

12 GHz TE_{103} EXPERIMENTAL FILTER

========== INPUT DATA ==========

TYPE OF FILTER:	CHEBYSHEV		
ARITHMETIC CENTER OF PASSBAND:	(FO)	11900.00	MHZ.
BANDWIDTH:	(BW)	38.00	MHZ.
PASSBAND RETURN LOSS:	(RL)	-26.00	DBS.
NUMBER OF SECTIONS	(N)	6	
WIDTH OF INTERFACING W/G	(A)	.750	INCH.
HEIGHT OF INTERFACING W/G	(B)	.375	INCH.
THIRD INDEX OF MODE	(NN)	3	
SQUARE CAVITY (SIZE)	(S)	.900	INCH.

========== INTERMEDIATE DESIGN DATA ==========

DESIGN CENTER OF PASSBAND:	(FR)	11899.95	MHZ.
CAVITY CUTOFF FREQUENCY:	(FC)	6557.14	MHZ.
CAVITY GUIDE WAVELENGTH AT FR	(CWL)	1.189	INCH.
INTERFACING GUIDE WAVELENGTH	(RGWL)	1.322	INCH.

========== THE FILTER ELEMENTS ARE ==========

INTERCAVITY COUPLINGS		INTRACAVITY COUPLINGS		CAVITY LENGTH (inch)
Aperture Susceptances $\lvert B/Y_o \rvert$	Length Apertures La (inch)	Coupling Coefficients K_c	Length of Coupling Screws (inch)	
3.913	0.384			
		0.00307	0.108	1.738
70.815	0.248			
		0.00197	0.041	1.771
70.815	0.248			
		0.00307	0.108	1.738
3.913	0.384			

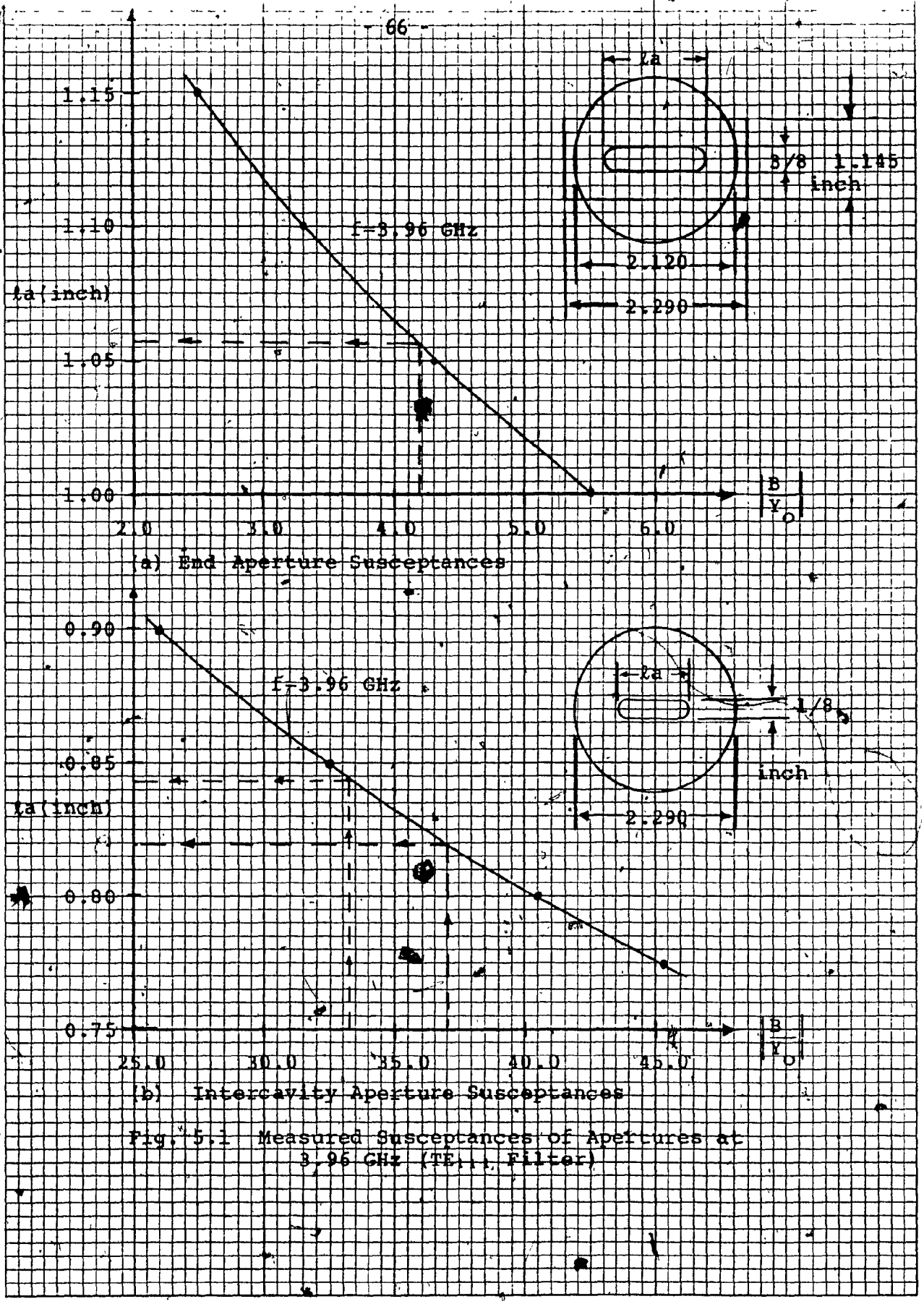

(a) End Aperture Susceptances

(b) Intercavity Aperture Susceptances

Fig. 5.1 Measured Susceptances of Apertures at 3.96 GHz (TE_{11} Filter)

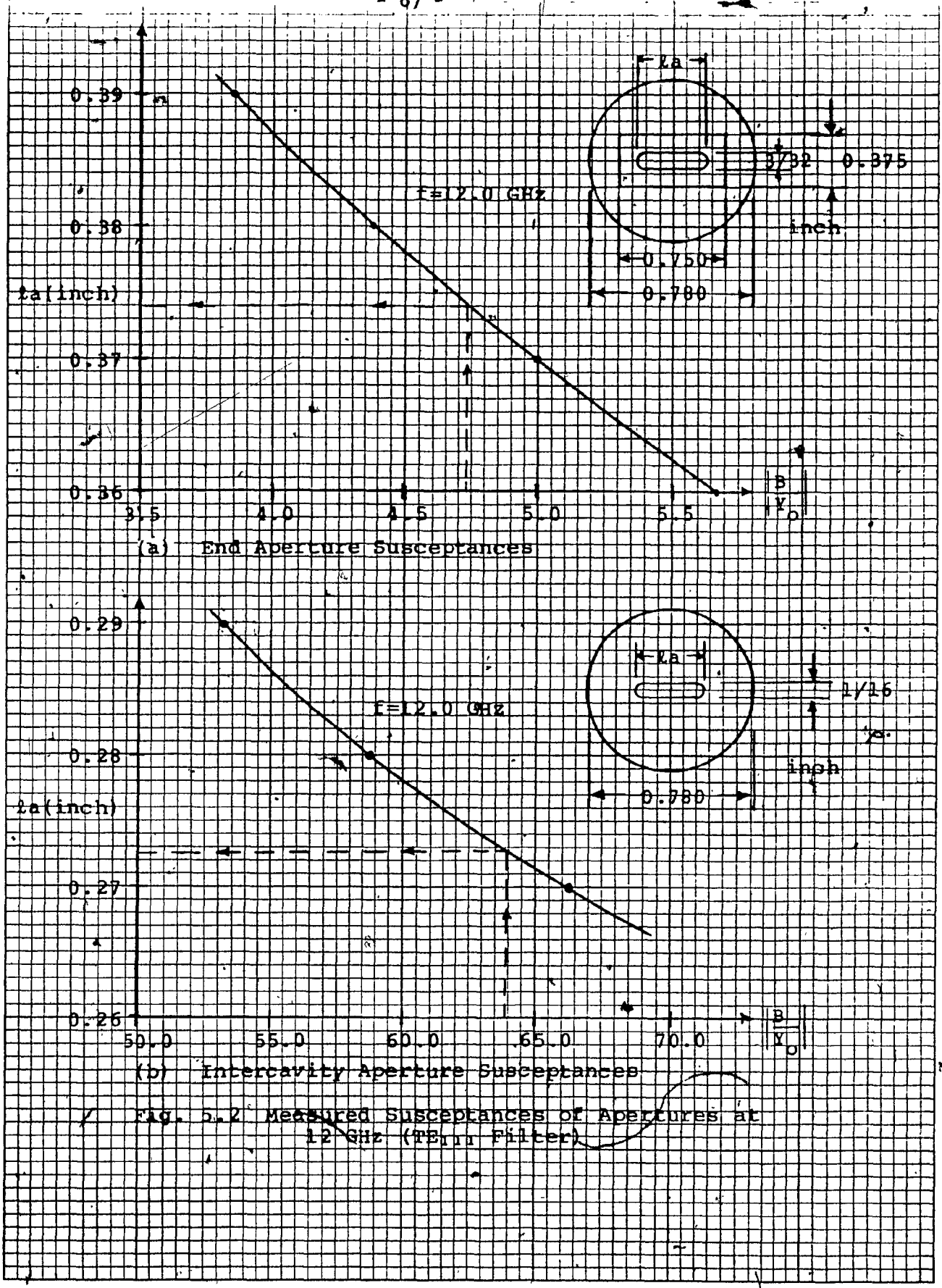

(a) End Aperture Susceptances

(b) Intercavity Aperture Susceptances

Fig. 5.2 Measured Susceptances of Apertures at 12 GHz (TE_{111} Filter)

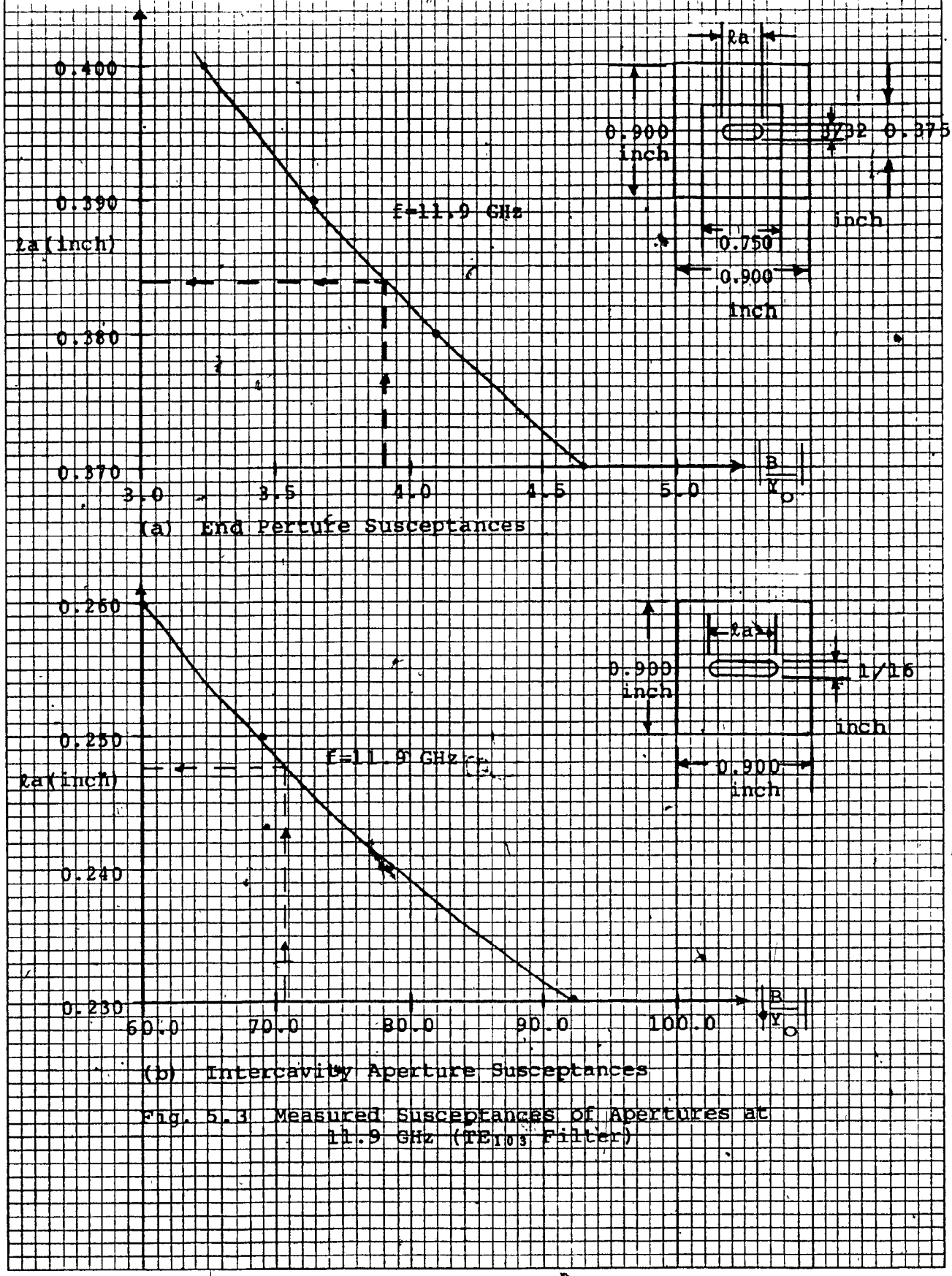

(a) End Perture Susceptances

(b) Intercavity Aperture Susceptances

Fig. 5.3 Measured Susceptances of Apertures at 11.9 GHz (TE_{103} Filter)

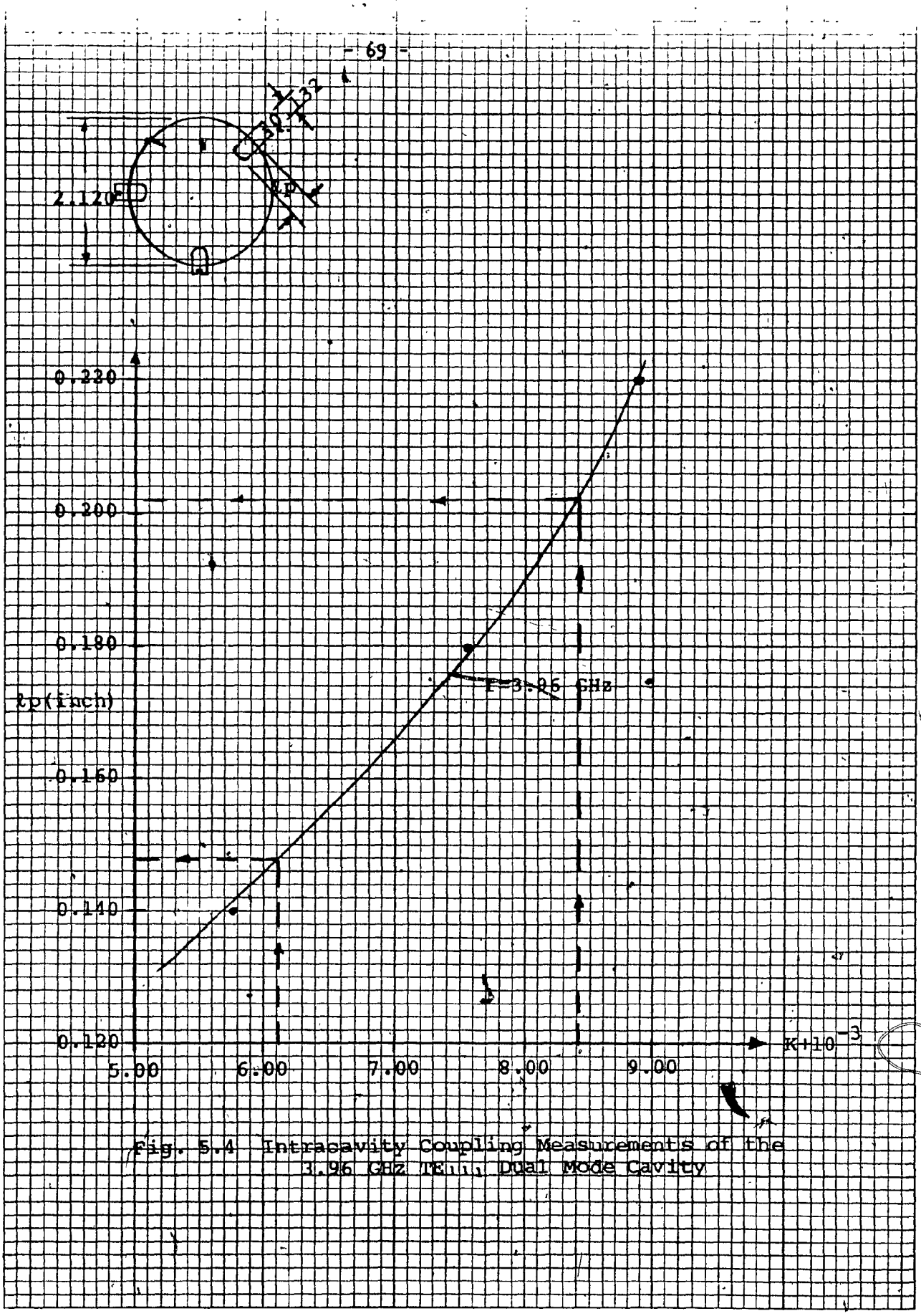

Fig. 5.4 Intracavity Coupling Measurements of the 3.96 GHz TE_{111} Dual Mode Cavity

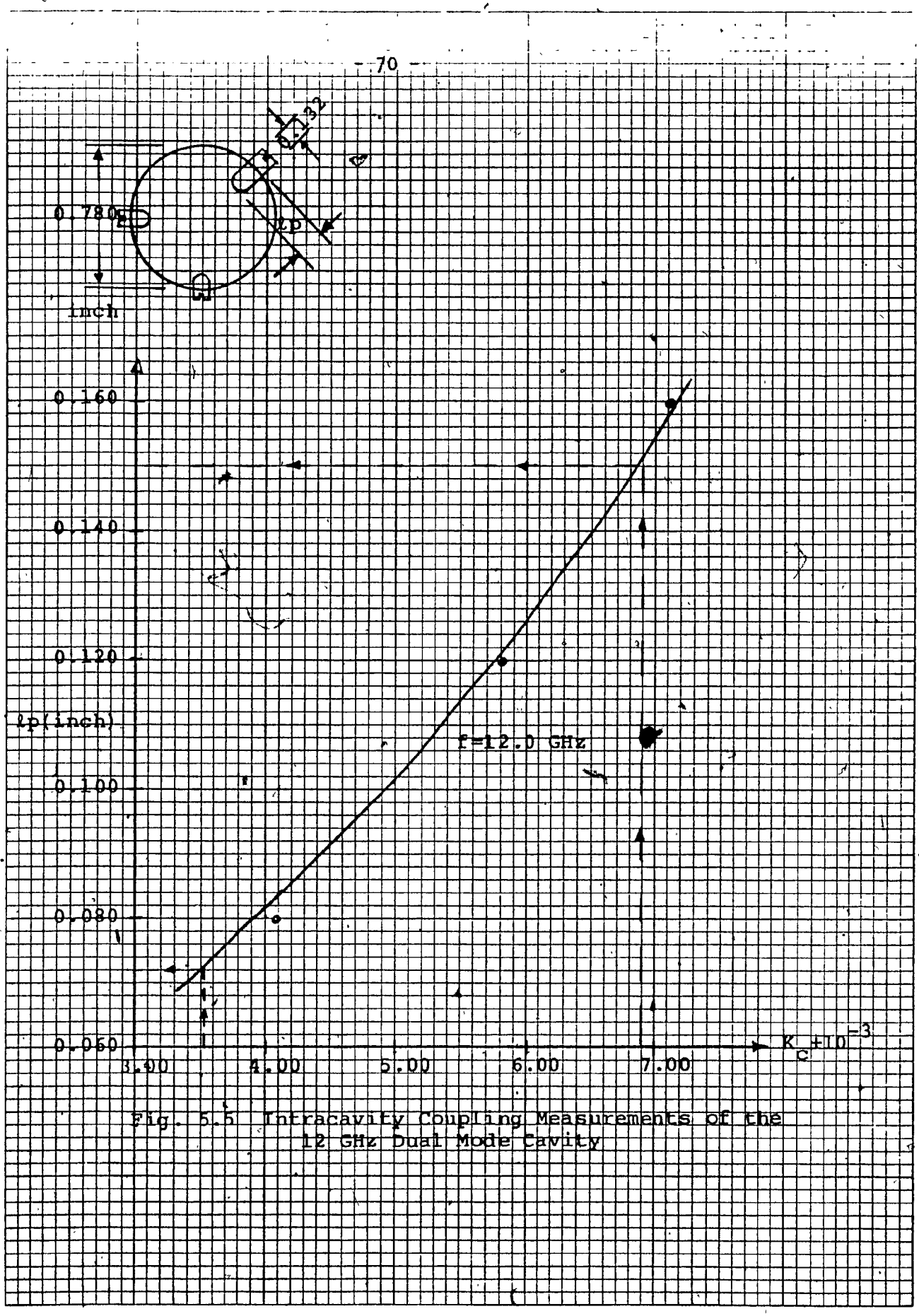

Fig. 5.5 Intracavity Coupling Measurements of the 12 GHz Dual Mode Cavity

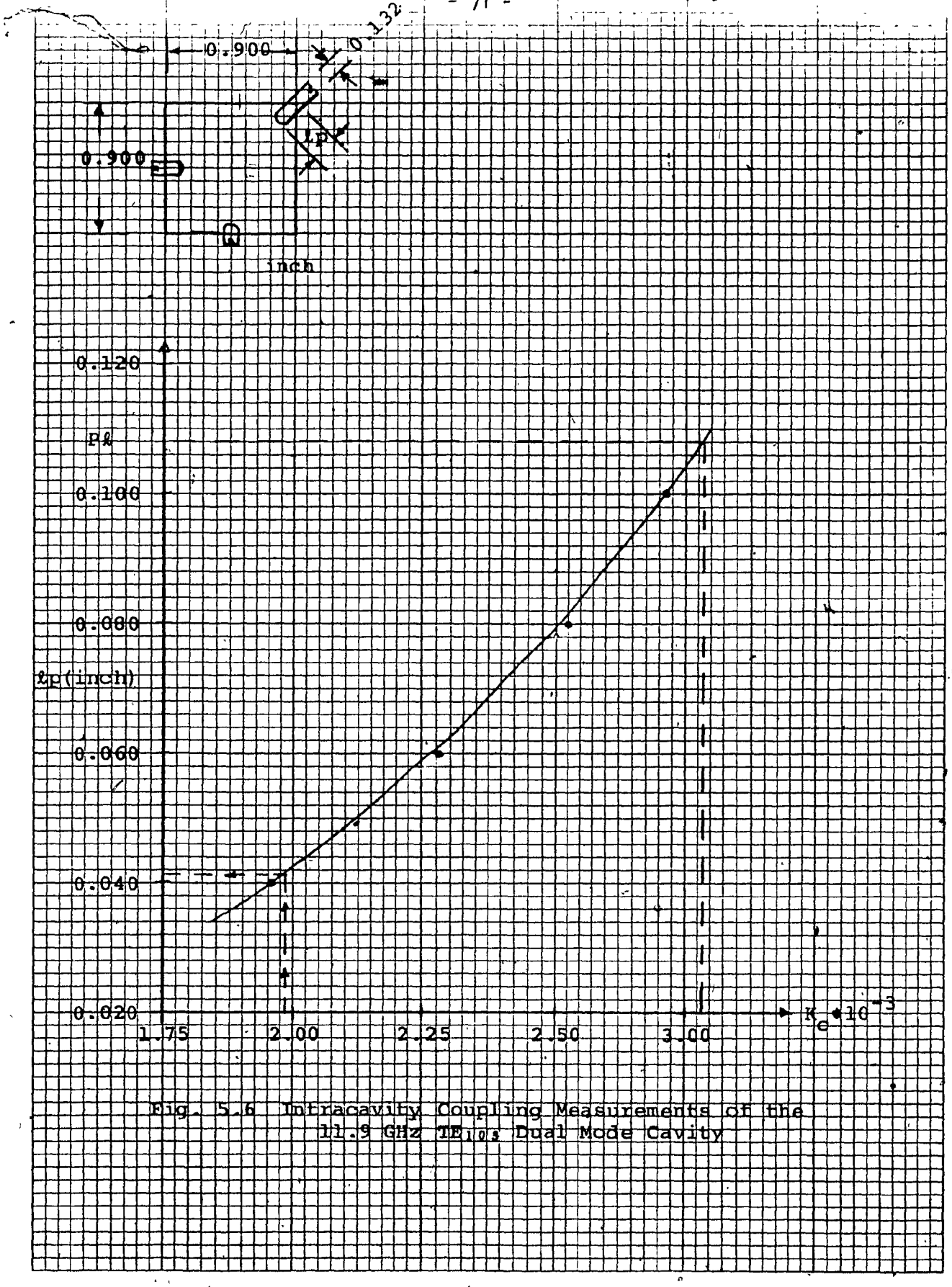

Fig. 5.6 Intracavity Coupling Measurements of the 11.9 GHz TE_{10s} Dual Mode Cavity

couplings. The physical cavities of the experimental filters are formed by placing coupling disks of 0.025 inch thickness between cylindrical or square waveguide sections as shown in the photographs.

5.3 COMPARISON OF DESIGNED AND MEASURED PARAMETERS

The designed and measured parameters fo, BW and A_r of the three experimental filters are given in Table 5.4.

From Table 5.4, it can be seen that the measured bandwidth of the 4 GHz filter is 1 MHz narrower than its design bandwidth. This is due to the width of the intercavity apertures which are made effectively smaller by the negative cross couplings employed by the filter. Such reduction in the bandwidth is corrected by increasing the length of the intercavity apertures by approximately 0.003 inch.

The measured parameters of the 12 GHz TE_{111} mode filter are also different from the design parameters. The larger bandwidth is due to the positive cross couplings which make the effective length of the intercavity apertures larger than its physical length. A reduction of the length of the intercavity apertures by about 0.002 inch will reduce the measured bandwidth to 80 MHz.

The increased level of the measured return loss is caused by incorrect end aperture lengths (approximately

TABLE 5.4

DESIGNED AND MEASURED PARAMETERS OF EXPERIMENTAL FILTERS

TYPE OF FILTER	DESIGN PARAMETERS			MEASURED PARAMETERS		
	fo(MHz)	BW(MHz)	A_r(dB)	fo(MHz)	BW(MHz)	A_r(dB)
4 GHz TE_{111}	3960	38.0	26.0	3960	37.0	26.0
12 GHz TE_{111}	12000	80.0	26.0	12002	83.0	26.6
12 GHz TE_{103}	11900	38.0	26.0	11900	38.0	26.0

0.002 inch error), due to errors in the susceptance measurements of the end apertures. Finally, the centre frequency of the filter can be shifted 2 MHz to the left by a uniform increase of the tuning screw penetrations.

The measured parameters of the 12 GHz TE_{103} filter are the same as its design parameters because this filter is less sensitive to the aperture dimensions since it is operating in a higher order mode. Further, in this filter the required corrections were applied prior to tuning.

Measured results of the passband return loss, relative group delay, and passband insertion loss of the experimental filters are shown in Figs. 5.8 to 5.11 for the 4 GHz filter, 5.13 to 5.15 for the 12 GHz TE_{111} filter and 5.17 to 5.20 for the TE_{103} filter.

5.4 COMPARISON OF COMPUTED AND MEASURED AMPLITUDE AND GROUP DELAY CHARACTERISTICS

The computed transmission characteristics of the experimental filters are obtained from the computer outputs of the second program which are given in the appendix. For comparison purposes, these results are also presented together with the measured ones.

From the amplitude and group delay responses shown in Figs. 5.9 to 5.11, 5.13 to 5.15 and 5.18 to 5.20, it is observed that there is close correlation between the computed

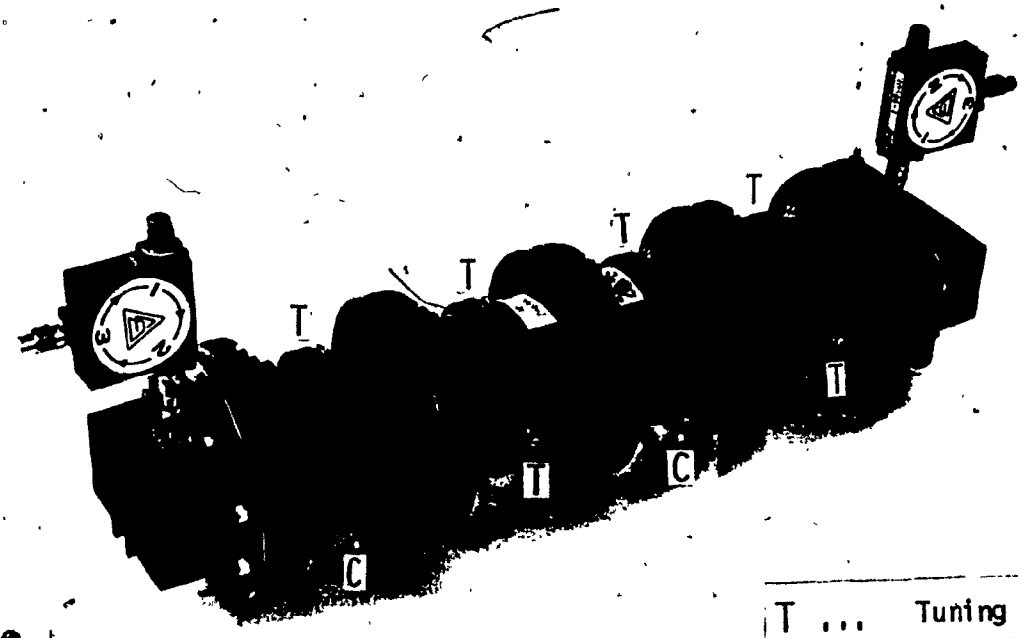

Fig. 5.7 Photograph of the 4 GHz, 8 Pole TE_{111} Dual Mode Experimental Filter.

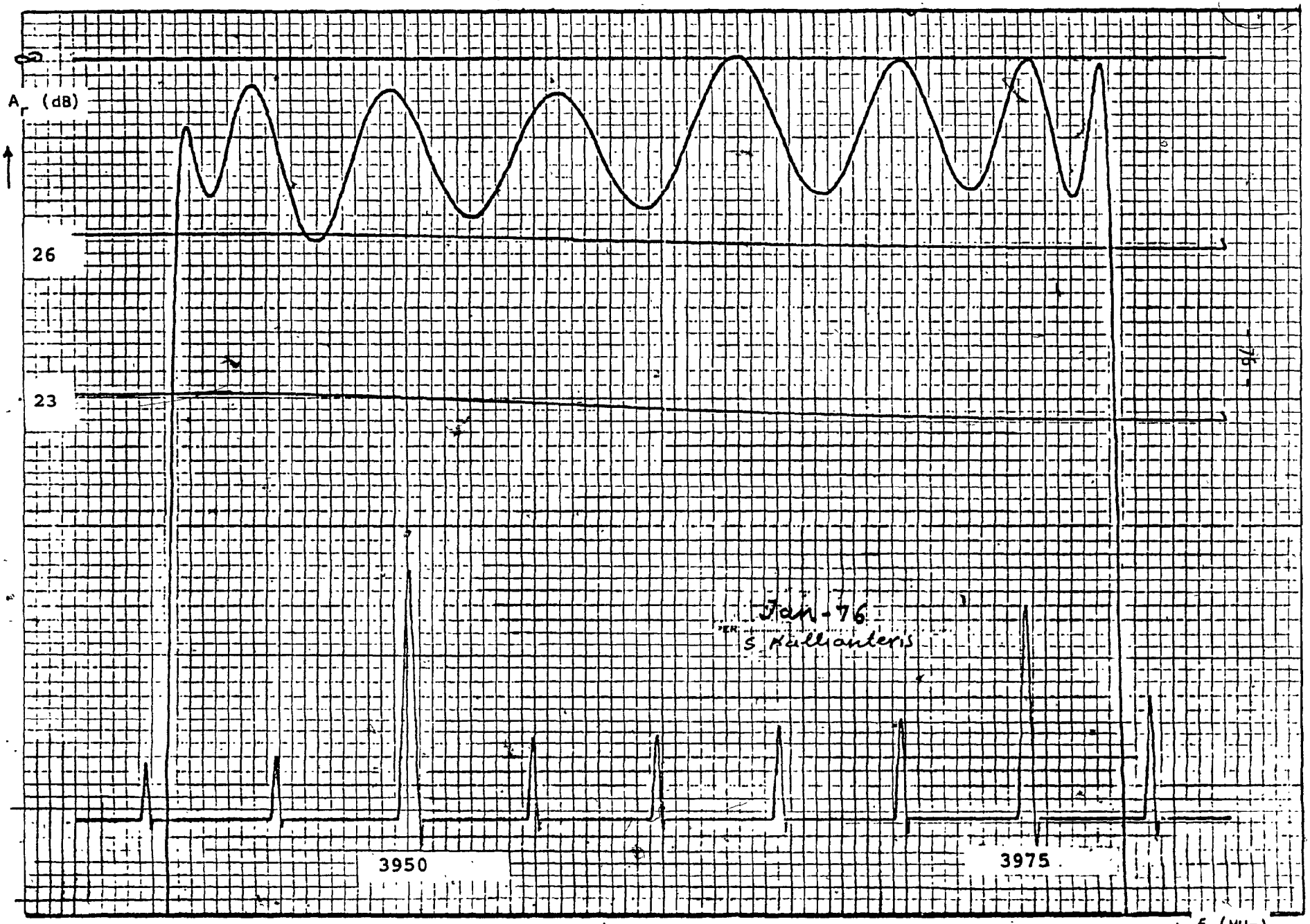

Fig. 5.8 Passband return loss of 4 GHz TE_{111} filter.

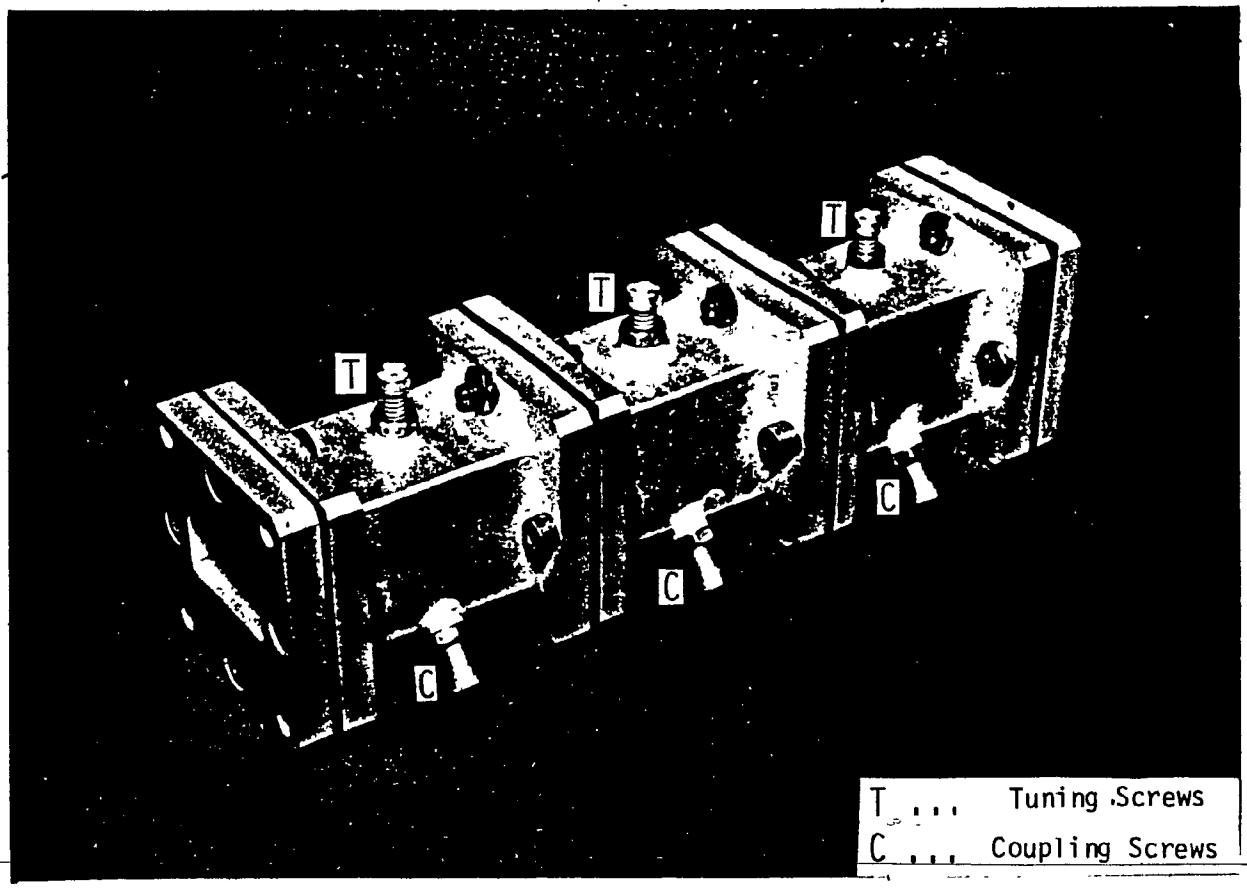

Fig. 5.16 Photograph of the 12 GHz, 6 Pole TE_{103} Dual Mode Experimental Filter.

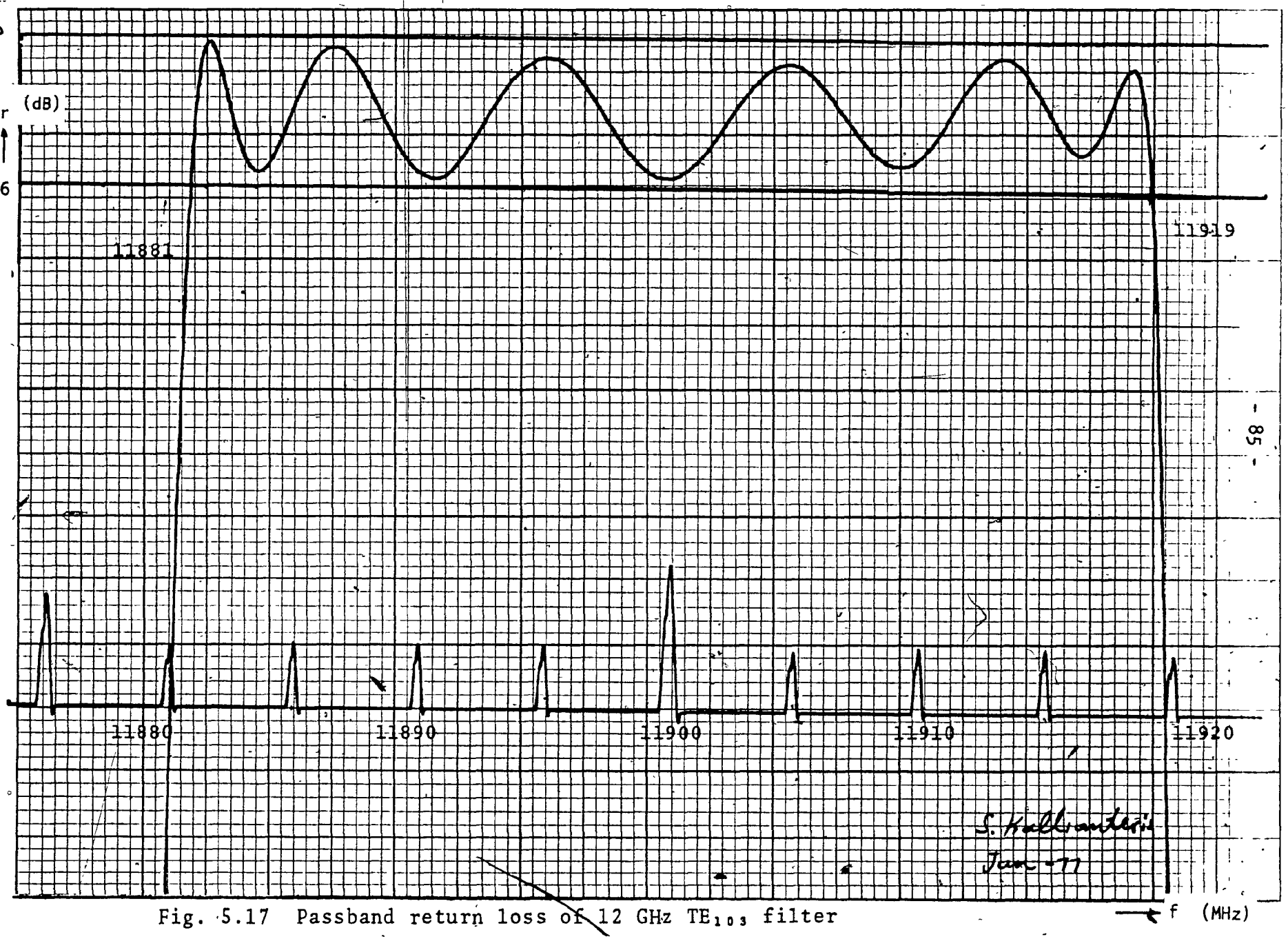

Fig. 5.17 Passband return loss of 12 GHz TE_{103} filter

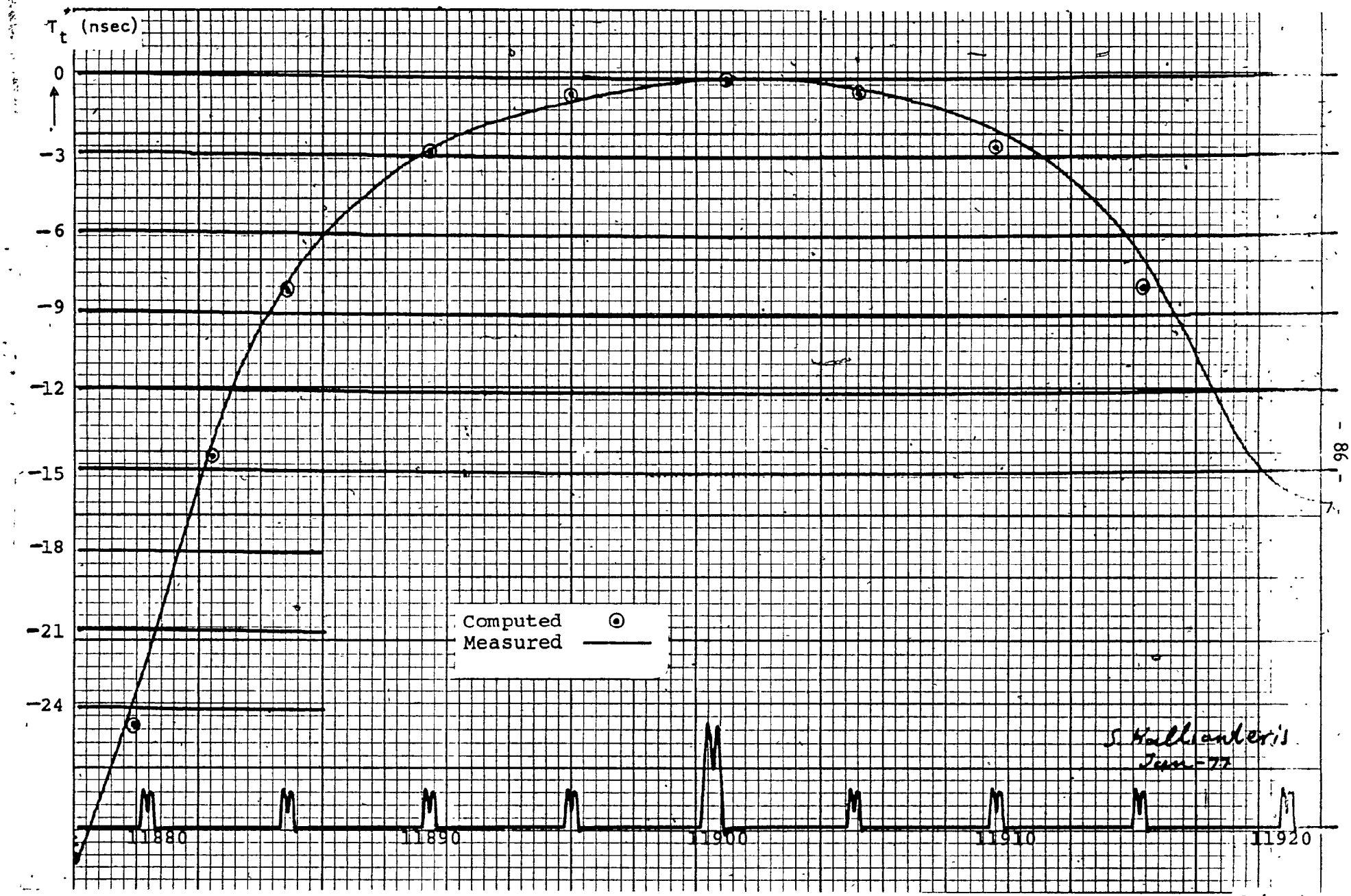

Fig. 5.18 Passband group delay of 12 GHz TE_{109} filter

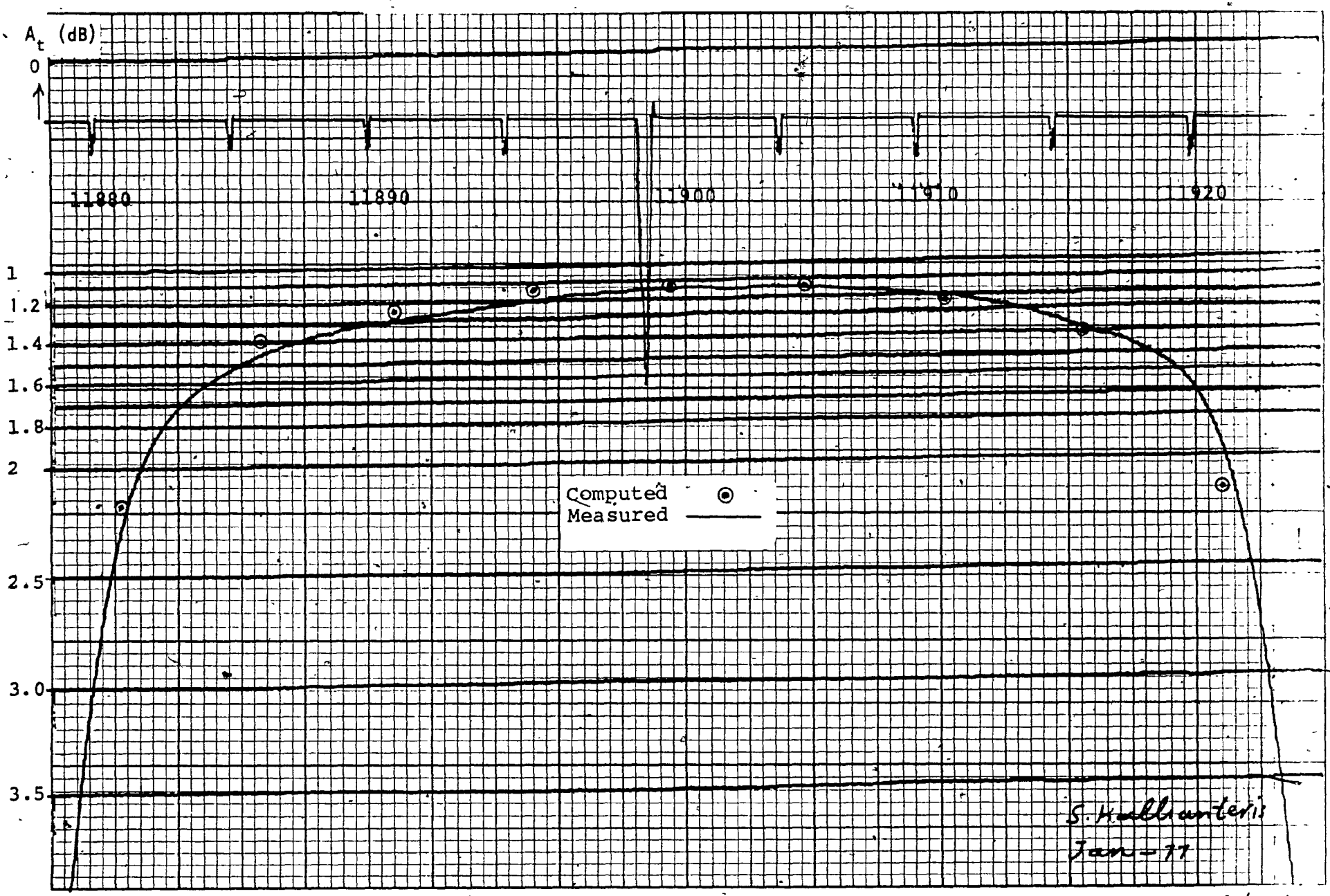

Fig. 5.19 Passband insertion loss of 12 GHz TE_{103} filter

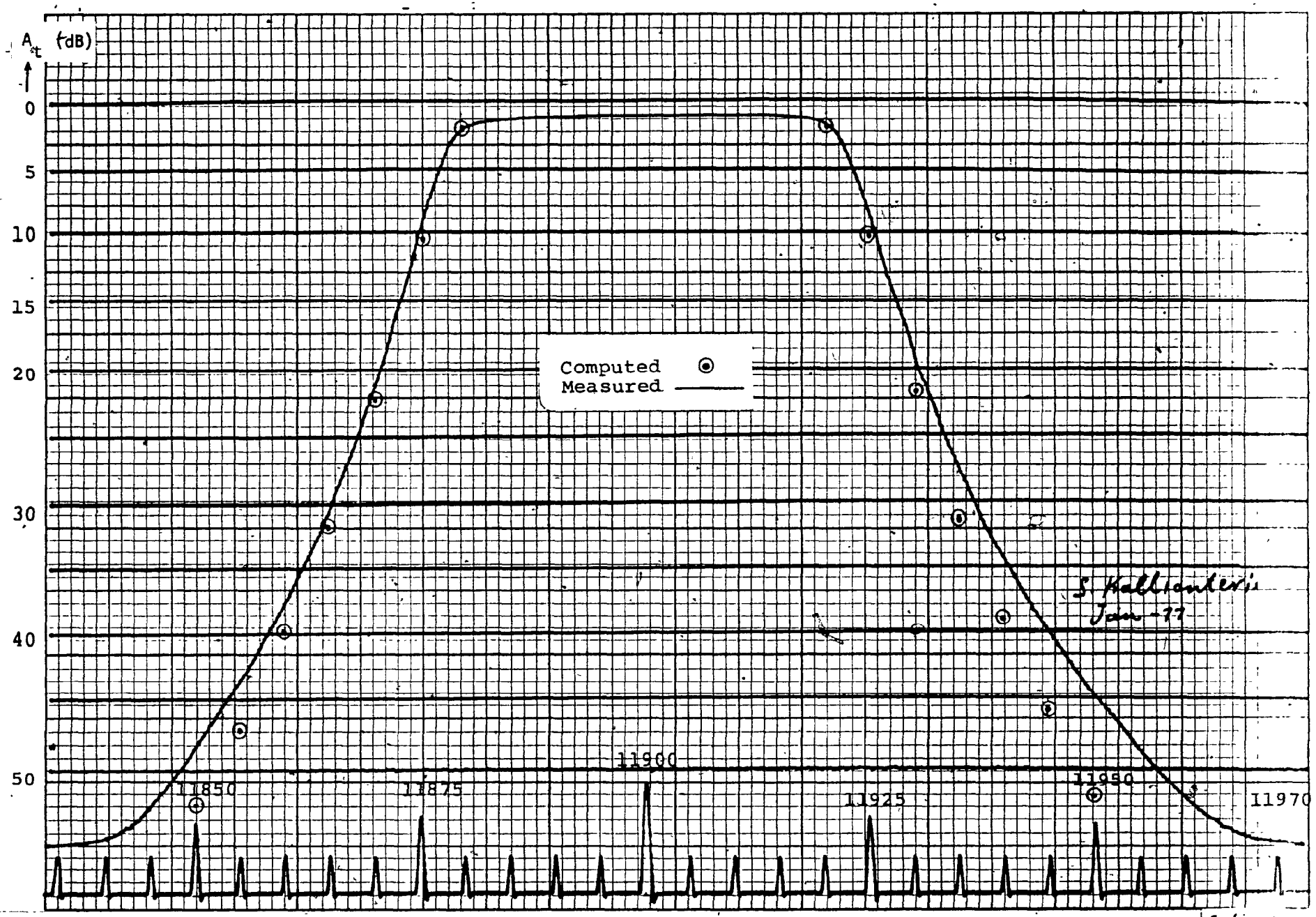

Fig. 5.20 Stopband isolation of 12 GHz TE_{10s} filter

and measured results. The only noticeable difference is in the stopband isolation of the 12 GHz filters shown in Figs. 5.15 and 5.20.

Figures 5.15 and 5.20 show that the measured stopband isolation of these filters is degraded in comparison to the computed one. This is due to the positive cross couplings employed by the 12 GHz filters, and the finite width of the intercavity apertures, which introduce the linear phase effects described in Section 3.2. These effects are eliminated either by reducing the width of the intercavity apertures or by employing negative cross couplings as in the 4 GHz filter.

Another difference between the computed and measured amplitude and group delay responses is due to the frequency dependence of the aperture susceptances. This dependence steepens the left side of the measured amplitude and group delay response and degrades its right side. Such an effect also exists in every direct coupled cavity filter and is more pronounced in filters with wider bandwidths.

5.5 UNLOADED Q EFFICIENCY OF EXPERIMENTAL FILTERS

The theoretical and measured unloaded Q's of the experimental filters are calculated using the procedures of Sections 4.6 and 4.8, the cavity dimensions, and the

measured centre frequency insertion loss of each filter. These Q's together with the unloaded Q efficiency of the filters are shown in Table 5.5.

From Table 5.5, it can be seen that the Q efficiency of the 12 GHz filters is considerably less than that of the 4 GHz filter. This reduction is caused by the effects on the Q of the surface roughness, tuning screw penetration, quality and thickness of plating, and electrical contact between adjacent cavities, all of which are more critical at higher frequencies.

Taking into consideration the above effects one can design and fabricate filters with higher unloaded Q efficiency. The electrical contact between the adjacent cavities can be improved either by electron beam welding the joints of the filters or by manufacturing the filter in such a way that the joints are at the minimum wall current areas of the cavities.

TABLE 5.5

THEORETICAL AND MEASURED UNLOADED Q'S OF EXPERIMENTAL FILTERS

TYPE OF FILTER	THEORETICAL UNLOADED Q	MEASURED UNLOADED Q	UNLOADED Q EFFICIENCY η
4 GHz TE_{111}	15519	12150	78.3%
12 GHz TE_{111}	8998	5300	58.9%
12 GHz TE_{103}	17198	9253	53.8%

CHAPTER VI

CONCLUSIONS

In this thesis, dominant and higher order mode dual mode Chebyshev filters have been considered. It was found that the higher order mode filters exhibit unloaded Q's significantly greater than those of dominant mode filters. They are, therefore, most suitable for applications at frequencies above 10 GHz.

Experimental models of both of the above filters were designed and thoroughly tested in the laboroatory. Good agreement between experimental results and predicted values was obtained.

Although higher order mode filters are superior to dominant mode ones in terms of unloaded Q and tunability, they exhibit unwanted spurious transmissions. These transmissions are more pronounced in filters with wider bandwidths and can be attenuated by employing dual mode cavities with different cross sectional dimensions.

The main advantages of the dual mode filter structure are its small volume, weight, manufacturing cost,

and its structural amenability to the realization of elliptic and linear phase function filters.

It is interesting to note that the experimental technique employed to determine the dimensions of the coupling apertures is accurate to within ±0.002 inch, and it is, therefore, the most suitable one for filters operating above 3 GHz and with fractional bandwidths less than 1%.

Further, the method for predicting the amplitude and phase characteristics of BP filters from the pole-zero locus of the LP prototype filter has been proven to be the most suitable for computer programming. An additional advantage of this method is that the dissipative losses of the filter can be considered by applying the predistortion technique on the pole-zero locus of the LP prototype filter. Suitable also for computer programming is the filter design technique by which the coupling elements and dimensions of the filter are determined from the prototype elements of the LP Chebyshev filters.

The large cross sectional dimensions and low loss of the higher order mode filter enable it to handle high microwave powers. Carefully design TE_{103}, TE_{113} and TE_{105} dual mode filters can withstand power levels up to 3 KW without voltage breakdown and excessive heat dissipation. The

measured unloaded Q's of such filters at 12 GHz and 14 GHz is in the range of 9,000 to 15,000. The increased unloaded Q of the higher order dual mode filter makes possible the multiplexing of channels with fractional bandwidths less than 0.5% at the output circuits of communications satellites.

Output multiplexers employing TE_{103}, TE_{113} and TE_{105} dual mode filters have been designed and successfully fabricated, and a considerable amount of development work is in progress to improve their performance. In the never ending drive toward better performance, the dual mode filter is today the state-of-the-art in the area of direct coupled cavity filters. It is hoped that this thesis demonstrates clearly the operating principles of the dual mode filter and enables the reader to design dual mode Chebyshev filters and predict their amplitude and phase characteristics.

REFERENCES

1. R.W. Daniels, "Approximation methods for design of passive, active and digital filters," McGraw-Hill, Co., New York, 1974.

2. V. Valkenburg, "Introduction to modern network synthesis", John Wiley and Sons, Inc., New York, 1960.

3. L. Weinberg, "Network analysis and synthesis", McGraw-Hill, Co., New York, 1962.

4. S.B. Cohn, "Direct coupled resonator filters", Proc., IRE, 45, (1957), 187-196.

5. S.B. Cohn, "Dissipation loss in multiple-coupled resonator filters", Proc., IRE 47, (1959), 1342-1348.

6. A.E. Williams, "A four cavity elliptic waveguide filter," Trans. IEEE, MTT-18, (1970), 1109-1114.

7. G.C. Temes, "A method for the estimation and precorrection of losses in terminated LC networks", Proc. of the National Electronics Conference, XVII, (1961), 341-346.

8. E.A. Gillemin, "Synthesis of passive networks", John Wiley and Sons, Inc., New York, 1967.

9. J.D. Rhodes, "The generalized direct-coupled cavity linear phase filters", Trans., IEEE, MTT-18, (1970), 308-313.

10. S. Kallianteris, "Low loss linear phase filters", IEEE-MTT-S, INternational Microwave Symposium, (1977), 394-396.

11. A.E. Atia and A.E. Williams, "Narrow-bandpass waveguide filters", Trans IEEE, MTT-20, (1972), 258-265.

12. R.D. Wanselow, "Prototype characteristics for a class of dual-mode filters", Trans. IEEE, MTT-23, (1975), 708-711.

13. G.C. Montgomery, R.H. Dicke and E.M. Purcell, "Principles of microwave circuits", Dover Publications Inc., New York, 1965.

14. A.E. Atia and A.E. Williams, "Nonminimum-phase optimum amplitude bandpass waveguide filters", Trans. IEEE, MTT-22, (1974), 425-431.

15. S. Kallianteris, C.M. Kudsia and M.N.S. Swamy, "A new class of dual-mode microwave filters for space applications", Proceedings of the 7th European Microwave Conference, (1977), 51-58.

16. S. Kallianteris and M.V. O'Donovan, "Technology advances in the realization of filter networks for communication satellite operation at frequencies above 10 GHz", 6th Communications Satellite Systems Conference, AIAA-76-292, (1976).

17. S. Kallianteris, "Design of low loss 12 GHz output multiplexer for the second genration Telesat Canada satellite", Proceedings of the 6th European Microwave Conference, (1976), 64-68.

18. N. Marcuvitz, "Waveguide handbook", McGraw-Hill, Co., New York, 1951.

19. G.L. Mathaei, L. Young and E.M.T. Jones, "Microwave filters, impedance matching networks and coupling structures", McGraw-Hill, Co., New York, 1964.

20. G.C. Montgomery, "Technique of microwave measurements", MIT, Radiation Laboratory, Boston Technical Publishers, Inc., 1964.

21. S.B. Cohn, "Microwave coupling by large apertures", Proc. IRE, (1952), 696-699.

22. S. Kallianteris, "Low Loss Dual Mode Filters Employing Square or Cylindrical Cavities Operating in TE_{10_N} Modes", Canadian Patent application, Nov. (1975).

23. S. Kallianteris, "Dual Mode Self Equalized Bandpass Filters", Canadian Patent application, Dec. (1976).

APPENDIX A

COMPUTED AMPLITUDE AND PHASE CHARACTERISTICS OF EXPERIMENTAL FILTERS

BAND PASS CHEBYSHEV FILTER

THE TRANSMISSION CHARACTERISTICS ARE

NUMBER OF SECTIONS	8	
RETURN LOSS	±26.00	(DB)
FILTER BANDWIDTH	37.00	(MHZ)
CENTER FREQUENCY	3960.00	(MHZ)
LOWER LIMIT	3925.00	(MHZ)
UPPER LIMIT	3995.00	(MHZ)
UNLOADED Q	12150.00	
NUMBER OF FREQUENCY POINTS	29	

TABLE A1.1

COMPUTED TRANSMISSION RESPONSE OF 4 GHz TE_{111} EXPERIMENTAL FILTER

FILTER RESPONSE

	AMPLITUDE				PHASE			
FREQUENCY	AMPLITUDE	RELATIVE AMPLITUDE	1ST DERIV		PHASE	GROUP DELAY	RELATIVE DELAY	1ST DERIV
MHZ	DB	DB	DB/MHZ		RADIANS	NSECS	NSEC	NSEC/MHZ
3925.0	-55.6197	55.170	2.354		-14.05	-8.75	-40.598	-.729
3927.5	-49.4229	48.973	2.614		-14.21	-10.93	-38.414	-1.058
3930.0	-42.4866	42.037	2.951		-14.40	-14.23	-35.121	-1.655
3932.5	-34.5639	34.114	3.413		-14.67	-19.71	-29.640	-2.925
3935.0	-25.2418	24.792	4.091		-15.05	-30.53	-18.817	-6.432
3937.5	-13.8638	13.414	5.018		-15.72	-60.10	10.751	-20.853
3940.0	-2.5851	2.135	2.572		-10.93	-126.31	76.961	-1.706
3942.5	-.7473	.298	.087		-12.59	-83.80	34.453	11.094
3945.0	-.5979	.148	.033		-7.48	-67.62	18.275	4.204

3947.5	-.5377	.088	.023		-8.47	-59.79	10.438	2.166
3950.0	-.4909	.041	.011		-3.09	-55.44	6.093	1.413
3952.5	-.4753	.026	.006		-3.93	-52.45	3.102	.889
3955.0	-.4539	.004	.008		-4.74	-50.79	1.441	.449
3957.5	-.4452	-.005	-.001		.75	-49.80	.456	.294
3960.0	-.4497	-.000	.000		-.03	-49.35	-.003	-.014
3962.5	-.4449	-.005	.001		-.81	-49.73	.378	-.305
3965.0	-.4553	.006	-.009		4.69	-50.60	1.250	-.461
3967.5	-.4762	.026	-.006		3.88	-52.17	2.825	-.910
3970.0	-.4923	.043	-.011		3.04	-55.04	5.691	-1.405
3972.5	-.5400	.090	-.023		8.43	-59.22	9.868	-2.164
3975.0	-.6000	.150	-.033		7.45	-66.82	17.472	-4.131
3977.5	-.7489	.299	-.086		12.58	-82.48	33.131	-10.825
3980.0	-2.5090	2.059	-2.444		10.95	-123.71	74.363	.253
3982.5	-13.4353	12.986	-4.926		15.75	-60.47	11.121	20.816
3985.0	-24.6382	24.188	-4.033		15.08	-30.68	-18.664	6.460
3987.5	-33.8268	33.377	-3.363		14.69	-19.77	-29.575	2.923
3990.0	-41.6285	41.179	-2.904		14.43	-14.26	-35.086	1.648
3992.5	-48.4505	48.001	-2.569		14.23	-10.96	-38.393	1.050
3995.0	-54.5377	54.088	-2.311		14.08	-8.77	-40.584	.722

BAND PASS CHEBYSHEV FILTER

THE REFLECTION CHARACTERISTICS ARE

NUMBER OF SECTIONS	8	
RETURN LOSS	+26.00	(DB)
FILTER BANDWIDTH	37.00	(MHZ)
CENTER FREQUENCY	3960.00	(MHZ)
LOWER LIMIT	3940.00	(MHZ)
UPPER LIMIT	3980.00	(MHZ)
UNLOADED Q	12170.00	
NUMBER OF FREQUENCY POINTS.	17	

TABLE A1.2

COMPUTED REFLECTION RESPONSE OF 4 GHz TE_{111} EXPERIMENTAL FILTER

FILTER RESPONSE

FREQUENCY	AMPLITUDE	RELATIVE AMPLITUDE	1ST DERIV	PHASE	GROUP DELAY	RELATIVE DELAY	1ST DERIV
MHZ	DB	DB	DB/MHZ	RADIANS	NSECS	NSEC	NSEC/MHZ
3940.0	-6.6033	6.603	-6.552	1.81	-117.20	117.196	6.861
3942.5	-27.5167	27.517	5.486	-3.27	-19.65	19.650	-150.383
3945.0	-36.1864	36.186	17.123	-1.54	68.90	68.899	-556.114
3947.5	-27.1143	27.114	-1.987	-2.15	-49.92	49.924	4.966
3950.0	-40.6924	40.692	20.388	-.38	128.34	128.336	-869.452

I	3952.5	-26.5518	26.552	.674	I	-.81	-46.46	46.464	-.497
I	3955.0	-31.5763	31.576	-5.839	I	-1.49	-33.96	33.963	22.745
I	3957.5	-32.3470	32.347	6.417	I	.63	-30.36	30.356	-28.720
I	3960.0	-26.4232	26.423	-.145	I	-.03	-44.50	44.505	.154
I	3962.5	-33.5861	33.586	-7.674	I	-.66	-23.86	23.861	45.753
I	3965.0	-30.6765	30.677	4.984	I	1.45	-36.95	36.945	-15.824
I	3967.5	-26.6754	26.675	-.972	I	.76	-45.99	45.991	.950
I	3970.0	-43.6033	43.603	-25.231	I	.55	302.39	302.395	2090.214
I	3972.5	-26.9367	26.937	1.649	I	2.12	-49.71	49.709	-4.054
I	3975.0	-37.3004	37.300	-19.073	I	1.58	108.56	108.561	793.154
I	3977.5	-27.6230	27.623	-5.751	I	3.27	-16.40	16.396	158.565
I	3980.0	-6.8026	6.803	6.582	I	-1.78	-114.53	114.530	-8.347

BAND PASS CHEBYSHEV FILTER

THE TRANSMISSION CHARACTERISTICS ARE

NUMBER OF SECTIONS	6	
RETURN LOSS	+26.60	(DB)
FILTER BANDWIDTH	83.00	(MHZ)
CENTER FREQUENCY	12002.00	(MHZ)
LOWER LIMIT	11875.00	(MHZ)
UPPER LIMIT	12150.00	(MHZ)
UNLOADED Q	5300.00	
NUMBER OF FREQUENCY POINTS	56	

TABLE A1.3

COMPUTED TRANSMISSION RESPONSE OF 12 GHz
TE_{111} EXPERIMENTAL FILTER

FILTER RESPONSE

FREQUENCY	AMPLITUDE	RELATIVE AMPLITUDE	1ST DERIV	PHASE	GROUP DELAY	RELATIVE DELAY	1ST DERIV
MHZ	DB	DB	DB/MHZ	RADIANS	NSECS	NSEC	NSEC/MHZ
11875.0	-60.9694	60.067	.438	-10.35	-1.29	-13.154	-.024
11880.0	-58.7324	57.831	.457	-10.40	-1.41	-13.029	-.027
11885.0	-56.3911	55.489	.479	-10.44	-1.56	-12.883	-.032
11890.0	-53.9346	53.033	.504	-10.49	-1.73	-12.712	-.037
11895.0	-51.3500	50.448	.531	-10.55	-1.93	-12.510	-.045
11900.0	-48.6220	47.720	.561	-10.62	-2.18	-12.267	-.054
11905.0	-45.7323	44.830	.596	-10.69	-2.47	-11.971	-.066
11910.0	-42.6586	41.757	.635	-10.77	-2.84	-11.603	-.083
11915.0	-39.3734	38.471	.680	-10.87	-3.31	-11.138	-.106
11920.0	-35.8420	34.940	.734	-10.98	-3.91	-10.531	-.140

11925.0	-32.0203	31.118	.797	-11.12	-4.73	-9.713	-.193
11930.0	-27.8514	26.950	.873	-11.28	-5.89	-8.556	-.280
11935.0	-23.2629	22.361	.965	-11.49	-7.63	-6.814	-.436
11940.0	-18.1742	17.272	1.072	-11.77	-10.48	-3.961	-.744
11945.0	-12.5657	11.664	1.161	-12.17	-15.56	1.118	-1.350
11950.0	-6.8655	5.964	1.057	-12.79	-23.91	9.472	-1.805
11955.0	-2.8314	1.930	.503	-7.36	-28.75	14.308	.260
11960.0	-1.5145	.613	.104	-8.20	-24.02	9.577	1.093
11965.0	-1.2337	.332	.033	-8.88	-19.93	5.487	.551
11970.0	-1.1040	.202	.020	-3.19	-17.91	3.463	.302
11975.0	-1.0266	.125	.011	-3.73	-16.65	2.205	.207
11980.0	-.9802	.078	.008	-4.24	-15.77	1.331	.138
11985.0	-.9435	.042	.007	-4.73	-15.21	.766	.086
11990.0	-.9161	.014	.004	-1.09	-14.85	.402	.057
11995.0	-.9038	.002	.001	.62	-14.60	.152	.037
12000.0	-.9019	.000	.000	.17	-14.46	.015	.011
12005.0	-.9020	.000	-.000	-.29	-14.46	.022	-.019
12010.0	-.9056	.004	-.002	-.74	-14.61	.166	-.043
12015.0	-.9217	.020	-.005	5.08	-14.86	.414	-.063
12020.0	-.9520	.050	-.007	4.61	-15.23	.788	-.096
12025.0	-.9900	.088	-.008	4.12	-15.83	1.384	-.152
12030.0	-1.0407	.139	-.013	3.61	-16.74	2.296	-.220
12035.0	-1.1278	.226	-.022	3.06	-18.05	3.610	-.326
12040.0	-1.2705	.369	-.037	8.75	-20.29	5.850	-.631

I 12045.0	-1.6351	.733	-.143	I	8.05	-24.76	10.316	-1.120
I 12050.0	-3.3359	2.434	-.608	I	7.20	-28.30	13.862	.217
I 12055.0	-7.7460	6.844	-1.083	I	12.67	-22.02	7.579	1.776
I 12060.0	-13.3996	12.498	-1.131	I	12.10	-14.34	-.102	1.194
I 12065.0	-18.8320	17.930	-1.036	I	11.73	-9.82	-4.618	.664
I 12070.0	-23.7493	22.847	-.933	I	11.47	-7.24	-7.200	.396
I 12075.0	-28.1882	27.286	-.845	I	11.27	-5.64	-8.805	.259
I 12080.0	-32.2267	31.325	-.772	I	11.11	-4.56	-9.886	.179
I 12085.0	-35.9326	35.031	-.712	I	10.98	-3.79	-10.658	.131
I 12090.0	-39.3594	38.458	-.660	I	10.87	-3.21	-11.234	.100
I 12095.0	-42.5487	41.647	-.616	I	10.77	-2.76	-11.679	.079
I 12100.0	-45.5333	44.631	-.578	I	10.69	-2.41	-12.031	.063
I 12105.0	-48.3393	47.437	-.545	I	10.62	-2.13	-12.316	.051
I 12110.0	-50.9882	50.086	-.515	I	10.56	-1.89	-12.551	.042
I 12115.0	-53.4974	52.596	-.489	I	10.50	-1.70	-12.747	.036
I 12120.0	-55.8816	54.980	-.465	I	10.45	-1.53	-12.912	.030
I 12125.0	-58.1532	57.251	-.444	I	10.41	-1.39	-13.054	.026
I 12130.0	-60.3228	59.421	-.424	I	10.36	-1.27	-13.176	.022
I 12135.0	-62.3994	61.498	-.407	I	10.33	-1.16	-13.282	.020
I 12140.0	-64.3909	63.489	-.390	I	10.29	-1.07	-13.375	.017
I 12145.0	-66.3043	65.402	-.375	I	10.26	-.99	-13.456	.015
I 12150.0	-68.1455	67.244	-.361	I	10.23	-.91	-13.529	.013

BAND PASS CHEBYSHEV FILTER

THE REFLECTION CHARACTERISTICS ARE

NUMBER OF SECTIONS	6
RETURN LOSS	+26.60 (DB)
FILTER BANDWIDTH	83.00 (MHZ)
CENTER FREQUENCY	12002.00 (MHZ)
LOWER LIMIT	11955.00 (MHZ)
UPPER LIMIT	12045.00 (MHZ)
UNLOADED Q	5300.00
NUMBER OF FREQUENCY POINTS	19

TABLE A1.4

COMPUTED REFLECTION RESPONSE OF 12 GHz
TE_{111} EXPERIMENTAL FILTER

FILTER RESPONSE

FREQUENCY	AMPLITUDE			PHASE			
		RELATIVE AMPLITUDE	1ST DERIV		GROUP DELAY	RELATIVE DELAY	1ST DERIV
MHZ	DB	DB	DB/MHZ	RADIANS	NSECS	NSEC	NSEC/MHZ
11955.0	-8.6425	8.642	-1.824	2.37	-24.27	24.269	1.369
11960.0	-23.4239	23.424	-4.639	1.94	14.02	14.016	29.795
11965.0	-27.6076	27.608	.628	-2.70	.03	.033	-8.046
11970.0	-32.3704	32.370	-2.634	3.48	7.96	7.965	14.414
11975.0	-33.4419	33.442	2.565	-.97	10.48	10.483	-16.959

11980.0	-27.5637	27.564	.278	-1.13	-10.32	10.320	-.480
11985.0	-29.1748	29.175	-.955	-1.46	-8.70	8.702	1.364
11990.0	-39.9152	39.915	-3.798	5.01	57.49	57.493	62.845
11995.0	-32.3901	32.390	1.794	.38	-2.26	2.259	-5.161
12000.0	-27.6829	27.683	.335	-.12	-10.44	10.436	-.315
12005.0	-28.2817	28.282	-.596	-.21	-9.82	9.821	.648
12010.0	-35.1891	35.189	-2.618	-.36	9.07	9.074	14.412
12015.0	-35.6248	35.625	2.831	1.51	12.21	12.212	-17.483
12020.0	-28.2062	28.206	.613	1.38	-9.88	9.876	-.685
12025.0	-28.0931	28.093	-.606	1.06	-9.32	9.316	1.099
12030.0	-37.0322	37.032	-3.524	1.16	47.55	47.554	54.290
12035.0	-29.9528	29.953	1.750	-3.47	-2.08	2.076	-5.232
12040.0	-28.7354	28.735	-1.544	2.74	14.78	14.779	22.771
12045.0	-19.3272	19.327	3.713	-1.92	-5.09	5.090	-12.206

BAND PASS CHEBYSHEV FILTER

THE TRANSMISSION CHARACTERISTICS ARE

NUMBER OF SECTIONS	6	
RETURN LOSS	+26.00	(DB)
FILTER BANDWIDTH	38.00	(MHZ)
CENTER FREQUENCY	11900.00	(MHZ)
LOWER LIMIT	11845.00	(MHZ)
UPPER LIMIT	11955.00	(MHZ)
UNLOADED Q	9253.00	
NUMBER OF FREQUENCY POINTS	23	

TABLE A1.5

COMPUTED TRANSMISSION RESPONSE OF 12 GHz
TE_{103} EXPERIMENTAL FILTER

FILTER-RESPONSE

FREQUENCY	AMPLITUDE	RELATIVE AMPLITUDE	1ST DERIV	PHASE	GROUP DELAY	RELATIVE DELAY	1ST DERIV
MHZ	DB	DB	DB/MHZ	RADIANS	NSECS	NSEC	NSEC/MHZ
11845.0	-58.3590	57.231	1.013	-10.41	-3.18	-28.662	-.136
11850.0	-53.0170	51.889	1.128	-10.52	-3.99	-27.852	-.195
11855.0	-47.0232	45.895	1.276	-10.66	-5.19	-26.657	-.296
11860.0	-40.1784	39.050	1.472	-10.85	-7.09	-24.758	-.491
11865.0	-32.1680	31.040	1.749	-11.12	-10.48	-21.364	-.942
11870.0	-22.4654	21.337	2.159	-11.55	-17.94	-13.904	-2.350

I 11875.0	I-10.5123	I 9.384	I 2.519	I	I -12.40	I -40.87	I 9.024	I -7.807 I
I 11880.0	I -2.2003	I 1.072	I .476	I	I -7.88	I -57.19	I 25.341	I 5.145 I
I 11885.0	I -1.4085	I .280	I .061	I	I -3.07	I -40.11	I 8.264	I 1.583 I
I 11890.0	I -1.2269	I .098	I .022	I	I -4.23	I -34.75	I 2.905	I .660 I
I 11895.0	I -1.1430	I .015	I .009	I	I 1.00	I -32.60	I .751	I .260 I
I 11900.0	I -1.1284	I .000	I -.000	I	I -.01	I -31.85	I -.000	I -.003 I
I 11905.0	I -1.1439	I .016	I -.010	I	I -1.02	I -32.53	I .685	I -.262 I
I 11910.0	I -1.2285	I .100	I -.022	I	I 4.22	I -34.61	I 2.760	I -.671 I
I 11915.0	I -1.4108	I .282	I -.061	I	I 3.06	I -39.84	I 7.990	I -1.570 I
I 11920.0	I -2.1951	I 1.067	I -.468	I	I 7.88	I -56.50	I 24.654	I -5.040 I
I 11925.0	I-10.3289	I 9.209	I -2.480	I	I 12.42	I -40.87	I 9.024	I 7.686 I
I 11930.0	I-22.1434	I 21.015	I -2.138	I	I 11.57	I -17.99	I -13.852	I 2.349 I
I 11935.0	I-31.7501	I 30.622	I -1.731	I	I 11.14	I -10.50	I -21.342	I .939 I
I 11940.0	I-39.6742	I 38.546	I -1.456	I	I 10.87	I -7.10	I -24.747	I .488 I
I 11945.0	I-46.4368	I 45.308	I -1.260	I	I 10.68	I -5.20	I -26.651	I .293 I
I 11950.0	I-52.3508	I 51.222	I -1.112	I	I 10.54	I -4.00	I -27.848	I .193 I
I 11955.0	I-57.6146	I 56.486	I -.997	I	I 10.42	I -3.19	I -28.659	I .135 I

BAND PASS CHEBYSHEV FILTER

THE REFLECTION CHARACTERISTICS ARE

NUMBER OF SECTIONS	6
RETURN LOSS	+26.00 (DB)
FILTER BANDWIDTH	38.00 (MHZ)
CENTER FREQUENCY	11900.00 (MHZ)
LOWER LIMIT	11880.00 (MHZ)
UPPER LIMIT	11920.00 (MHZ)
UNLOADED Q	9253.00
NUMBER OF FREQUENCY POINTS	17

TABLE A1.6

COMPUTED REFLECTION RESPONSE OF 12 GHz
TE_{103} EXPERIMENTAL FILTER

FILTER RESPONSE

FREQUENCY	AMPLITUDE			PHASE			
		RELATIVE AMPLITUDE	1ST DERIV		GROUP DELAY	RELATIVE DELAY	1ST DERIV
MHZ	DB	DB	DB/MHZ	RADIANS	NSECS	NSEC	NSEC/MHZ
11880.0	-16.4860	16.486	-6.847	2.12	-21.33	21.329	40.521
11882.5	-28.1426	28.143	2.915	-2.76	50.49	50.491	-127.295
11885.0	-29.9696	29.970	-4.122	3.56	6.76	6.758	37.405
11887.5	-33.4551	33.455	5.492	-1.06	44.95	44.955	-109.710
11890.0	-27.0872	27.087	.518	-1.13	-20.32	20.323	-2.637
11892.5	-29.3018	29.302	-2.422	-1.44	-13.73	13.730	10.519

I 11895.0	I-40.6010	I 40.601	I -.795	I	I 5.66	I 218.01	I 218.014	I 42.693 I
I 11897.5	I-29.6974	I 29.697	I 2.501	I	I .30	I -12.54	I 12.536	I -11.448 I
I 11900.0	I-26.9407	I 26.941	I -.042	I	I -.01	I -21.78	I 21.783	I .099 I
I 11902.5	I-29.9512	I 29.951	I -2.648	I	I -.30	I -11.32	I 11.323	I 12.846 I
I 11905.0	I-40.4398	I 40.440	I 2.621	I	I -5.53	I 208.58	I 208.582	I-142.499 I
I 11907.5	I-29.1024	I 29.102	I 2.286	I	I 1.43	I -14.52	I 14.516	I -9.439 I
I 11910.0	I-27.1278	I 27.128	I -.600	I	I 1.12	I -20.01	I 20.008	I 2.955 I
I 11912.5	I-33.7713	I 33.771	I -5.616	I	I 1.08	I 51.16	I 51.160	I 120.195 I
I 11915.0	I-29.8165	I 29.817	I 3.975	I	I -3.56	I 5.35	I 5.352	I -34.366 I
I 11917.5	I-28.1870	I 28.187	I -2.928	I	I 2.77	I 51.94	I 51.939	I 128.533 I
I 11920.0	I-16.5600	I 16.560	I 6.799	I	I -2.12	I -20.66	I 20.658	I -40.195 I

APPENDIX B

FLOW CHARTS FOR THE DESIGN AND RESPONSE PREDICTION PROGRAMS

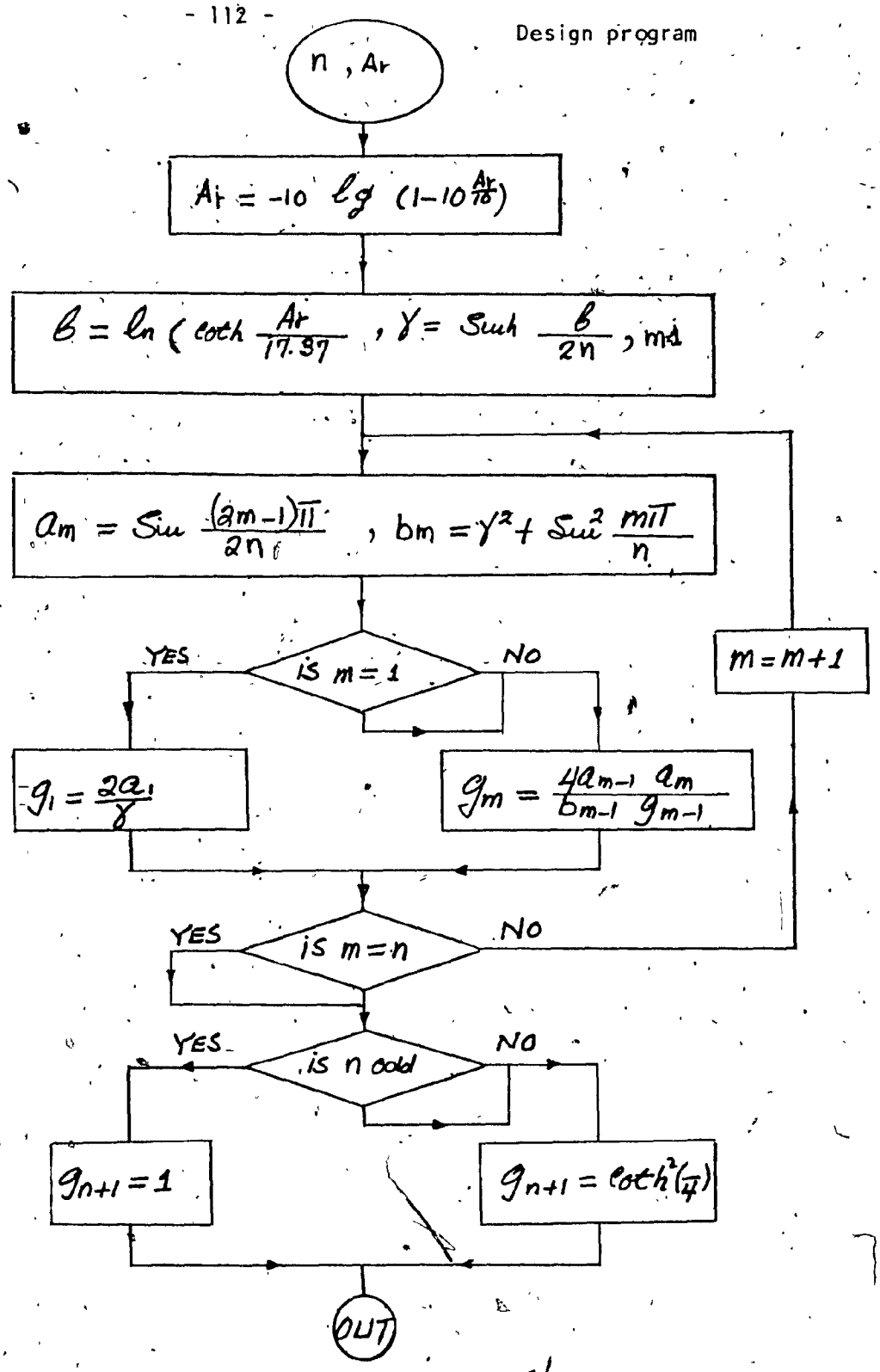

Fig. A2.1 Computation of g_m elements of doubly terminated LP Chebyshev filters

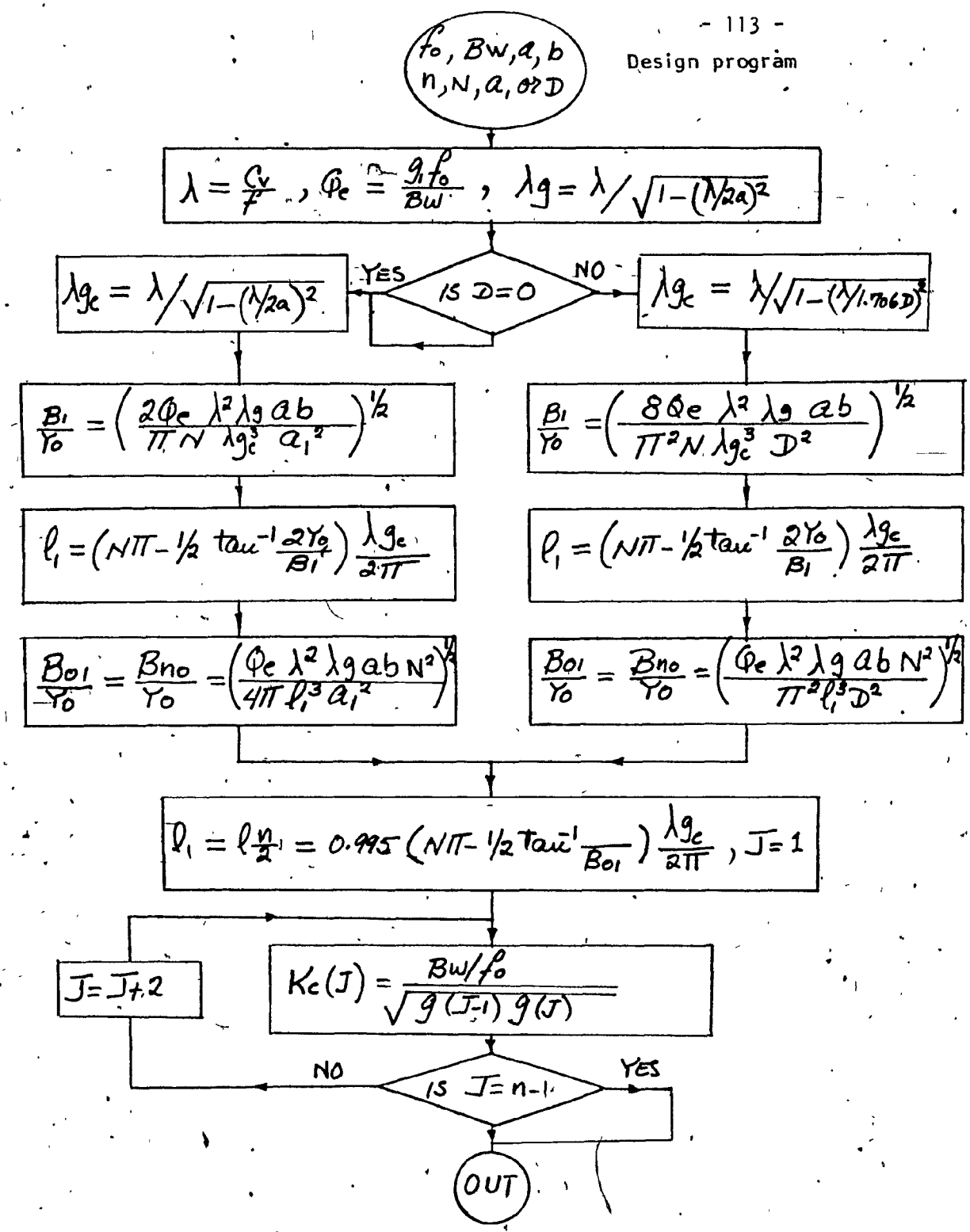

Fig. A2.2 Computation of cavity length and susceptance for the end apertures, and of the intracavity coupling coefficients

Design program

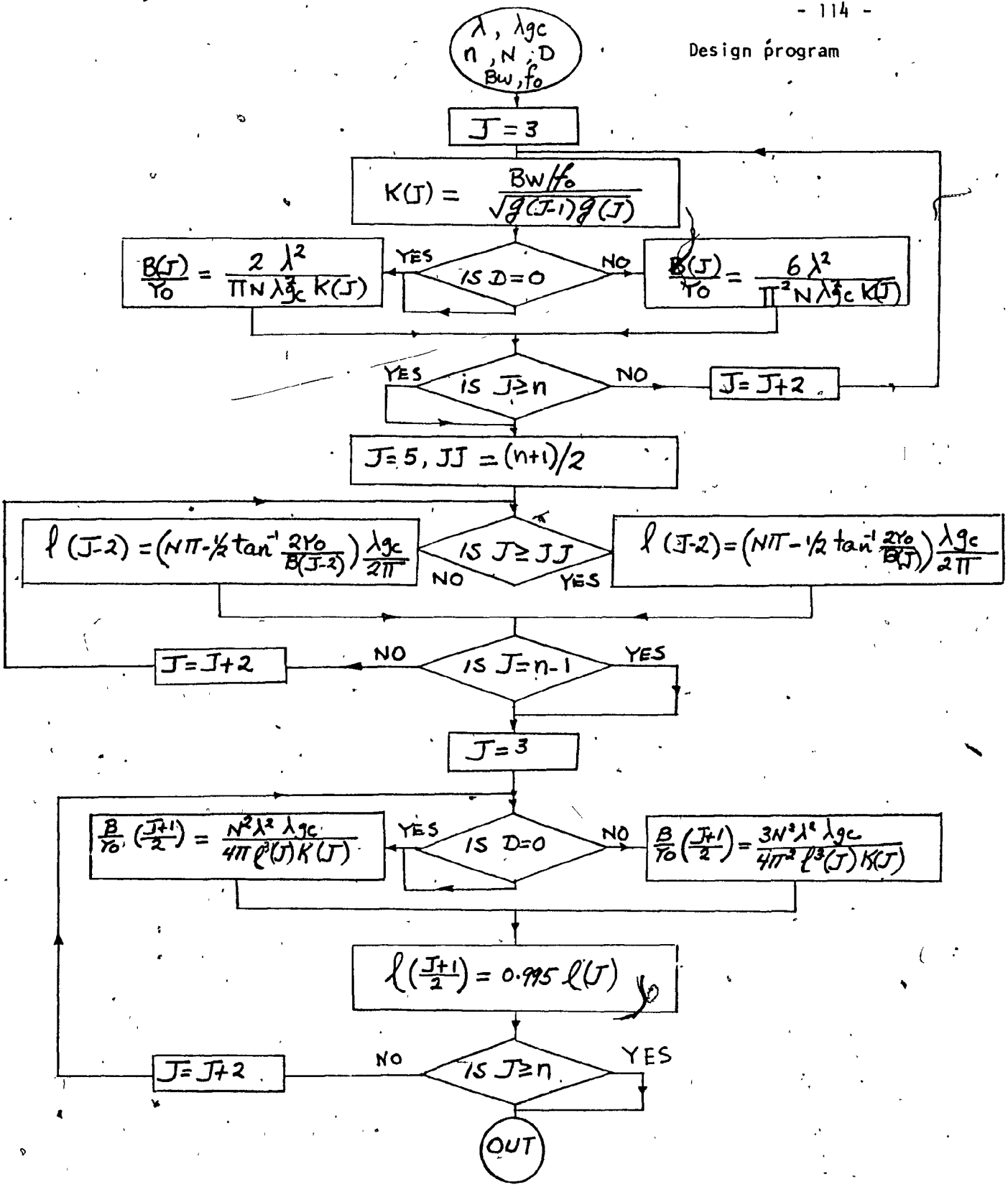

Fig. A2.3 Computation of intercavity susceptances and length of cent . cavities.

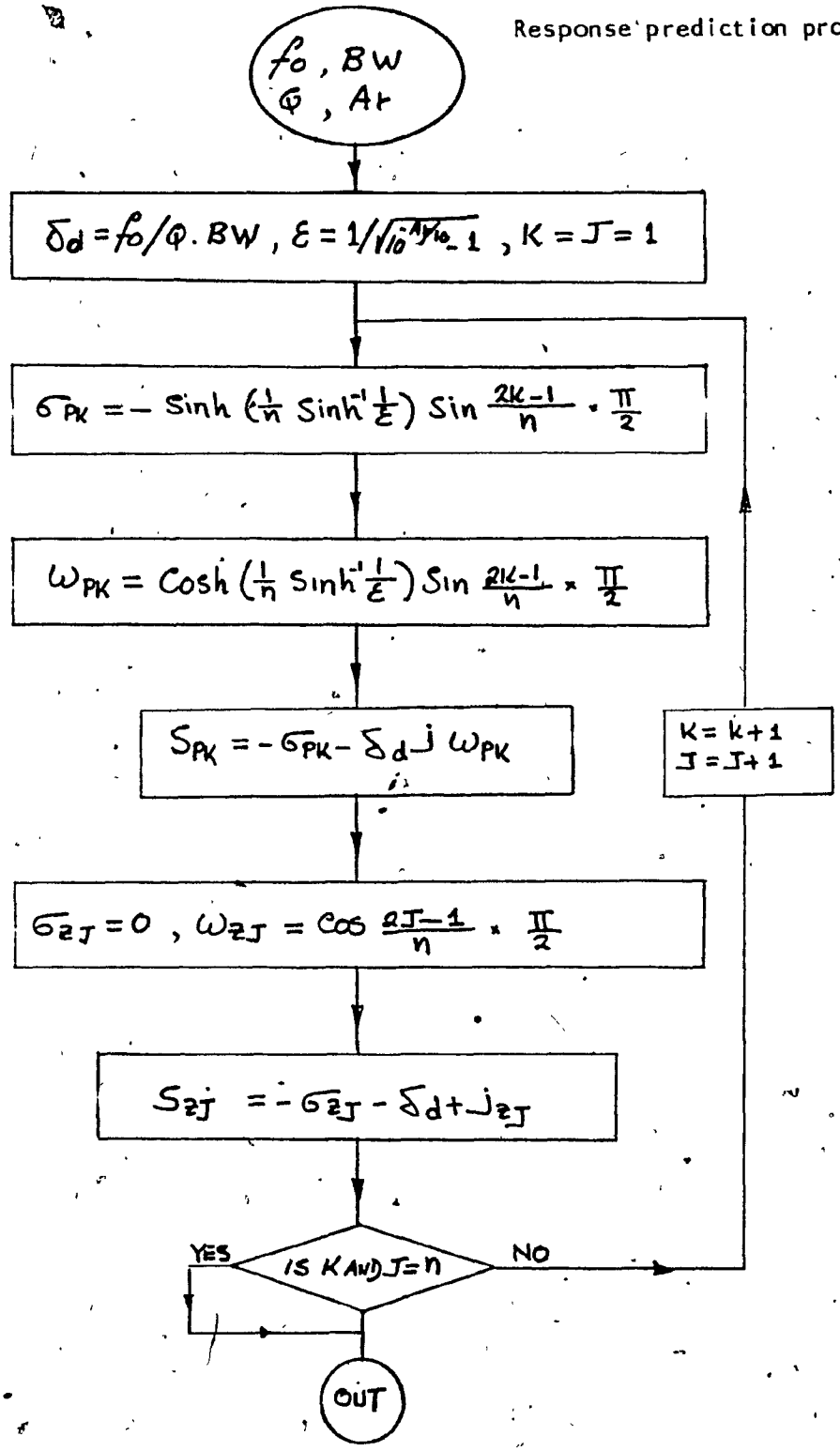

Fig. A2.4 Computation of poles and reflection zeros of L.P. Chebyshev filters.

Response prediction program

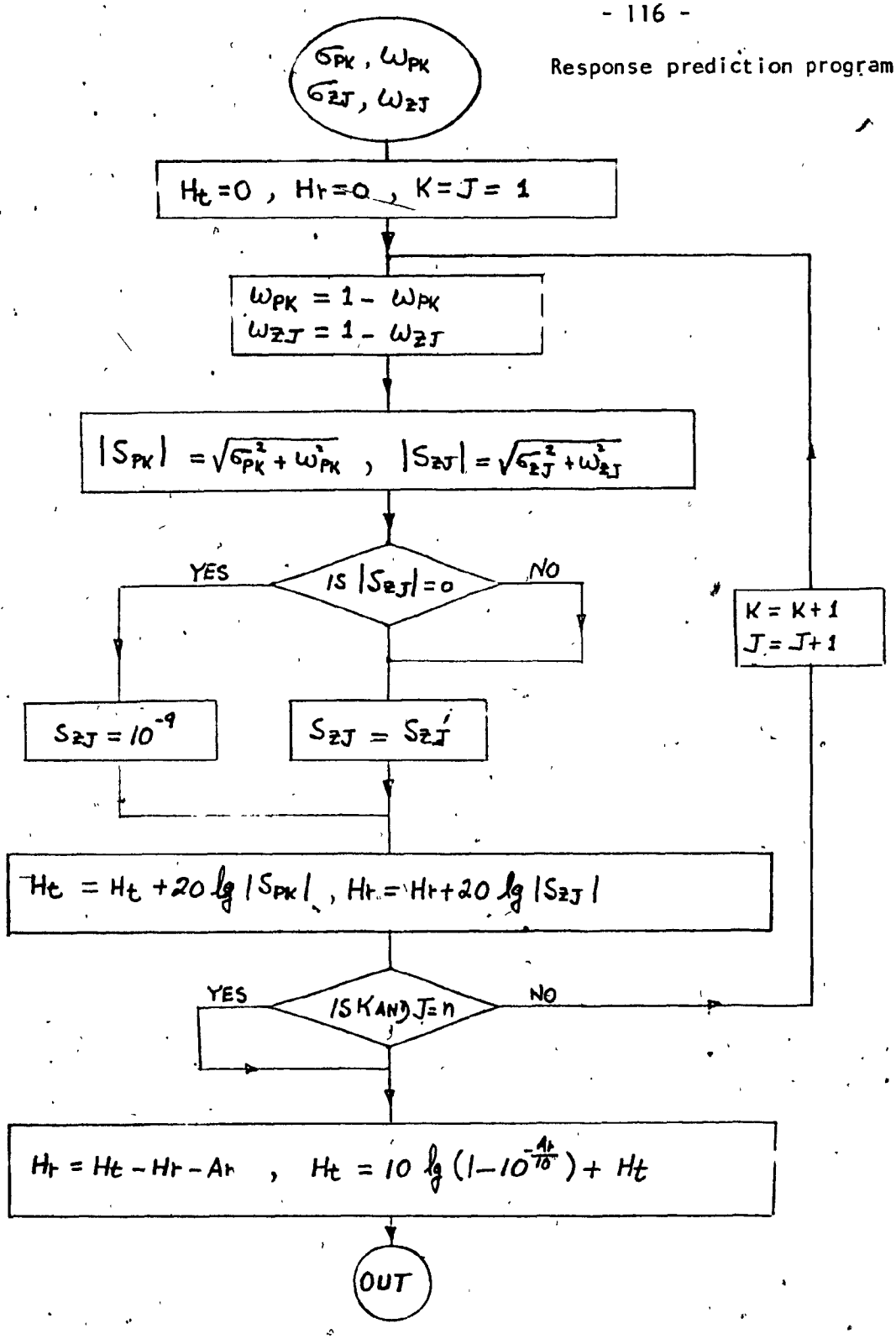

Fig. A2.5 Computation of H_t and H_r of LP Chebyshev filters

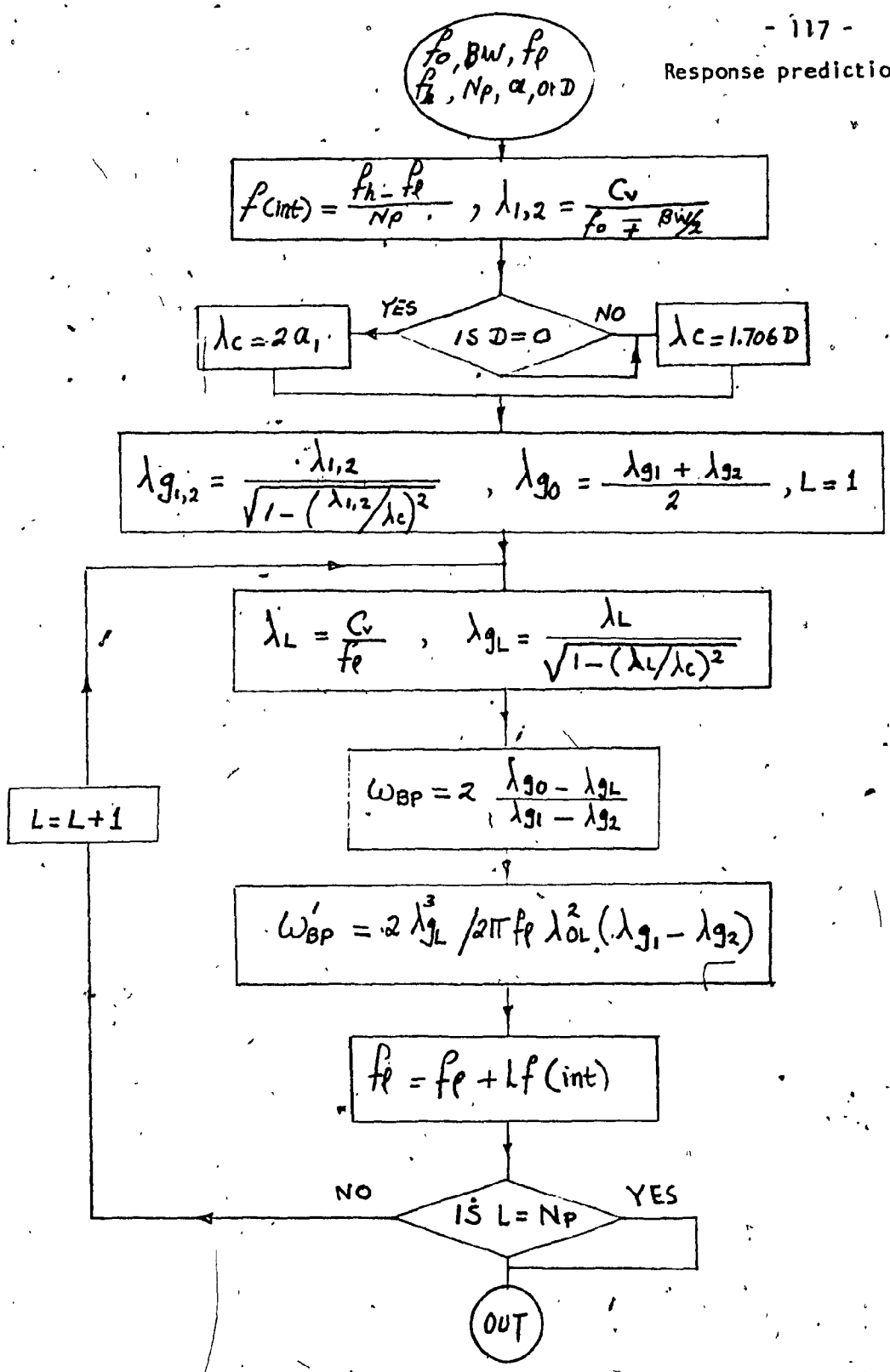

Fig. A2.6 Computation of ω_{BP} and ω'_{BP} for every frequency print out point N_p

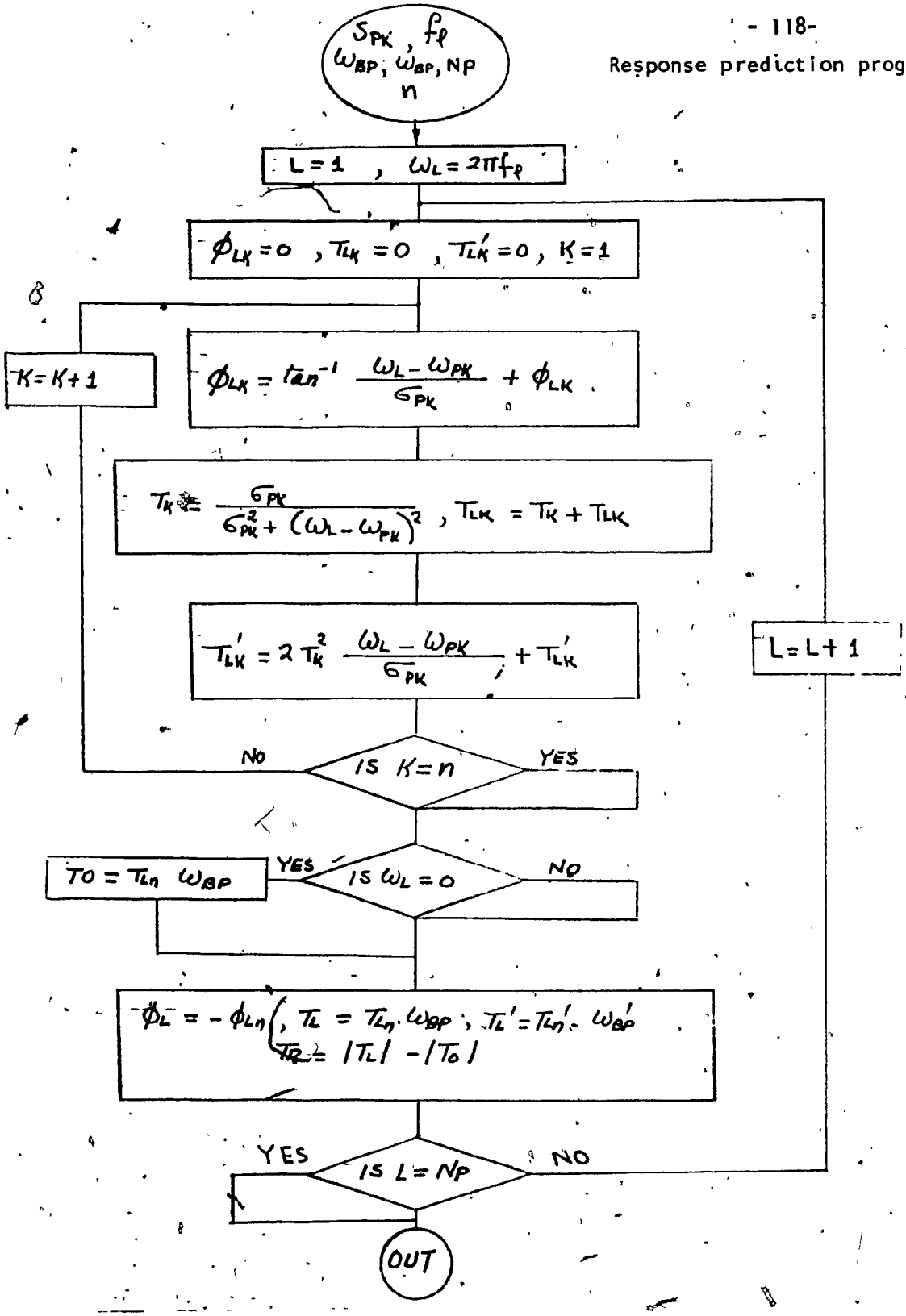

Fig. A2.7 Computation of the transmission characteristics ϕ_t, and T_t for every frequency print out point N_P

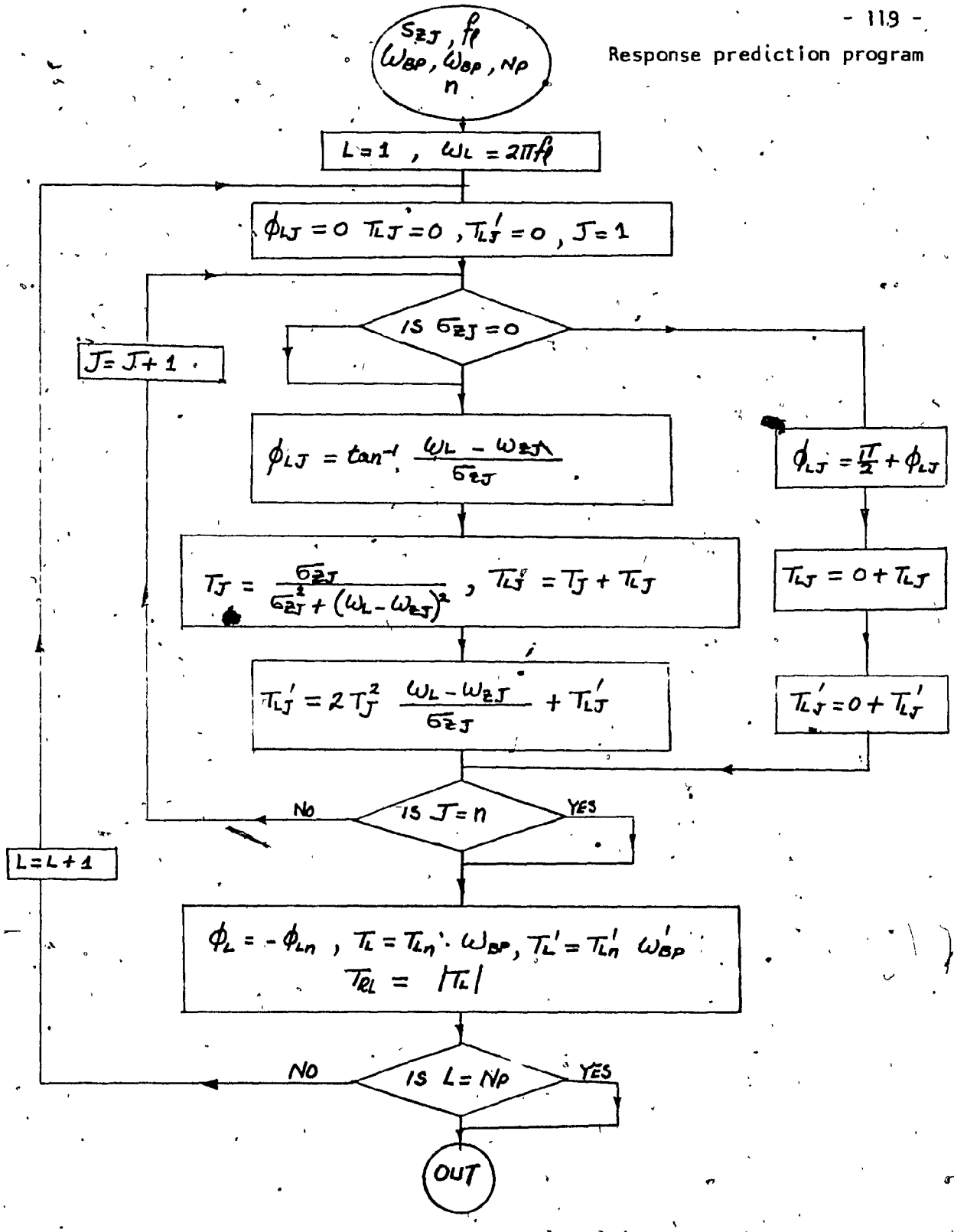

Fig. A2.8 Computation of reflection characteristics Φ_r, T_r for every frequency print out point N_P